

Functionalized Nano-channels in Polymeric Membranes for Hydrogen Separation

Ph.D. Thesis

RAJESH KUMAR

2014RPY9043



DEPARTMENT OF PHYSICS

MALAVIYA NATIONAL INSTITUTE OF TECHNOLOGY JAIPUR

April 2019

Functionalized Nano-channels in Polymeric Membranes for Hydrogen Separation

Submitted in

fulfillment of the requirements for the degree of

Doctor of Philosophy

by

RAJESH KUMAR

(2014RPY9043)

Under the Supervision of

Dr. KAMLENDRA AWASTHI



DEPARTMENT OF PHYSICS

MALAVIYA NATIONAL INSTITUTE OF TECHNOLOGY JAIPUR, INDIA

April 2019

Thesis is dedicated to my Family
For their unconditional Love and Motivation.

DECLARATION

I, **Rajesh Kumar**, declare that this thesis titled, ” **Functionalized Nano-channels in Polymeric Membranes for Hydrogen Separation**” and the work presented in it, are my own. I confirm that:

- This work was done wholly or mainly while in candidature for a research degree at this university.
- Where any part of this thesis has previously been submitted for a degree or any other qualification at this university or any other institution, this has been clearly stated.
- Where I have consulted the published work of others, this is always clearly attributed.
- Where I have quoted from the work of others, the source is always given. With the exception of such quotations, this thesis is entirely my own work.
- I have acknowledged all main sources of help.
- Where the thesis is based on work done by myself, jointly with others, I have made clear exactly what was done by others and what I have contributed myself.

Date:

Rajesh Kumar
(2014RPY9043)

CERTIFICATE

This is to certify that the thesis entitled ” **Functionalized Nano-channels in Polymeric Membranes for Hydrogen Separation**” being submitted by **Rajesh Kumar (2014RPY9043)** is a bonafide research work carried out under my supervision and guidance in fulfillment of the requirement for the award of the degree of **Doctor of Philosophy** in the Department of Physics, Malaviya National Institute of Technology, Jaipur, India. The matter embodied in this thesis is original and has not been submitted to any other University or Institute for the award of any other degree.

Place: Jaipur
Date:

Dr. Kamendra Awasthi
Assistant Professor
Dept. of Physics
MNIT Jaipur

ACKNOWLEDGEMENT

First of all, I would like to express my thanks and gratitude to the Almighty, the most beneficent and merciful who granted me health, ability and strength for successful completion of this venture, which helped me to overcome the troubles and difficulties with vigor and vitality. I am highly indebted and hence would like to express my sincere gratitude to my supervisor Dr. Kamendra Awasthi, Assistant Professor, Department of Physics, MNIT Jaipur, who enlightened my way to complete this work.

I would like to thank specially Dr. Kamendra Awasthi, I feel blessed to have the opportunity to work and learn under his guidance. He is a great human being, during my Ph.D. he was like guardian for me. He was always supportive through various discussions. As a mentor, he knew precisely when to give me the freedom to pursue a new avenue of research, when to cheer me up and exactly how to provide motivative and constructive criticism. It is my pleasant opportunity to place my sincere thanks to Dr. Manoj Kumar, Department of Physics, MNIT Jaipur for his help, and valuable discussions during the course of the study. I would like to thank Dr. Anjali Awasthi and Mrs. Sarika Kashyap for endless help and moral support throughout my study.

It is great opportunity to acknowledge Prof. Kanupriya Sachdev, Department of Physics, MNIT Jaipur and other faculty members of the department for allowing me to complete this work. I extend my sincere thanks to DREC members and Head, Department of Physics for their constant help and permitting me to carry out my research activity within or outside the department. Their valuable and critical suggestions were a constant source of encouragement through the entire course of this work. I am also thankful to all office and technical staff for their valuable help and support.

I express my heartiest thanks to my friends and labmates Dr. Yogita Kumari, Dr. Lokesh Kumar Jangir, Dr. Anil Kumar, Dr. Kamakshi, Dr. Sonalika, Rini Singh, Anoop MD, Shivani Shishodia, Prashant Sharma, Pooja Kumari, Sandeep Gupta, Jyoti Yadav, Khushbu Sharma, Nisha Yadav, Sanjay, and Shiv Ratan for their co-operation and making the journey memorable. I would like to thank Dr. Rishi Vyas, Dr. Vikas Sharma, Shushant Kumar Singh, and Himanshu Sharma for always motivating me. I would like to thank Material Research Center MNIT Jaipur for providing access to characterization facilities during my thesis work.

During my research work, I visited IUAC, New Delhi many times for ion irradiation measurements, I would like to thank Dr. Fouran Singh, IUAC, New Delhi for providing me various facilities during my Ph.D work. I would like to thank the team of INUP CeNSE, IISc

Bangalore for providing me the hands on training during my IISc, Bangalore visit. During my Ph.D., I visited various research labs, attended workshops, conferences, symposia and seminars and came in touch with academicians, scientists and researchers. I learnt many things from them. It is impossible for me to list them all. I acknowledge and thank them for the impact they had on my lessons in both science and life. I especially acknowledge the IUAC, New Delhi and CSIR for providing me financial assistance under JRF and SRF scheme, respectively to carry out my research work.

My deepest sense of gratitude goes to my father Mr. Mahaveer Prasad Jangir and my mother Mrs. Chukesh Devi, who were always there during ups and downs, for their unending support, selfless love and affection, never-ending patience and constant encouragement. I would like to express my deep and sincere obligations to my elder brother Gauttam Jangir and sister in law Mrs. Ayushi Jangir, who deserve a special word of thanks, without whom it would have been almost impossible for me to pursue and complete this work successfully. Their immense help and affection inculcated enthusiasm within me to work even in the distressed hours of my thesis. The moral support and encouragement provided by my elder sister Sarita Jangir and my brother in law Mr. Bhaskar Jangir in countless ways will always be appreciated by me. Anushka, Harsh and Lavik, my nephew, arrived with the beginning of my research work. I feel very sorry that I could not spend much time with them, but their single smile helped me to forget all my problems.

Last but not the least, I would like to thank my friends Sohail, Balwant, Bhera Ram, Nakul, Sonika, Ankita, Meenakshi, Pooja, Khusbhu, Mahendra and Rakesh for their support. I would also like to thank my all the teachers, relatives and well-wishers who supported me by prayers and kindness. This thesis is an important milestone of my journey in obtaining my Ph.D. degree. I have not travelled in a vacuum in this journey. This thesis has been kept on track and been through to completion with the support and encouragement of numerous people including my teachers, family, well-wishers, friends, and colleagues. At the end of my thesis, I would like to thank all those people who made this thesis possible and unforgettable experience for me.

Rajesh Kumar

ABSTRACT

As the fossil fuels are depleted rapidly, and the byproducts of fossil fuels are responsible for polluted environment, it becomes a necessity to develop an eco-friendly and renewable energy source. To overcome the problem of air pollution by the fossil fuel and due to energy requirement, our energy dependence on renewable energy sources should be high. Hydrogen has been widely deliberated as an attractive energy carrier with high efficiency for developing an environmental friendly and cost-effective sustainable energy system. However, besides the hydrogen energy, the main issue with other energy sources is energy density and area dependency.

Fuel cell is that unit, which is used to convert hydrogen in the other form of energy. The advantage with the H₂ fuel cell has water, the only byproduct obtained after the energy generation. But the primary requirement for lifetime and efficiency of the fuel cell is the purified H₂ from the impurities or separated H₂ from other gases. So the separation/purification of the H₂ is the solution for a new renewable energy source, prevent the environment from global warming as well as useful for controlling the air pollution.

The primary aim of our research work is to find out the eco-friendly technology through which we can separate/purify hydrogen. There are many types of method or process, which are used to separate/purify the hydrogen gas from the mixture of other gases. Moreover, membrane-based technology for the H₂ separation/purification has attracted considerable response due to inherent benefits over other separation methods. The membrane-based separation process is not only cost-effective but also environmentally friendly as well.

Membrane-based gas separation, suffer from a problem in the form of trade-off relationship between selectivity and permeability. So, the control over selectivity and permeability of the gases is the main goal for the membrane-based gas separation. For the gas separation with the membrane is depends on two parameters; diffusion coefficient (D) and solubility coefficient (S). For gas separation application, we have used different types of porous polymeric membranes and functionalized these membranes to attach the gas sensitive nanoparticles. For the H₂ selective membranes, we have synthesised and deposited palladium nanoparticles in the functionalized porous membranes.

Functionalization is an effective method for different functionalities for the membrane and subsequently desired nanomaterials can be incorporated into the polymer matrix. Initially, Polycarbonate (PC) with functionalized and non-functionalized MWCNTs composite membranes have been prepared. The alignment of the MWCNTs is controlled by high magnetic field. Pd nanoparticles were synthesised chemically and deposited on PC-MWCNTs composite membranes. In the obtained of permeability and selectivity data, significant improvement has been found with the use of functionalized MWCNTs and Pd nanoparticles.

If membranes will be functionalized by a specific functional group then it can improve the selectivity of hydrogen. We have functionalized porous PET membranes having pore diameter $\sim 0.2 \mu\text{m}$ with carboxyl group. The effect of functionalization time on permeability and selectivity of hydrogen over other gases in PET membranes have been observed. Functionalized PET membranes were also used for the H₂ separation application with 6 hours attachment of the Pd nanoparticles. Functionalization the specific group and attachment of Pd nanoparticles enhanced the H₂ permeability as well as selectivity.

Further, to functionalized porous PC membranes, we have used a reliable and low-cost UV irradiation method with the fixed time difference. To enhance hydrogen selectivity, palladium nanoparticles have deposited into the pores as well as on the surface membranes. We have also use binder polyvinylpyrrolidone (PVP), for the palladium nanoparticles to improve the hydrogen selectivity over other gases. Due to the functionalization and maximum attachment of palladium nanoparticles, these membranes have high permeability as well as selectivity of hydrogen. Significant results, easy fabrication process and low cost of these membranes gives an opportunity to use for commercial use.

CONTENTS

DECLARATION	
CERTIFICATE	
ACKNOWLEDGEMENT	
ABSTRACT	i
CONTENTS	iii
LIST OF FIGURES	vii
LIST OF TABLES	x
LIST OF ABBREVIATIONS	xi
Chapter-1	
General Introduction	1
1.1 Gas Separation	1
1.2 Membrane Based Gas Separation	3
1.2.1 Solution-Diffusion	4
1.2.2 Molecular Sieving	4
1.2.3 Knudsen Diffusion	6
1.3 Types of Membrane	6
1.3.1 Composite Membranes	7
1.3.2 Carbon Based Membranes	9
1.3.3 Track-Etched Membranes	10
1.4 Functionalization of Membranes	12
1.5 Outline of the Thesis	13
Chapter-2	
Literature Review	16
2.1 Introduction	16

2.2	Gas Separation	16
2.3	Hydrogen Separation	20
2.4	Gas Separation by Using Carbon-Based Composite Membranes	23
2.5	Gas Separation by Using Track-Etched Membranes	24
2.6	Gas Separation by Using Functionalized Membranes	27
Chapter-3		
	Materials and Methods	30
3.1	Introduction	30
3.2	Materials	30
3.2.1	Polyethylene Terephthalate (PET) Track-Etched Membrane	30
3.2.2	Polycarbonate (PC) Track-Etched Membrane	31
3.2.3	Functionalization of Membranes	32
3.2.4	Functionalization of MWCNTs	33
3.2.5	Synthesis of Palladium Nanoparticles	33
3.3	Characterizations Techniques	34
3.3.1	Scanning Electron Microscopy (SEM)	34
3.3.2	Transmission Electron Microscopy (TEM)	35
3.3.3	Fourier Transform Infra-Red Spectroscopy (FTIR)	36
3.3.4	Raman Spectroscopy	37
3.3.5	UV-Vis Spectroscopy	38
3.3.6	Gas Permeability	39
3.4	Conclusion	40
Chapter-4		
	Functionalized and Aligned MWCNTs in Polycarbonate	41
4.1	Introduction	41
4.2	Experimental Details	42
4.2.1	Sample Preparation	42
4.2.2	Characterization Details	43

4.3	Result and Discussion	44
4.3.1	Transmission Electron Microscopy (TEM)	44
4.3.2	Raman Spectroscopy	45
4.3.3	Fourier-Transform Infrared Spectroscopy (FTIR)	47
4.3.4	Scanning Electron Microscope (SEM)	48
4.3.5	Current-Voltage Measurement (I-V)	49
4.3.6	Permeability and Selectivity Measurements	50
4.4	Conclusions	54

Chapter-5

	Chemical Functionalized PET Membranes	55
5.1	Introduction	55
5.2	Experimental Details	56
5.2.1	Sample Preparation	56
5.2.2	Characterization Details	57
5.3	Results and Discussion	57
5.3.1	Fourier Transform Infrared Spectroscopy (FTIR)	57
5.3.2	Scanning Electron Microscopy (SEM)	60
5.3.3	Permeability and Selectivity	62
5.4	Conclusions	65

Chapter-6

	UV Functionalized PC Membranes	66
6.1	Introduction	66
6.2	Experimental Details	67
6.2.1	Sample Preparation	67
6.2.2	Characterization Details	68
6.3	Results and Discussion	68
6.3.1	UV-Visible Spectroscopy	69
6.3.2	Raman Spectroscopy	70
6.3.3	Fourier Transform Infrared Spectroscopy (FTIR)	72

6.3.4	Scanning Electron Microscopy (SEM)	73
6.3.5	Permeability and Selectivity	74
6.4	Conclusions	77
Chapter-7		
Conclusions and Future Scope of the Work		78
7.1	Conclusions	78
7.2	Future Scope of the Work	80
References		81

LIST OF FIGURES

Figure 1: Schematic representation of the gas permeation models.	3
Figure 2: Typical molecular sieving mechanism for gas-polymer interaction phenomena	5
Figure 3: Generalised classification of the membranes	6
Figure 4: Schematic representation of Mixed Matrix Membrane (MMMs)	7
Figure 5: Swift Heavy Ion (SHI) irradiation and track creation process	11
Figure 6: A schematic representation for track-etched nanochannels with different shapes with the type of chemical etching.	11
Figure 7: Schematic diagram of the work process for the hydrogen separation application.	13
Figure 8: Literature data for H ₂ /N ₂ separation factor versus H ₂ permeability [108].	17
Figure 9: Trade-off relation between separation factor and permeability coefficient for the helium/ methane system at 35°C [111].	18
Figure 10: The concept of hybrid membrane/FT process for biodiesel production from biomass [129].	22
Figure 11: Gas permeance change with temperature for the γ -Fe ₂ O ₃ /PHFMs [139].	23
Figure 12: Schematic for composite membrane generation: (a) PET porous membrane (b) Block copolymer with additive coated on PET (c) Block copolymer coated PET after removal of additive [148].	26
Figure 13: A schematic illustration of tunable, remote-controllable molecular selectivity by a photo-switchable MOF membrane.	28
Figure 14: Basic unit of PET polymer	30
Figure 15: Basic unit of PC polymer	31
Figure 16: Process of Solution cast method for membrane synthesis	31
Figure 17: Synthesis process for the Pd nanoparticles.	33
Figure 18: A schematic diagram of SEM system	34
Figure 19: A schematic diagram of TEM system	35
Figure 20: A schematic diagram for the FTIR technique	36
Figure 21: A schematic diagram for the Raman technique	37
Figure 22: A schematic diagram for the UV-Vis technique	38
Figure 23: A schematic diagram for the gas permeability setup.	40

Figure 24: Schematic diagram of the process (a) Random distribution of MWCNTs in PC membrane (b) Magnetically alignment of non-functionalized MWCNTs in PC membrane (c) Pd deposition in the aligned non-functionalized MWCNTs-PC composite membrane (d) Magnetically alignment	42
Figure 25: TEM image of (a) Pd nanoparticles distribution (b) histogram for average particle size.	44
Figure 26: Energy-dispersive X-ray spectra (EDS) of Pd nanoparticles.	44
Figure 27: Raman spectra of (a) Non-functionalized and functionalized MWCNTs (b) all composite membranes (symbols; N: non, F: functionalized, R: random, A: aligned, Pd: Palladium, PC: Polycarbonate).	45
Figure 28: FTIR spectra of (a) Polycarbonate membrane (b) Non-functionalized MWCNTs.	47
Figure 29: SEM image of (a) MWCNTs distribution in random orientation (b) in aligned orientation (c) aligned MWCNTs with Pd nanoparticles (d) non-functionalized MWCNTs.	49
Figure 30: I-V curve of (a) non-functionalized MWCNTs composite samples (b) functionalized MWCNTs composite samples.	50
Figure 31: Graph of gas permeability for (a) non-functionalized MWCNTs (b) functionalized MWCNTs in both orientation (c) Pd deposited aligned sample.	52
Figure 32: Selectivity data for (a) non-functionalized MWCNTs (b) functionalized MWCNTs in both orientation (c) Pd deposited aligned sample.	53
Figure 33: Schematic diagram of the process (a) Gas permeation through the non-functionalized membrane (b) Gas permeation through the functionalized membrane (c) Gas permeation through the Pd nanoparticles deposited functionalized membrane	55
Figure 34: FTIR spectra of (a) functionalized membranes (b) correspond to carboxylation peak	58
Figure 35: FTIR spectra of (a) functionalized Pd deposited membranes (b) correspond to carboxylation peak.	59
Figure 36: FTIR spectra for comparison of functionalization peak of PET, F24 and F24-Pd6	59
Figure 37: Scanning electron micrograph of 3 hours functionalized PET membrane (a) before Pd deposition (b) after Pd deposition for 6 hours.	60
Figure 38: Scanning electron micrograph of 6 hours functionalized PET membrane (a) before Pd deposition (b) after Pd deposition for 6 hours.	61

Figure 39: Scanning electron micrograph of 12 hours functionalized PET membrane (a) before Pd deposition (b) after Pd deposition for 6 hours.	61
Figure 40: Scanning electron micrograph of 24 hours functionalized PET membrane (a) before Pd deposition (b) after Pd deposition for 6 hours.	61
Figure 41: Graph of gas permeability for all functionalized samples.	63
Figure 42: Selectivity data for functionalized samples	63
Figure 43: Graph of gas permeability for all functionalized Pd deposited samples	64
Figure 44: Selectivity data for all functionalized Pd deposited samples	64
Figure 45: Schematic diagram of process Gas permeation through (a) Pristine PC membrane (b) UV irradiated PC membrane and (c) Pd Nanoparticles deposited in UV irradiated PC membrane.	66
Figure 46: A schematic representation of the photo-degradation process	68
Figure 47: UV-Vis spectra for the sample S0, S1 and S4 in the range of 300-700 nm, those are resembled to the pristine PC, UV irradiated PC for 36 hours and UV irradiated PC for 48 hours respectively	70
Figure 48: Raman spectra of all the samples (S0-S6) in the range of 500-200 cm^{-1} .	71
Figure 49: Raman spectra of all the samples (S0-S6) in the range of 2750-3150 cm^{-1} .	72
Figure 50: FTIR spectra of the all the samples (S0-S6) in the range of 400 cm^{-1} - 3100 cm^{-1} .	72
Figure 51: Scanning electron microscope (SEM) of the sample (a) Pristine PC (S0) (b) UV irradiated for 48 hours (S4) (c) UV irradiated for 48 hours with deposition of Pd Nanoparticles for 24 hours (S5) (d) UV irradiated for 48 hours with deposition of Pd nanoparticles	73
Figure 52: Energy Dispersive Spectroscopy (EDS) spectra of the Sample S2 for the confirmation of palladium (Pd) NP's.	74
Figure 53: Graph of the gas permeability data for the samples (S0 - S3). S0 is for the without UV irradiation pristine PC and S1-S3 samples having the UV irradiation time of 36 hours.	75
Figure 54: Graph of the gas permeability data for the samples (S0, S4 – S6). S0 is for the without UV irradiation pristine PC and S4-S6 samples having the UV irradiation time of 48 hours.	75
Figure 55: Graph of selectivity data of H ₂ over CO ₂ and N ₂ for all the samples (S0-S6).	76

LIST OF TABLES

Table 1: Gases with their kinetic diameter, molecular weight specific gravity and volume.	5
Table 2: Reframed table for permeation rate, permeability, overall resistance and permeation rate ratio data for the all the mentioned gases from the publication of A. T. Mohammadi et al. [112].	19
Table 3: Sample representation according to Type of MWCNTs, orientation and Pd deposition time	43
Table 4: Raman peaks and corresponding bond for all the composite samples.	46
Table 5: Permeability data for composite membrane.	51
Table 6: Selectivity data for composite membrane.	54
Table 7: Sample representation based on the carboxylation and Pd nanoparticles deposition time (c; carboxylated, C-Pd; carboxylated membranes with Pd nanoparticles, numbers represents hours).	56
Table 8: FTIR peaks and corresponding bond.	60
Table 9: Permeability data for all functionalized and Pd deposited PET samples.	62
Table 10: Selectivity data for all functionalized and Pd deposited PET samples	62
Table 11: Sample representation based on the UV irradiation time and Pd nanoparticles deposition time.	67
Table 12: Raman peaks and corresponding bonds.	71

LIST OF ABBREVIATIONS

AFM	Atomic force microscopy
CA	Cellulose acetates
CO₂	Carbon Dioxide
CO	Carbon monoxide
CH₄	Methane
DI	Deionized (DI) water
FESEM	Field Emission scanning electron microscopy
FTIR	Fourier transform infrared spectroscopy
He	Helium
H₂	Hydrogen
I-V	Current-Voltage
MMMs	Mixed matrix membranes
MWCNTs	multi wall carbon nanotubes
N₂	Nitrogen
PC	Polycarbonate
Pd	Palladium
PDMS	Polydimethylsiloxane
PET	Polyethylene terephthalate
PEG	Polyethylene glycol
PES	Polyethersulphone
PSA	Pressure Swing Adsorption
PP	Polypropylene
Pd	Palladium
PMMA	Polymethyl methacrylate
PSU	Polysulfone
PI	Polyimide
PVF	Polyvinylidene fluoride
PVP	Polyvinylpyrrolidone
RMS	Root mean square
TEM	Transmission electron microscopy
THF	Tetrahydrofuran
UV-Vis	Ultraviolet-visible

General Introduction

1.1 Gas Separation

At present situation of the world, main requirement of the human life is to develop an eco-friendly and renewable energy source. The current energy disaster urges us to explore a variety of alternate methods to fulfil the world's energy demands. To satisfy the energy requirement of the world, fossil fuels are not only sufficient but also very harmful and dangerous for the life. In current global energy consumption, it is predicted that it will be double by 2050 [1]. All the fossil fuels are very limited, and the use of these fuels produce injurious byproducts such as carbon dioxide, carbon monoxide, chlorofluorocarbon and many more. These byproducts affect the human's life as well as the degrading environment. So, overall air pollution and energy requirement are two main issue in the present scenario.

To overcome the problems of air pollution by the fossil fuel and energy requirement, our energy dependence on renewable energy sources should be high. Because the availability of renewable energy sources is unlimited and main advantage is no harmful byproduct [2]. However, beside the hydrogen energy, the main issue with these energy sources is energy density and area dependency. In case of solar energy, per area density of energy is low also not possible in the cold states. Similarly ocean energy is possible only area near to the ocean, which is not applicable in the dry states etc. [3]. But the acceptance in the form of hydrogen energy is high because of the hydrogen (H_2) obtainability. H_2 has been widely deliberated as an attractive energy carrier with high efficiency for developing an environmental friendly and cost-effective sustainable energy system. H_2 has been accepted as a clean and effective energy carrier to alleviate the mounting worldwide energy and environmental crisis, directing towards developing efficient H_2 separation technologies.

The unit which is used to convert hydrogen in the other form of energy is called the hydrogen fuel cell [4–6]. But the primary requirement of the fuel cell is the purified H_2 from the impurities or separated H_2 from other gases [7]. Otherwise, the lifetime and the efficiency of the fuel cell decreases drastically. So, the purity of the H_2 is a leading parameter to decide the effectiveness of the fuel cell system. The most important

advantage with the hydrogen fuel cell is having water as the only byproduct obtained after the energy generation. Produced water can be used in other useful applications. That's way the main advantage of using H₂ as an energy source is a "green fuel source" which does not damage the ecological system. Hydrogen energy is not only the clean energy source but also the offshoot in the form of pure water. So the separation/purification of the H₂ is the solution for a new renewable energy source as well as useful for controlling the air pollution. So to utilise hydrogen as an energy source and prevent the environment from global warming, it is required to purify H₂ gas from the other gases and impurities.

In order to resolve these problems of separation, it might be helpful to combine the separation process with membrane technology [8]. There are many types of method or process, which are used to separate/purify the hydrogen gas. Some of them are membrane technology, pressure swing adsorption, chemical absorption, catalytic purification, metal hydride separation, and cryogenic separation etc. Membrane-based technology for the H₂ separation/purification has attracted considerable response due to inherent benefits over other separation methods [9–11]. The membrane-based separation process is not only cost-effective but also environmentally friendly as well [12,13]. Except for membrane technology, all other mentioned methods are not so popular and also not cost effective. Some of the advantages of the membrane-based gas separation are mentioned below:

- Mechanical strength and durability
- Controlled pore shape and size
- Chemical stability
- Thermal stability
- Manufacturing reproducibility
- Space saving
- Low weight
- Flexibility
- Low energy consumption
- Easy to manufacture
- Easy to clean
- High potential of adaptability
- Low capital cost over other conventional separation methods.

Despite several advantages of the membrane based gas separation, this process suffer from a problem in the form of trade-off relationship between selectivity and permeability. So the control over selectivity and permeability of the gases is main goal for the membrane based gas separation.

1.2 Membrane Based Gas Separation

In the membrane-based separation process, gas molecules separate by the difference in permeation rate of gas molecules. Adolph Fick gives the fundamental law's called "Fick's law" and it explain the basic mechanism of the gas diffusion or permeation through the membrane [14]. For the gas separation/permeation with the membrane is measured by the two key parameters 1) diffusion coefficient (D) and 2) solubility coefficient (S) [15,16]. Basically based on the membrane structure (pores & non-pores)/morphology gas permeation can be explained in three models. Schematic representation of these models is shown in the figure 1.

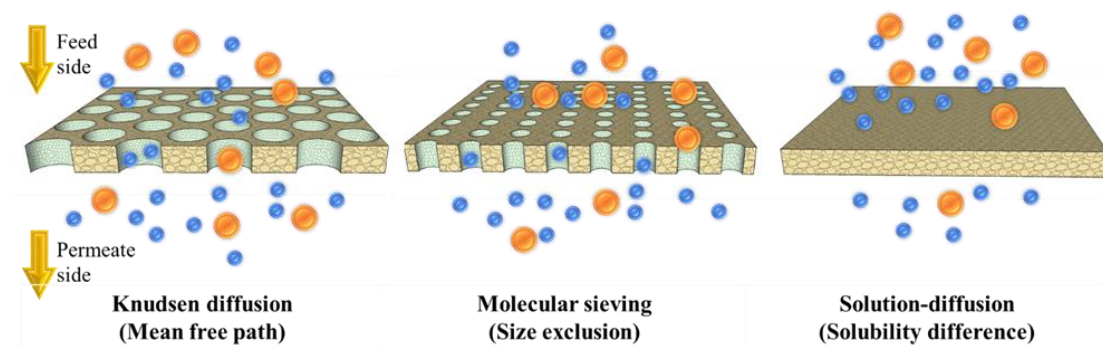


Figure 1: Schematic representation of the gas permeation models.

As according to equation 1, Knudsen number (K_n), which is the fraction of the gas molecule mean free path to the pore size of the membrane, is normally used to distinguish among the three mechanisms.

$$K_n = \frac{\lambda}{d_p} \quad (1)$$

In the equation, d_p is the diameter of the pore, and the λ is the mean free path of the gas molecules. Mean free path of the gas is depends on the pressure (p), temperature (T) and the effective diameter of the as molecule (d_g) as according to the given equation

$$\lambda = \frac{K_B T}{\sqrt{2} p \pi d_g^2} \quad (2)$$

Where K_B is the Boltzmann constant.

Based on the porosity of the membrane there is three basic permeation process: Knudsen diffusion, molecular sieving, and solution-diffusion.

1.2.1 Solution-Diffusion

The gas permeation in the case of the dense membrane can be explained by the solution-diffusion model. The solution-diffusion model has been described widely in many articles [17–19] and books [20,21] as well. In this model, gas permeation is cross product of the solubility coefficient (S) and diffusion coefficient (D). The overall equation can be shown as;

$$P = D \times S \quad (3)$$

Both the coefficient D and S depends on the membrane material and the type of gas chosen for permeation. Every material has a different value of diffusion coefficient and solubility coefficient according to the gas type. Also, both the coefficient changes with temperature, as the temperature changes the polymer structure and mobility of gas molecules. As mentioned above temperature depends on P, D and S can be represented by the Arrhenius type equation.

$$P = P_0 \exp\left(\frac{-E_p}{RT}\right) \quad (4)$$

$$S = S_0 \exp\left(\frac{-\Delta H_s}{RT}\right) \quad (5)$$

$$D = D_0 \exp\left(\frac{-E_d}{RT}\right) \quad (6)$$

Where P_0 , S_0 and D_0 represented as pre-exponential value for the corresponding equation. R is used for universal gas constant and T for the temperature. E_d , ΔH_s and E_p are the activation energy for diffusion, heat of solution/sorption and activation energy for permeation respectively.

1.2.2 Molecular Sieving

In terms of gas separation, molecular sieve membranes have been recognized as a very promising applicant for gas separation [22,23]. These molecular sieves are porous solids that contain constrictions of apertures that approach molecular dimensions of diffusing gas molecules. A typical schematic diagram of molecular sieving mechanism for gas-polymer interaction phenomena is shown in the figure 2.

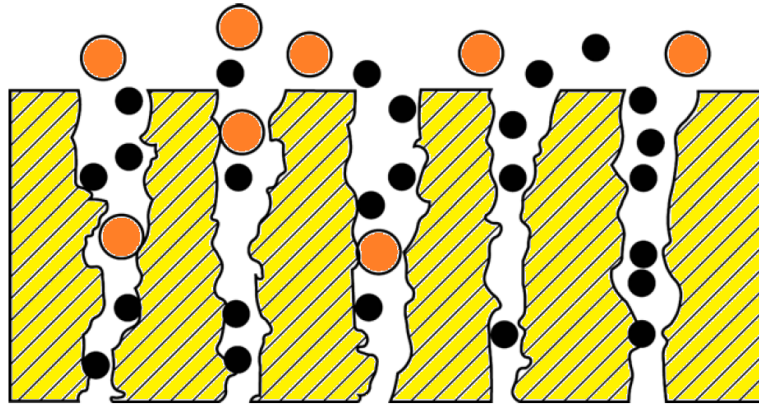


Figure 2: Typical molecular sieving mechanism for gas-polymer interaction phenomena

When pore diameter or opening of membrane is relatively small to the gas molecule, then repulsive force dominates. In this case, higher activation energy is required for the permeation [24]. In the same situation, when gas molecule has suggestively small diameter compared to opening or pore diameter, then it requires small amount of energy for the permeation. Molecular sieving is dominating mechanism for the above mentioned conditions [25].

Overall, pore diameter and gas molecule size are key element to control the separation performance such type of membranes. The molecular diameter of the gases and other important properties are listed in the table 1 [26].

Gas	State	Kinetic diameter (Å)	Molecular weight	Specific gravity at 70°F (1 atm)	Specific volume (cf/lb)
H ₂	Compressed Gas	2.89	2.02	0.0696	192
N ₂	Compressed Gas	3.64	28.01	0.967	13.8
He	Compressed Gas	2.6	4.003	0.138	96.7
O ₂	Compressed Gas	3.46	32.0	1.105	12.1
CO ₂	Liquefied Gas	3.3	44.01	1.52	8.74
C ₃ H ₆	Liquefied Gas	4.4	42.08	1.501	9.05
C ₃ H ₈	Liquefied Gas	3.96	44.1	1.55	8.5
CH ₄	Compressed Gas	3.8	16.04	0.555	23.7
CO	Compressed Gas	3.76	28.01	0.97	13.8
Ar	Compressed Gas	3.4	39.95	1.38	9.7

Table 1: Gases with their kinetic diameter, molecular weight specific gravity and volume.

1.2.3 Knudsen Diffusion

When mean free path of the gas molecules is in the order of the pore diameter than the dominating mechanism for the gas permeation is Knudsen diffusion [27]. Because the walls of the pore involve in the mechanism, so the walls of the membrane also effects the gas permeability. The general equation for the Knudsen diffusion for the gas is given by equation 7.

$$J_{iK} = -D_{iK} \frac{\partial c_i}{\partial x} \quad (7)$$

where, D_{iK} is representation for the Knudsen diffusivity. D_{iK} can be calculated by equation 8. In this mechanism, the molecules collision with pore walls are more repeated than the collision among molecules. Also, the selectivity of gases is inversely proportional to square root of the molecular weights.

$$D_{iK} = \frac{d_p}{3} \sqrt{\frac{8RT}{\pi M_i}} \quad (8)$$

where, M_i showing the molecular weights for gas species i , and d_p is the average pore size of porous membrane. Generally, Knudsen diffusion is useful for the low pressure, because due to the bigger pore diameter the permeation rate in such membrane is high at low pressure. This mechanism is ruled in the zeolites membranes [28], CNT-polymer composite membranes [29], swift heavy ion irradiated membranes, fiber membranes and the membranes have porous structure across the thickness etc.

1.3 Types of Membrane

Commercially, various types of membranes are used for application on hydrogen separation like metal membranes, track-etched membranes, polymer membranes, ceramic membranes, etc. [30,31].

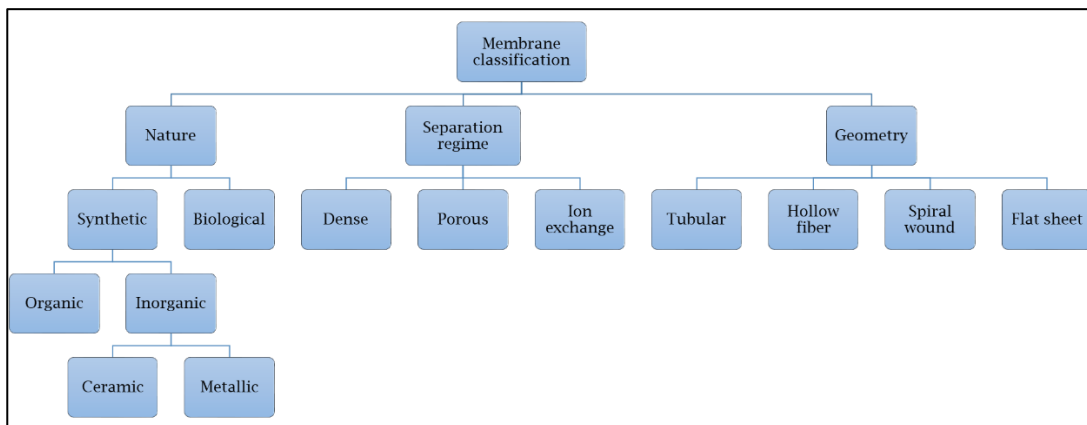


Figure 3: Generalised classification of the membranes

Because the membrane material is most critical portion for the selectivity and permeability of the gas, so the selection of the membrane material is very important for the required application. Based on the properties and approach, the membrane can be classified in many categories. M De Falco *et al.* [32] has reported the generalised classification of the membrane as shown in the figure 3.

In the field of gas separation, most of the samples are in the form of mixed matrix membranes (MMMs) [33,34], as shown in the figure 4. In these MMMs materials, 2 phase are present, one is the polymer matrix which acts as a bulk phase and another one the filler material like zeolite, carbon nanotubes, different form of metal (nanoparticles, nanorod, nonoflakes, etc.) [35]. MMMs is one of the advantageous form of the samples to overcome this problem relatively to pristine polymer or pure filler material. At the same time, the cost of the MMMs is low compared to the pure material, at the same time MMMs have high flexibility.

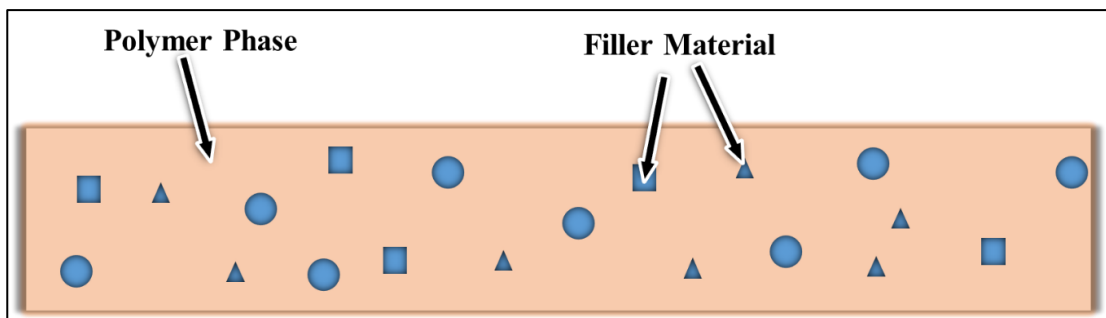


Figure 4: Schematic representation of Mixed Matrix Membrane (MMMs)

For the hydrogen gas separation, following membranes are being used by various researchers:

1.3.1 Composite Membranes

The amazing properties of nanomaterials result in a new class of composite material, which helps to improve the separation properties [36,37]. In the composite membranes, it covers metallic alloys [38,39], organic polymers and inorganic oxides [40,41]. Here we will critically compare the diverse composite membrane materials, which are using for the H₂ separation/purification in the composite form. The simplest way for the classification of the composite membrane is to categorise them based on the filler material. It can be as follow; pure metals [16], alloys [42], oxides, ceramics [43,44], zeolites [45], glasses and carbon products (CNT, graphene, graphene

oxide, graphite) etc. carbon-based composite membranes have broad area and different approach. So carbon-based membranes will be explained in the next section.

During the selection of composite membranes, some of the targeted key points are like H₂ selectivity, and the permeability should be high. Composite materials cost should be low. In the commercial point of view, the durability of the sample should be long time. The last production/fabrication process cost is not to be expansive. In broad sense, a composite membrane effects only H₂ molecules for the selectivity. That means only H₂ molecules or other gas molecules (impurities) interact with the composite membrane.

Typically metallic composite membranes are dense membranes, in which a specific metal is used as a filler material. The selectivity of such membranes is high, but the permeability is low. Metal can be used in the different form of structures such as; nanoparticles, nanorods, nano-tubes, nano-frames, ribbons etc. the most suitable and reliable metal for H₂ is Palladium (Pd). Because Pd has high diffusivities or solubility for the hydrogen, and have excellent thermal stability [46,47]. Platinum (Pt) is one more metal which is used as a spare filler material for palladium [16,48]. Both Pt and Pd also used with Ni, Ag, Au and Cu as alloy metals in composite membranes. The performance, fundamental concept and mechanism for the metallic membranes have been explained in the various researcher [47,49,50].

Due to some of the limitation with the metallic membranes, silica composite membranes are an alternative approach for H₂ separation application. Compare to metallic membranes, silica membranes are easy to fabricate, controllable filler porosity and low cost of production. Silica has pores network matrix in which the approximate diameter of the pore is 0.5 nm. Such small pores can control permeation of the small gas molecules such as H₂, CO₂, He, CO, O₂, and N₂. Such type of composite membranes are not 100% selective for an individual component [51,52]. The separation of gas mixtures is centred on a competitive process of different molecules move in the micropores network [53]. Commonly two type of synthesis methods are used for silica-based composite membranes; chemical vapor deposition (CVD) and sol-gel method [54]. In comparison of both methods, sol-gel provides good permeability as well as selectivity. While the problem with the sol-gel method is reproducibility of the samples and which can be the achieved by CVD method by the controlled condition of deposition.

From last few years, zeolite membranes have achieved considerable attention in the field of gas separation [55,56]. Zeolite membranes have controlled pore shape and

size with the enhanced properties of mechanical, thermal and chemical stability. Such type of membranes have long lifetime and can be used multiple times. The optimised thickness of the zeolite membranes is the key parameters for the selectivity and permeability data. Zeolites have a uniform and molecular-sized pores with crystalline inorganic nature. Most of the zeolites are made with the TO_2 unit, where T represents a tetrahedral framework atom (Si, Al, B, Ge, etc.) [57].

Due to the long life time, stability at high temperature and the ability of the regeneration makes these membranes as a competitive candidate for H_2 separation/purification application.

1.3.2 Carbon Based Membranes

In the comparison with other materials, the composite material of carbon with polymer have been centre of demand due to their unique properties and technological usage, especially for gas separation application [58–60]. Carbon-based polymer composites such as carbon nanotubes (CNT's), graphite, graphene, graphene oxide (GO) have been reported widely.

Since the discovery by Iijima [61,62] of carbon nanotubes (CNTs) has been made supreme impacts on nanotechnology and nanoscience. Especially application part of the composite in the reference of electrical, thermal and mechanical properties [63,64]. Mostly CNT's are categorised in the single wall carbon nanotubes (SWCNT's), double wall carbon nanotubes (DWCNT's) and multiwall carbon nanotubes (MWCNTs). The arc discharge is one of the oldest and worthy technique to produce the CNT's. As according to physical and chemical properties of CNT's, these have a potential application in the gas separation. There is large variation in the ratio of length and diameter of the CNT's. Many types of CNT's composites are used for gas separation applications. Structure and orientation of CNT's key parameters for the conductivity as well as the permeability & selectivity of the gases. In the field of the hydrogen separation, many researchers used the aligned orientation of CNT's to improve the selectivity of gases [65,66]. It is expected that alignment of CNT's in polymer matrix provides more number of the channels and dissolution opportunity in comparison to randomly distributed MWCNTs. Also, the separation application is based on the functionalization of the CNT's [67,68]. Functionalization of the CNT's is useful for the attachment of gas sensitive nanomaterials which helps to enhance the selectivity of a specific gas. Based

on the diameter of the CNT in the composite membrane permeation of the gases can be combined effect of solution diffusion and molecular sieving model. These features make CNT's highly useful in reinforcement nano filter, probes, energy storage, gas filters, bio applications and various electronic and thermal devices.

Graphene also has a great opportunity for membrane-based gas separation applications because of critical thickness, chemical stability, flexibility, and mechanical strength. Molecular Dynamic (MD) simulation and Density Functional Theory (DFT) calculation shows that the graphene-based membranes are one of good choice for the H₂ separation application [69,70]. H₂ have a significant difference in its kinetic diameter (2.9 Å for H₂) compared with other gases molecules (3.64 Å for N₂, 3.8 Å for CH₄ and 3.76 Å for CO etc.) [71]. DFT calculation explained that the pore size in graphene is nearly the molecular diameter of the H₂. So there are much possibility that H₂ molecule will separate from other gas molecules by a candidate having nearly equal pore size and other gas molecules will block due to bigger kinetic diameter than H₂. The approach with graphene polymer composite membrane can enhance the H₂ selectivity over other gases multiple times. However, the drawback is that due to smaller pore size the permeability decreases.

Functionalized graphene (graphene oxide) [72] can be used with polymer matrix to reduce the lower permeability problem. GO can also utilise as a unique material for gas separation application. Functionalization of the graphene can enhance the H₂ attachment probabilities. Separation mechanism for the GO composite membranes follows the molecular sieving as explained in the previous part. Nanoparticles, nanowires and other nanostructures can interact with the GO lays and helpful to expand the gaps [73–75]. This explanation offers fast permeation of the gas molecules through the channels. Such approach is useful for the high permeability with high selectivity of H₂.

1.3.3 Track-Etched Membranes

Now these days, track-etched membranes are new class of the gas separation/purification applications. Track-etched polymeric membranes have received considerable attention in gas separation applications due to tunable pore shape and size due to chemical etching and choice of the ion [76–79]. Swift Heavy Ion (SHI) irradiation process is used to create the tracks, and subsequently, the tracks are converted into

nanopores by selective chemical etching. Basically the ions beam having the heavy energy in the range of 100 MeV were bombarded on the membranes.

Due to heavy energy these ion passed throughout the membrane, and local damaged zones (latent tracks) were created along the ion path. In details, the passing ion interacts with the loosely bound electrons of the polymer and transfer its energy to them. Such electrons of the polymer gradually transfer this energy in the outward direction of the ion path. Due to this phenomena, a cylindrical zone is created, which called as the latent tracks.

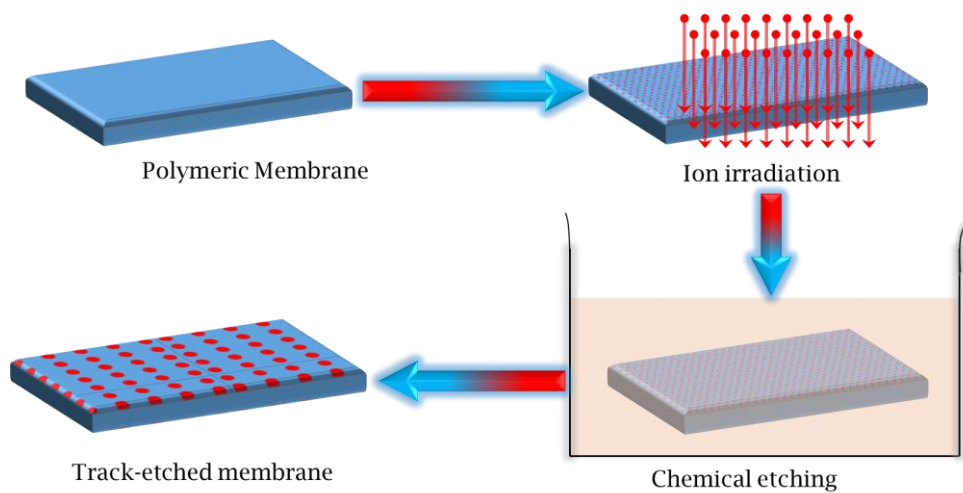


Figure 5: Swift Heavy Ion (SHI) irradiation and track creation process

These tracks can be converted into the pores by the chemical etching. The schematic representation of the followed process is shown in the figure 5.

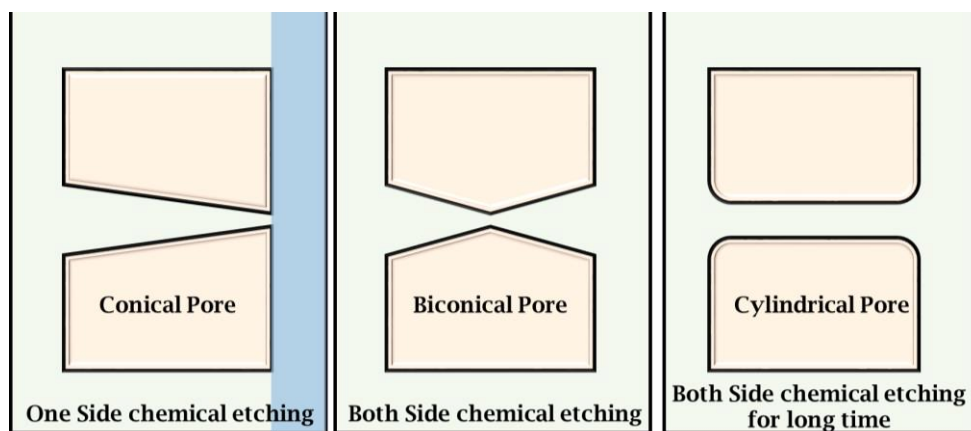


Figure 6: A schematic representation for track-etched nanochannels with different shapes with the type of chemical etching.

Type of the ion and his energy affect the damaged area of the membrane matrix, which is one the responsible factor for the pore size. But the chemical etching process is responsible for the pore shape and size [80]. To control the control the pore size chemical etching time need to be optimised and the shape of the pore depends on the one or both side etching. One side chemical etching generates the conical shape of the pore. Both side chemical etching leads for the double conical/bi-conical shape, and later it's converted into the cylindrical shape as shown in the figure 6.

The main advantage of such membranes is that we can control pore shape, size, length and the distribution. So, based on the application, we can obtain the required pores. The most natural example of such track etched nanochannels is living human skin. Human skin can selectivity permeate water and ions in the form of sweat, not the blood cell.

Separation and selectivity of the gases also depend on the interaction of the gas within the pore wall and the surface of the membranes. These track-etched membranes are able to modify them after or before the irradiation process. These modified membrane have more benefit then the pristine form of these membranes.

1.4 Functionalization of Membranes

Functionalization of the membrane is that process, in which we have modified a specific physical property of the membrane [81,82]. Modification of the membrane is done according to our required application [83,84]. In the field of the gas separation, gas permeation capabilities of the membranes depend on the type of functionalization. Such as with the functionalization if the gas sensing material is attached to the surface or the pore wall on the membrane. Then it favours to enhance the gas selectivity. Similarly, if the functionalized of the membrane controls the porosity of the membrane then it will be in the support of permeability improvement of the gases.

In the context of the membrane functionalization, different methods and approaches have been developed to manipulate the membrane properties. Membrane functionalization is possible via targeted chemical reaction [85,86], UV irradiation [87,88], plasma process [89], alteration in the synthesis/fabrication process and many more. Selection of the functionalization process depends on the sample material and application.

The most common process for the functionalization is the targeted chemical method. In this method, a chemical reaction proposed after the sample synthesis to generate or enhance a specific number of the functional group [90]. Such as carboxylic group is generated with chemical reaction on the PET membranes for improvement of attachment capabilities of gas sensitive nanomaterial with the surface of the membrane. The UV-irradiation process is also low cost and effective method for the functionalization of the membranes. In this method, UV-lamp is used in the process having specific wavelength. The specified wavelength has sufficient energy that it can break polymeric bonds (bond splitting). Due to the unsaturated state of these break bonds, they always ready to accept or attach with gas sensitive materials. But the difficulty with this method is only applicable on the some specific polymer. And also the process time is long as compared to the targeted chemical reaction method.

Use of track-etched membranes instead of the dense membranes will provide the opportunity for the much larger area of the membrane for functionalization. In the track-etched membranes not only the surface but also we are getting the pore walls area of the membrane. Higher functionalization adds the extra control on the permeability and selectivity of the membranes. In present study, we are using the track-etched PET and PC membranes for the higher functionalization.

1.5 Outline of the Thesis

The directed problem with gas separation application is to achieve remarkable change in selectivity when we were getting high permeability and vice versa.

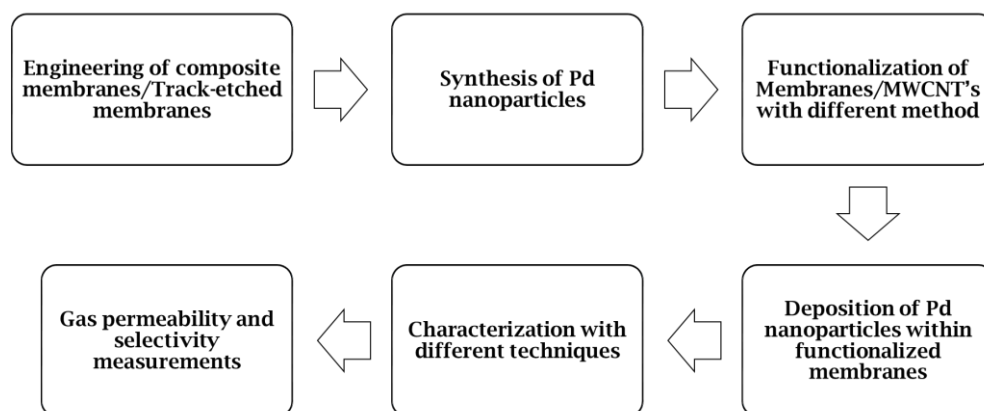


Figure 7: Schematic diagram of the work process for the hydrogen separation application.

Therefore, the aim and motivation of this study to enhance the hydrogen permeability and selectivity of the hydrogen over other gases with the help of the functionalized nano-channels of polymeric membranes. For controlled separation of gases, high selectivity along with the high permeability is needed. To achieve high selectivity with high permeability, optimization of various parameters of functionalized membranes such as nature of nanomaterials, deposition time etc. The overall methodology of the work is represented in the figure 7.

To improve the selectivity as well as permeability of hydrogen, the objectives of proposed plan are given below:

- Preparation of different polymeric membranes
- Ion irradiation of polymeric membranes to create the tracks.
- Chemical etching of ion irradiated membranes
- Functionalization of porous membranes
- Synthesis of nanomaterials
- Deposition of nanomaterials into the functionalized membranes
- Characterization of samples by SEM, AFM, FTIR, TEM, Raman spectroscopy and XRD.
- Gas permeability and selectivity measurements

To follow the proposed plan, initially Polycarbonate (PC) and functionalized and non-functionalized MWCNTs composite membranes have been prepared by solution cast method. Track-etched polymeric membranes of PC and PET were prepared by ion irradiated and having different pore size.

For functionalized MWCNTs and PET membranes with carboxylic group, we follow targeted chemical method. Beside chemical method, to functionalized track-etched PC membranes, we have also used the UV irradiation method. To optimise the functionalization time, different samples were UV-irradiated from 0 to 48 hours.

For the H₂, Pd is most common and the perfect gas sensitive materials to enhance permeability as well as selectivity. So we have synthesised Pd nanoparticles by using the chemical method. As compared to pristine samples, functionalized samples always shows more attachment of Pd nanoparticles.

UV-Vis, FTIR and Raman spectroscopy were used for the confirmation of the functionalization of the membranes. SEM technique is used for the morphological studies

and observation. The characterization of the nanoparticles is done by TEM technique. Deposition of Pd nanoparticles can be confirmed by the by the EDX and the SEM images.

All the gas permeability measurements were done with the help self-developed gas permeability setup [91,92]. Details of the setup has been explained in the section 3.3.6. For the gas permeability application, we have used hydrogen (H₂), nitrogen (N₂) and carbon dioxide (CO₂) gases.

Literature Review

2.1 Introduction

From last few decades, the membranes based technology have noteworthy advantage from wastewater treatment for water purification to the high efficiency of the solar cell [93–96]. In considering the future energy requirement membrane equipment and technology can be a good option because of its eco-friendly nature, low cost, economical processing capabilities and modification acceptability. As per current fossil fuel consumption rate direct us for clean, eco-friendly and sustainable fuel [97–100]. Hydrogen is one of the respectable fuel for coming time and hydrogen fuel cell will the unit, which converts hydrogen in another form of energy. Compare to other conventional vehicles hydrogen fuel cell vehicles are more profitable also there not any toxic gas explosion [101–103]. In the essential stuffs for fuel cell is pure hydrogen for the better efficiency and lifetime. Many methodologies has been followed by the researcher for the improvement of selectivity of hydrogen over other gases and impurities. But separation/purification by selective transport with the help of polymeric membranes is one of the fastest growing branch. In the reference of original polymeric membrane, composite membrane always beneficial in the goal of selectivity and permeability alteration. Because in the composite membranes many parameters can be tune like concentration, size, shape, distribution of filler material etc.

2.2 Gas Separation

In the membrane-based separation process, gas molecules separate by the difference in permeation rate of gas molecules. For the gas separation/permeation with the membrane is measured by the two key parameters 1) diffusion coefficient (D) and 2) solubility coefficient (S). Thomas Graham in the Application of membrane technology [104] gives the detail of the gas permeation phenomena polymeric membrane. Graham provides the systematic study about the permeation rate of all gases by obtainable diaphragm option. Graham defines the solution-diffusion model for gas permeation. In the 1943-45 first commercial use done to separate $U^{235}F_6$ from $U^{238}F_6$ with the help of microporous metal membrane. In the duration 1940-50, some of the researcher like

Amerongen [105], Barrer [106], Stern [107] directed the groundwork of the gas permeation theories. But that time the membrane fabrication techniques are limited, so only pristine polymeric membranes used for the gas permeability. In 1991 M. Robeson *et al.* [108] presented the relative upper limit performance of the different polymer for the gas combination of O₂/N₂, H₂/CH₄, CO/H₂, H₂/N₂, He/CH₄, He/N₂, He/H₂, He/O₂, H₂/O₂. Figure 8 shows the separation factor of H₂ over N₂ including the upper limit boundary.

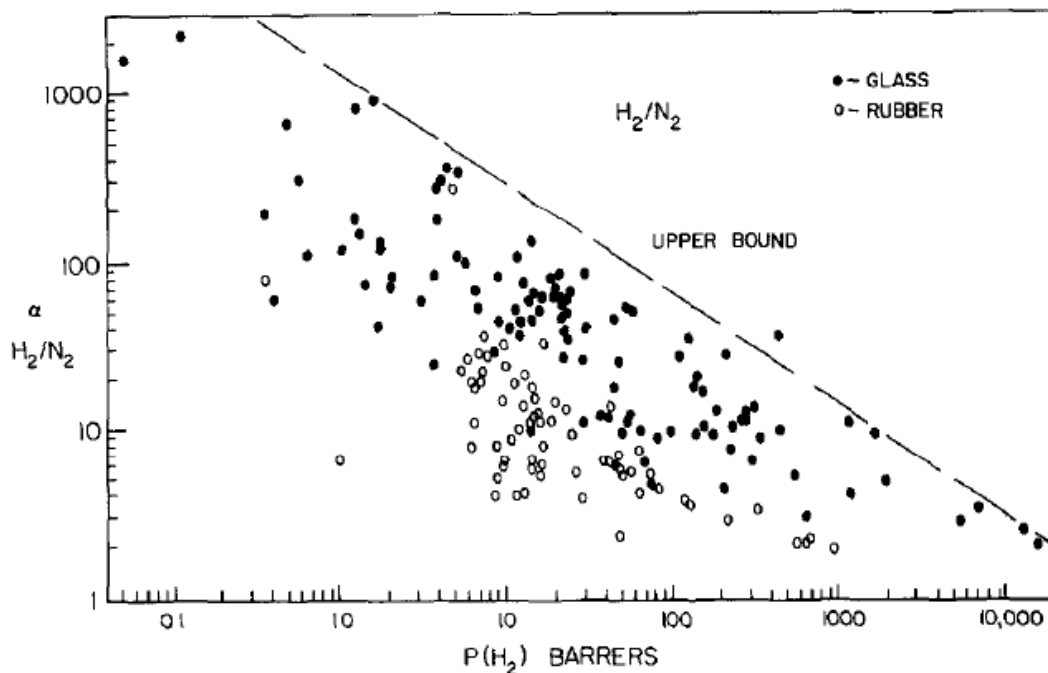


Figure 8: Literature data for H₂/N₂ separation factor versus H₂ permeability [108].

But there are some limitations with pristine polymers such as mechanical strength, interaction phenomena with gases, chemical stability etc. to overcome these problems/limitation, most of polymers and inorganic composites are used for improvement of desired properties. In these composite membranes, two phase are present, one is the polymer matrix which acts as a bulk phase and another one the filler material like zeolite, carbon nanotubes, different form of metal (nanoparticles, nanorod, nonoflakes, etc.).

The study about the Mix Matrix membranes (MMMs) for the gas separation have been explained nearly 1970 by D Paul *et al.* [109]. D. Paul *et al.* introduced delayed diffusion time lag concept for CH₄ and CO₂ gas. For this work, authors use zeolite into the polymer matrix and found that there are very large increases in the diffusion time lag.

In one of the US patent [110] in 1992, silicalite powder and cellulose acetate MMMs are used for the gas separation application. In this patent, 150 psi pressure difference was used for various gas and the selectivity factor (α_{O_2/N_2}) was found nearly 3.4-4.0 and (α_{CO_2/H_2}) 5.3 – 9.0. In 1989 T.A. Barbari *et al.* [111] used five bisphenol based polymer (Polycarbonate, Polysulfone, Polyarylate, Polyetherimide and Polyhydroxyether) to examine the effect of the attached group with bisphenol on the gas separation properties. 50:50 CO₂ and CH₄ combination were used to check the gas permeability coefficient for all the polymeric membranes. Based on the study for all polymers, it's observed that polyetherimide is suitable candidate for He/CH₄ or H₂/CH₄ and polycarbonate or polysulfone for CO₂/CH₄ combination. As figure 9 from the same article shows that there is always inversely-proportional relation between permeability and separation factor (selectivity).

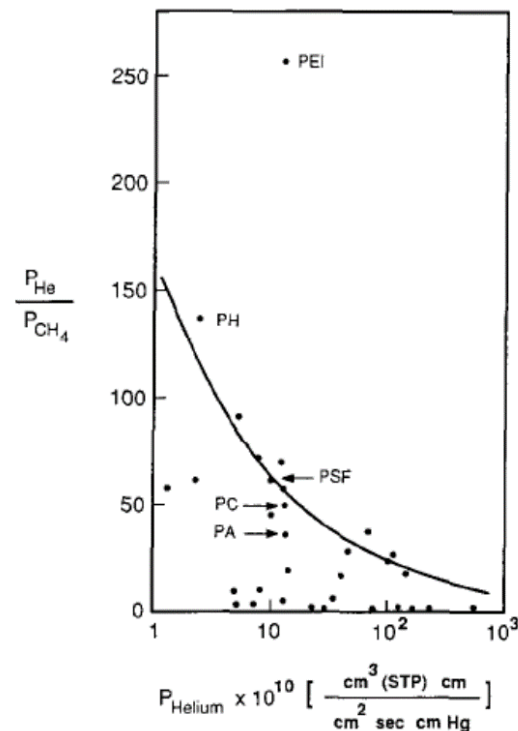


Figure 9: Trade-off relation between separation factor and permeability coefficient for the helium/ methane system at 35°C [111].

In 1995 A. T. Mohammadi *et al.* [112] used, a coating layer of silicone over the surface of polyimide membrane and use for the separation factor of different gases. In this study, they found that the permeation rate of H₂, He and CO₂ is not affected, but the permeation rate of N₂ and CH₄ is changed. This layer structure of silicon and Polyimide enhanced the selectivity of CO₂/CH₄ from 64 to 166, as the silicon layer covers the large

pores (due to the phase-inversion process) of the Polyimide membrane. As a results, permeation decreases and separation factor increases. In the same publication authors have summarised data of permeation rate, permeability, overall resistance and permeation rate ratio in tabular form as shown in the table 2.

Pressure (gauge) (kPa)	He	H ₂	CO ₂	O ₂	N ₂	CH ₄
Q, permeation rate (mol s⁻¹ x 10⁷)						
700	6.70	1.65	0.67	0.14	< 0.037	< 0.037
1400	17.4	4.46	1.38	0.30	< 0.037	< 0.037
2100	30.8	7.59	2.05	0.43	< 0.037	< 0.037
P/I, permeability(mol m⁻² s⁻¹ Pa⁻¹×10⁻¹⁰) [cm s⁻¹ cm Hg⁻¹ x 10⁻⁶]						
700	9.94 [2.97]	2.45 [0.73]	0.99 [0.30]	0.21 [0.063]	< 0.055 < [0.016]	< 0.055 < [0.016]
1400	12.9 [3.76]	3.31 [0.99]	1.03 [0.31]	0.22 [0.066]	< 0.028 < [0.008]	< 0.028 < [0.008]
2100	15.2 [4.54]	3.76 [1.12]	1.02 [0.31]	0.21 [0.063]	< 0.018 < [0.005]	< 0.018 < [0.005]
R, overall resistance (Pa s mol⁻¹ x10¹²)						
700	1.05	4.2	10.5	51	> 200	> 200
1400	0.80	3.1	10.1	46	> 390	> 390
2100	0.68	2.8	10.2	48	> 590	> 590
α, permeation rate ratio						
700	1	4.0	10	48	> 1 90	> 1 90
1400	1	3.9	13	57	> 490	> 490
2100	1	4.1	15	71	> 860	> 860

Table 2: Reframed table for permeation rate, permeability, overall resistance and permeation rate ratio data for the all the mentioned gases from the publication of A. T. Mohammadi et al. [112].

In the parallel, scientists also used composite membranes based gas separation. Q. Hu *et al.* [113] used Poly(amide-imide) as a polymer matrix and TiO₂ as a filler. In this composite, they checked different gases such as s O₂, N₂, CO₂, H₂ and CH₄ for the

permeability and permselectivity. CO₂ and H₂ show intermolecular interaction with TiO₂ domains and it's interaction with specific gas responsible for higher separation factor of CO₂ and H₂.

Z. Jahan *et al.* [114] developed a series of the crystalline nanocellulose (CNC)/polyvinyl alcohol (PVA) nanocomposite membranes for the observation of CO₂ selectivity over CH₄. In this study, they optimised the CNC concentration and the pH of the casting solution. According to data 1wt% CNC concentration and pH 10 is an optimized condition for the maximum selectivity. On the above-optimized condition the highest selectivity of CO₂ over CH₄ is 43.

S. Kim *et al.* [115] used two-dimensional zeolitic imidazolate framework-L (ZIF-L) with polyimide (PI). ZIF-L have a leaf-like structure and have excellent absorption properties for CO₂ because of the strong interaction between ZIF-L and CO₂ molecule. Observed data shows that at 20 wt% of ZIF-L with PI, maximum permeability of MMMs is 260 Barrers and selectivity of H₂/CO₂ was 13.4.

B. Molki *et al.* [116] prepared composite membranes of different wt% of NiO nanoparticles and polyurethane (PU) polymer for the selectivity of CO₂ gas. The permeability of synthesised samples was checked by the CO₂, CH₄, O₂ and N₂ gases. Authors found that with the increment in the wt% of NiO permeability and selectivity of CO₂ over N₂ increased. The selectivity CO₂/N₂ increased by 161.1%, in the cases 5wt% of NiO nanoparticles loading.

T Rodenas *et al.* [117] prepared metal-organic metal (MOFs)-polymeric composite membrane for CO₂ separation from CO₂/CH₄ gas mixtures. They dispersed copper 1,4-benzenedicarboxylate MOFs in polymeric matrix and found that the resultant composite shows outstanding separation properties for CO₂. Such research work for the MOF-polymer composites opens the new doors for gas separation applications.

2.3 Hydrogen Separation

Due to the fact of that, the H₂ molecule has smallest kinetic diameter the selection of the H₂ over other gases is easy. Since H₂ molecule has the biggest diffusion coefficient, permeability and selectivity are of the H₂ can be tuned. In this section, we will go through some of the articles in which researcher attempted different type of samples and method to reach Higher H₂ permeability and selectivity.

Because Pd is one of the best Absorbent material for hydrogen, but it's also expensive compared to other metals. So researchers are also searching for the alternative to replace Pd by alloys. D. Liu *et al.* [118] fabricated alloy of Nb₃₅Mo₅Ti₃₀Ni₃₀ as an alternative of Pd for hydrogen purification/separation application. They presented the theoretical calculation by DFT for the optimisation of combination of the alloy. Experimental data indicate that Nb₃₅Mo₅Ti₃₀Ni₃₀ membrane shows remarkable H₂ separation and can be a replacement of palladium metal.

In the same direction of the Pd membrane, Y.S. Cheng *et al.* [119] compared the H₂ permeation from the commercial Towngas (49% H₂, 28.5% CH₄, 19.5% CO₂ and 3% CO) by using alumina, zeolite, Pd and Pd-Ag alloy membranes. Their results show that alumina and the zeolite are not suitable options for the H₂ separation from the Towngas. Whereas, Pd and Pd-Ag membranes show great results for H₂ separation from Towngas to achieve high purity of H₂, the purification efficiency further increased by the addition for the silver, due to larger lattice spacing in the resulting alloy material. Some of the previous review articles for the H₂ separation by Pd and Pd-alloys described significantly [11,26,120,121].

Beside Pd and it's alloy, Yan Chen *et al.* [122] used a Pt layer over the surface of the La_{5.5}W_{0.45}Nb_{0.15}Mo_{0.4}O_{11.25-δ} membrane for the reflection effect on H₂ permeation. With a combination of 50% H₂ – 50% He at 1000⁰C achieved permeation flux of H₂ is 0.483 mL/min. cm² from both sides. This permeation rate is twice the uncoated La_{5.5}W_{0.45}Nb_{0.15}Mo_{0.4}O_{11.25-δ} membrane, indicates that Pt layer exhibits positive effect on the H₂ selectivity. This enhancement is due to H₂ dissociation/combination on the Pt layer. S. Fasolin *et al.* [123] fabricated a vanadium-based multi-layer structure (Pd/V₉₃Pd₇/Pd) having the thickness of < 7 μm onto porous alumina. Results show that these membranes have high H₂ selective flux up to 0.26 mol m⁻² s⁻¹ at 375 ⁰C.

Since the discovery of CNT by Iijima [61] in 1991, CNT's have come to the forefront of nano-structured materials and research interest has grown exponentially. Extensive work has been done to characterise CNT's include their exceptional mechanical, thermal and electrical characteristics. CNT's also known as to show extremely high aspect ratios of its length and diameter. Many of the researchers observed some of the respectable results in the field of the H₂ separation/purification. Vijay *et al.* and his group doing a wide-ranging study on the CNT-polymer nanocomposite for the hydrogen gas separation [124–127]. Their results show that the alignment and uniform

distribution of the CNT's is beneficial to enhance the H₂ permeability as well as the selectivity.

Lin Li *et al.* [128] fabricated a hybrid membrane of C/CNT for the gas permeability of H₂, CO₂, O₂, N₂, and CH₄. In this work, authors used CNTs in the form of single-walled carbon nanotubes (SWCNTs) and multi-walled carbon nanotubes (MWCNTs) individually in the membranes. Their results show that MWCNTs incorporated Carbon membrane exhibits higher permeability but lower selectivity than SWCNTs embedded Carbon membrane. Further, acid treatment of the MWCNTs helps to open the blocked ends and which can help to enhance the selectivity.

Recently, a two-stage carbon membranes based system was developed by Xuezhong He *et al.* [129] for the separation of the H₂ and CO₂ from the mixture of both the gases. In the first stage of the system, operated at 20 bar and 120⁰C, H₂ selective membrane is used and in the second stage, operated at 20 bar and 20⁰C, CO₂ selective membrane was proposed. The proposed system provides a low cost <1\$/Kg of H₂ production with the high purity of CO₂ (>95 vol.%) and H₂ (>99.5 vol.%). The proposed concept of the system is shown in figure 10.

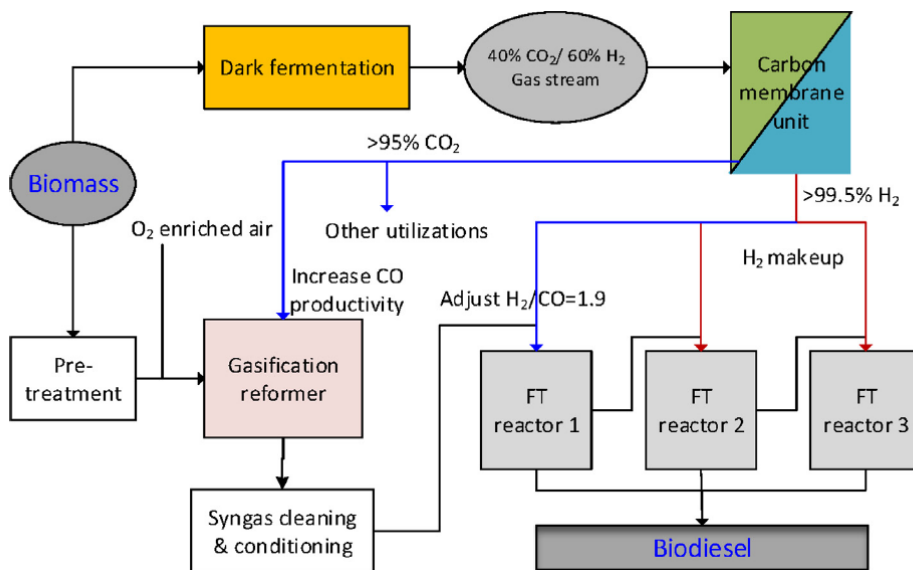


Figure 10: The concept of hybrid membrane/FT process for biodiesel production from biomass [129].

There are many review articles published for the composite polymeric membranes for the hydrogen separation. Some of them are Perovskite-based [130], graphene-based [131], dense metal membrane based [132]. silica-based membranes [133] and Non-Pd BCC alloy based membranes [134] etc.

2.4 Gas Separation by Using Carbon-Based Composite Membranes

Composite material of carbon with polymer have been the centre of demand because of their unique properties and technological usage, especially for the hydrogen separation application [135,136].

By using functionalization of carbon nanotubes A. D. Kiadehi *et al.* [137] Prepared mixed matrix membranes of F-CNFs and polysulfone (PSF) by immersion precipitation technique. Observed data shows that permeability of all gases enhanced with wt% of F-CNTs. But selectivity for CO₂/CH₄ and O₂/N₂ is maximum when 0.5 wt% of F-CNTs is loaded in the membrane.

Graphene and graphene oxide (GO) is the great product in the family of carbon-based materials. GO shows eye-catching properties for the gas separation application. To understand the gas separation mechanism from GO, Amr Ibrahim *et al.* [138] prepared the GO membrane with PETE made from the different size of GO sheets (17 and 33 μm). Their results explain that GO membranes show good H₂ selectivity over CO₂ for pure and binary gas feeds. Because GO exhibits higher permeability for the smaller gas molecules. Gas permeation mechanism of GO membranes is complex, and it is based on the solubility, diffusivity, porosity and tortuosity of the pores.

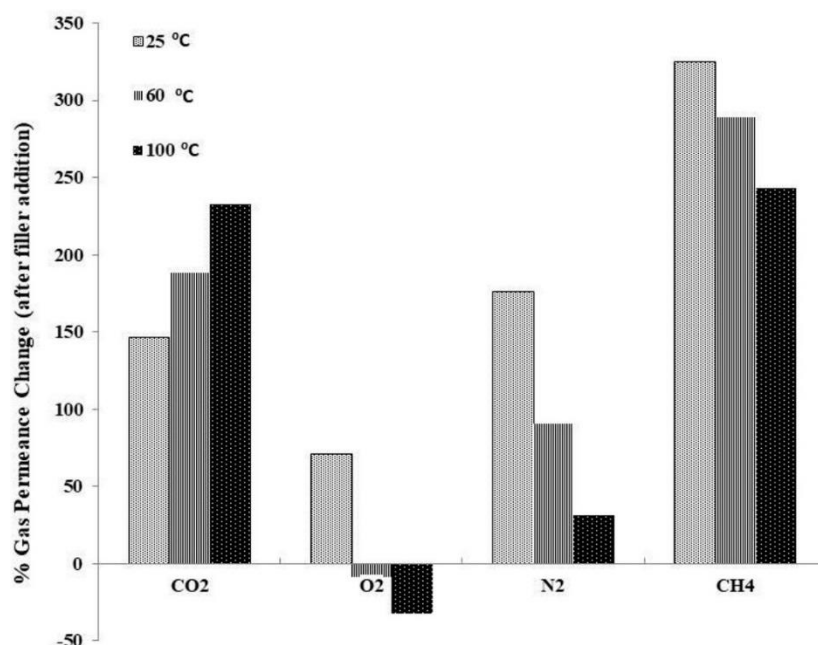


Figure 11: Gas permeance change with temperature for the γ -Fe₂O₃/PHFMs [139].

Graphene and GO membranes were also fabricated by T. V. Gestel *et al.* [140] over the specially designed 8YSZ mesoporous membrane with the help of reductive thermal treatment. The obtained results of selectivity with such membranes is 215, 80 and 170 the combination of the He/N₂, H₂/CO₂ and H₂/N₂, respectively.

Carbon hollow fiber and polyimide membranes composite membranes with or without Fe-based magnetic nanoparticles (γ -Fe₂O₃) were synthesised by E. P. Favvas *et al.* [139] for the gas separation application. These Fe based nanoparticles act as internal nanomagnets, which helps to alter the gas permeation properties of CO₂, O₂, N₂ and CH₄. Figure 11 shows the % change of permeability at different temperature comparing to the pristine sample of PHFMs.

Majid Nour *et al.* [141] synthesised composite membrane of the Polydimethylsiloxane (PDMS) and MWCNT (1, 5, 10 wt%) to evaluate permeation properties for H₂ and CH₄ gases. They found that by adding 1 wt% of MWCNT, the permeability of H₂ is increased by 94.8%. Furthermore, the permeability of the CH₄ is almost blocked for the 5wt%, doped sample of MWCNT. XPS and vibrational spectroscopy analysis of the samples revealed that, reduction in the CH₄ permeability. Incorporation of MWCNT decreases the number of Si-CH₃ and Si-O bonds as well as also increases the Si-C bond. Such membranes offer selective permeation of small gas molecules (H₂) over bigger gas molecules such as CH₄. Similar type of work is also done by the same group by using PDMS and carbon black composite membranes [142].

2.5 Gas Separation by Using Track-Etched Membranes

Track-etched membranes are one of the best categories of the membranes for the gas separation application. The reason behind it that track-etched membranes are capable of tuning the pore size as well as pore shape. Uniform and homogeneous distributed porous membranes have great potential for the selective and higher permeation of hydrogen. Swift heavy ion (SHI) irradiation is one the most known and advanced method for the creation of uniform pores in the membrane. During SHI irradiation process latent tracks are created, and subsequently, these tracks are converted into nanopores by selective chemical etching. Nanopores in polymer membranes have attracted various application as miniaturised devices, e.g. ion pumps, molecular sensors, gas separation and others. For the track-etched membrane, gas separation depends on the porosity of the membrane, chemical state of the pore, pore structure, temperature etc. Different chemical

modifications make it possible to improve the permeability and selectivity precisely in the gas separation process. H₂ separation and selectivity of a nanopore critically depend on the size and shape of its narrowest region, chemical modification and materials deposited inside and outside the pore. This tunability of pore shape and size helps to control the permeability and selectivity parameters.

Blended polymeric membranes of PSF and PC were synthesised by V. Kulshrestha *et al.* [143] in the (3:1), (1:1) and (0:1) ratio with the desired thickness of 27µm. It was observed that, as the concentration of PSF in blends increases, the permeability of hydrogen and carbon dioxide decreases. Further, these membranes were irradiated by Ni⁷⁺ ion having the energy of 100 MeV. Permeability was calculated from both sides; ion incidence side and ion emergence side. They noticed the higher permeability in ion incidence side. This difference in permeability from both the sides is due to the conical shape of the track generated by ions. Permselectivity of hydrogen over carbon dioxide also increases with increasing PSF concentration from both the sides and it observed maximum ~ 4.75 for 1:3 (PC : PSF) blend track-etched membrane.

Polymeric membranes of Polyimide having the thickness of 40 µm were irradiated by W. Ensinger *et al.* [144] for CO and CO₂ gases permeability measurement. The used fluence for the irradiation is 3 x 10⁵ to 1 x 10⁹ ions/cm² and after chemical etching obtained radii of pores is in the range of 10-100nm. According to their study over the 10⁸ fluence, pore gets overlapped. Such membranes cannot be used for a controlled permeation of gases. Gas chromatographic measurements results show that the CO has higher permeation rate than the CO₂. This is possible because gas permeation, in this case, depends on the mean free path of gas molecules and it was in the order of the pore radius.

K. Awasthi *et al.* [143] used 100 MeV Cl¹⁷⁺ ion for irradiation of PET membrane having a thickness of 25 µm, and fluence of irradiation is 10⁷ ions/cm². Because of the smaller size of H₂ molecule, hydrogen shows higher permeability than other gases. On the basis of permeability data hydrogen selectivity in H₂/N₂, H₂/O₂, H₂/CH₄ & H₂/CO₂ combination is around 3.4, 3.7, 2.8 & 4.4. In the other work membranes of thickness, 18 µm were irradiated by Ni⁷⁺ion of 100 MeV at fluence of 10⁶–10⁸ ions/cm² by V. Kulshrestha *et al.* [145] and it was observed by that permeability for H₂ is higher than CO₂ for all membrane. It was also noticed that the selectivity of the membrane increases as ion fluence increases. Y.K. Vijay *et al.* [146] reported that electron irradiation changes

the crosslinking density in the polymer at the surface as well as bulk. The SHI generated tracks can be etched further in a controlled manner to create the nanoscale filter.

Separation process depends on the absorption of gases in the sample material, and nanomaterial plays an essential role in the absorption of gases that why nanoparticles are very useful in selectivity improvement. Gas transport properties in polycarbonate (PC) nanocomposite membrane has been reported by Y.K. Vijay *et al.* [147] and they found that membrane containing nanoparticles displays low permeability with high permselectivity. After irradiation by swift heavy ions (SHI), high gas permeability and high permselectivity have been observed for these nanocomposite membranes.

NK Acharya *et al.* deposited thin film of Ti having a thickness within the range of 100nm-150nm on the surface of PC and Polyethylene terephthalate (PET) membranes [137]. The gas permeability and selectivity for hydrogen of these Ti-deposited membranes were improved because Ti has close affinity for hydrogen.

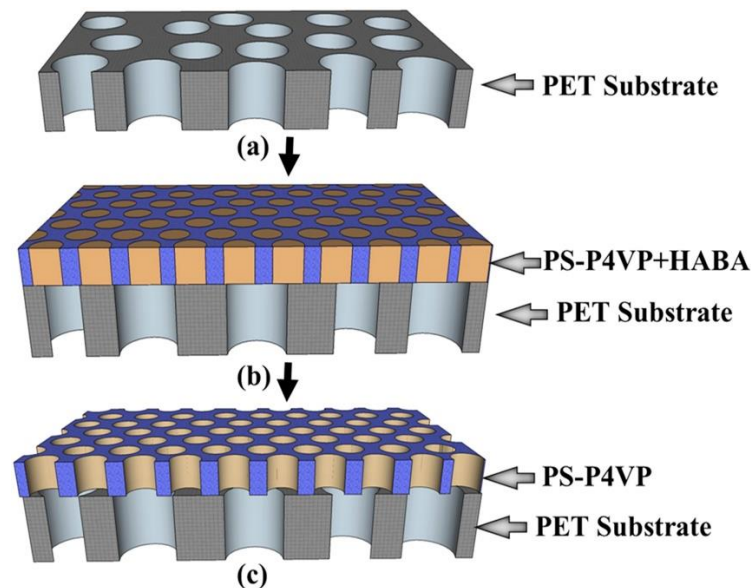


Figure 12: Schematic for composite membrane generation: (a) PET porous membrane (b) Block copolymer with additive coated on PET (c) Block copolymer coated PET after removal of additive [148].

An effective way was to control selectivity established by the Kamakshi *et al.* [148] and his group by using the Block copolymer (BC) membranes over the track etched PET membranes. Based on the molecular weight, BC membranes are used to control the pore diameters in the range of few nm with the uniform ordering of the pores. In this strategic research work, BC membrane is used to selective permeation of gas molecules

by controlling the pore size. Track-etched PET membranes are used to operative permeability of the gases. Schematic representation of the sampling process is shown in figure 12. Results of the work show that coated BC membranes plays significant role for the selectivity of H₂ over CO₂ in compare to pristine PET.

Graphene oxide shows promising results for gas separation, especially for H₂ gas. So, Amr F.M *et al.* [149] synthesised GO membrane over track etched hydrophilic polyester substrates. Synthesised samples have the combined effect of track-etched membrane as well as the graphene oxide on gas separation. Spray coating method was used to prepare the GO coating over track etched membrane, and the concentration of the GO solution is diluted. Because low concentration of GO minimize GO sheet edge-to-edge interactions and reduce extrinsic wrinkle formation. Minimization of wrinkles results in the reduction of over GO layer porosity, which restricts the transport of large gas molecules. This cost-effective method enhanced the H₂ selectivity over other gases.

2.6 Gas Separation by Using Functionalized Membranes

Beside the MMMs peoples are trying to modify the surface properties of the membrane with the help of chemical or other process. R Iwasa *et al.* [150] used vacuum ultraviolet (VUV) irradiation on the polyimide polymer membrane to enhance the hydroxyl groups. Enhancement in the hydroxyl group was always beneficial for the choosy permeation of the hydrogen. and helps to gets the selectivity improvement of H₂/CO₂, H₂/N₂, and H₂/CH₄ from 0.74 to 17, 13 to 230, and 14 to 600, respectively.

K. Awasthi *et al.* [151] used functionalization of membranes process for more attachment of Pd nanoparticle inside the pore of membrane. Palladium (Pd) is chosen because palladium modified membrane shows higher hydrogen selectivity and permeability. Pd nanoparticles are deposited onto pore walls and pore surfaces of PET membranes. SEM, TEM, and energy dispersive x-ray spectroscopy (SEM) results show the presence of Pd nanoparticles in functionalized PET membranes indicating to the improved binding capability of Pd nanoparticles that was used for hydrogen extraction from a mixture of gases. Observed data shows much more improvement in hydrogen selectivity and permeability. Hence nanomaterial modified membranes have high hydrogen permeability, excellent hydrogen selectivity and good chemical compatibility

In the same direction of work, functionalized track etched PET membranes were used by the Kamakshi *et al.* [92] for the for the H₂ and CO₂ gases. In this work authors

functionalized membranes with the carboxylic groups and the amino groups. Further, for the selective permeation of H₂, they deposited Pd nanoparticles (size of 5 nm) in functionalized membranes. Reported results show that H₂ have higher permeability and selectivity over CO₂ gas due to absorption phenomena of Pd nanoparticles.

Yong Wang *et al.* [73] computationally investigated the gas transport mechanism of the functionalized GO membranes for the gas separation applications. According to the study, functionalized GO membranes have the potential for higher selectivity of CO₂/N₂, CO₂/CH₄ and N₂/CH₄ gas combination. More important, their study explains that permeation performance of such membranes not only depends on the energy barrier to getting into the graphene layer but also depends on the energy barrier at the outlet of graphene pore. Both the energy barrier can be tuned by using the functionalization process. Such theoretical study provides a guiding factor for the future experimental study of such membranes for the gas separation application.

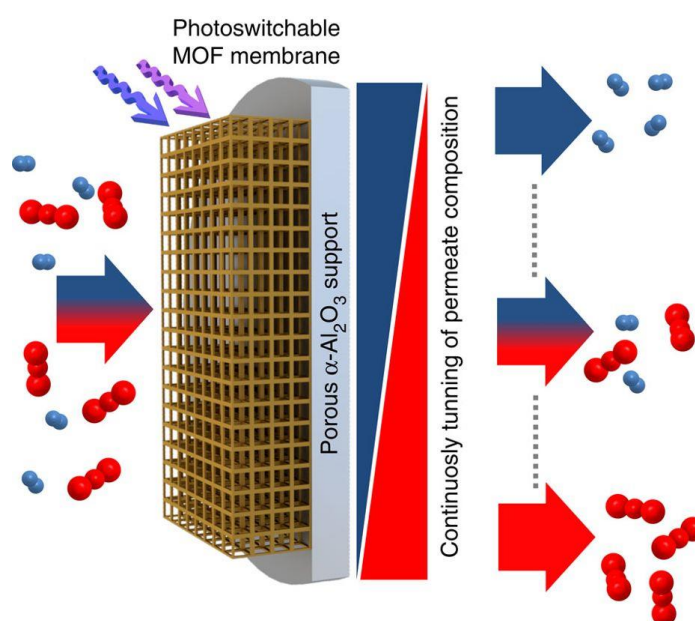


Figure 13: A schematic illustration of tunable, remote-controllable molecular selectivity by a photo-switchable MOF membrane.

Suitable functionalization and use of different pore sizes membranes can allow for an adjustment of the static selectivity. Based on that Z. Wang *et al.* [152] developed an amazing strategy to tune the separation factor of H₂ over CO₂, by assembling linkers having photo-responsive azobenzene side groups into monolithic, crystalline membranes of metal-organic frameworks. The schematic illustration of the sample is shown in figure 13. The azobenzene moieties can easily switch from Trans to Cis configuration by

controlled irradiation of the UV-Vis light and vice versa. Such type of membrane gives the option to enable the constant tuning of the separation and results shows that the separation factor of H₂ over CO₂ can be stepwise adjusted between 3 and 8.

Gas separation or purification based on functionalization of membranes is explained by Melinda L *et al.* [153] and explains the different functionalized strategies for membranes to enhance targeted gas permeation. Generated or enhanced functional as an outcome of the functionalization process, have a strong chemical interaction with a specific gas molecules. This interaction phenomenon can be used to enhance permeation pathway for gas molecules. Functionalization of the membrane has great potential to overcome the tradeoff relation between permeability and selectivity.

Materials and Methods

3.1 Introduction

In this chapter, we will describe the used materials, methods and characterization technique for the hydrogen separation experimental work. For gas separation application, we have used different types of porous polymeric membranes and functionalized these membranes to attach the gas sensitive nanoparticles. For the H₂ selective membranes, we have synthesized and deposited Pd nanoparticles in the functionalized porous membranes. All the samples were characterized by the different spectroscopy and microscopy techniques. Membrane-based gas separation (permeability and selectivity) data were recorded by gas permeability setup.

3.2 Materials

3.2.1 Polyethylene Terephthalate (PET) Track-Etched Membrane

Polyethylene terephthalate (PET) belonging to the polyester family have excessive physical properties for textile, fiber, film, food storage industry and other industrial applications. PET is a semi-crystalline polymer, aromatic, thermoplastic, and having characteristics such as superior mechanical properties temperature, chemical resistance, and high glass transition. Relatively, PET include high transparency, recyclability, and low cost. During the synthesis of PET, chain orientation and crystallinity are controlling parameters for the enhancement of the properties. The main advantage of the PET polymer over other is recycling. The basic unit for PET polymer is shown in the figure 14.

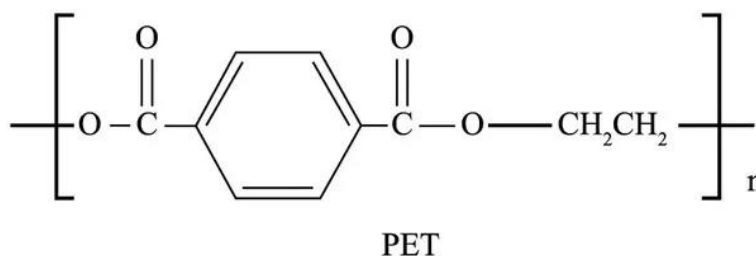


Figure 14: Basic unit of PET polymer

In our work, we have used porous PET membrane having the pore size of 0.2 μm and pore density 10^7 pores/ cm^2 . The pores in this PET membranes were generated through heavy ion irradiation process and followed by chemical etching. We have also purchased porous PET membranes from the Sterlitech Corporation, USA for gas separation application.

3.2.2 Polycarbonate (PC) Track-Etched Membrane

PC is in the one of the high-performance heterochain polymer that comprise the family of engineering thermoplastics. Form last many years, PC is chosen as good material in the industry not only due to its extraordinary characteristics but also processing. PC also has environmentally friendly nature, recycled capabilities and many other excellent properties such as high impact strength, high tensile, shear, and flexural strength, high modulus of elasticity, good electrical insulation etc.

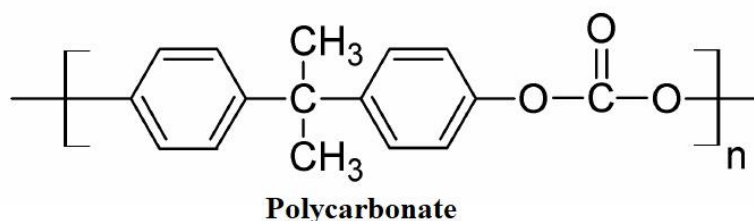


Figure 15: Basic unit of PC polymer

Due to its versatile properties, PC has a very broad range of applications e.g. electrical connectors, coil bobbins & forms, relay components, medical tubing, insulators, brush holders, machine guards, gamma sterilizable re-usable, dialysis equipment parts and instrument covers, fittings and many more.

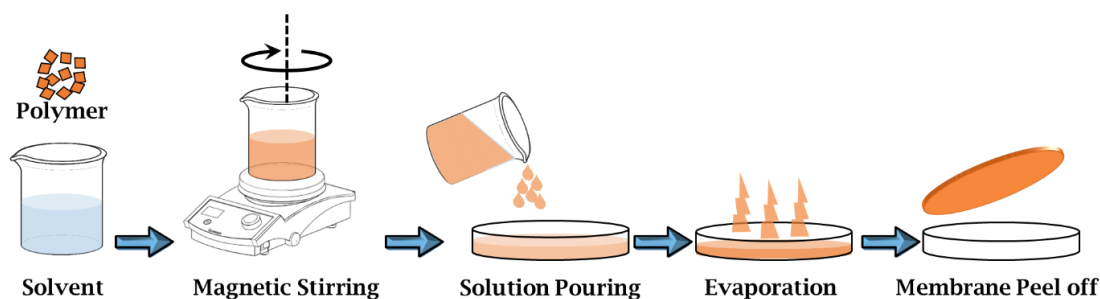


Figure 16: Process of Solution cast method for membrane synthesis

PC is composed of Bisphenol A and carbonate group. Bisphenol A is the backbone for the PC structure and its properties. The basic unit of the PC polymer is shown in the figure 15.

In our work, we have used porous PC membranes of pore size of 0.1 μm and pore density 10^7 pores/ cm^2 . Polycarbonate was used in granular form for the synthesis of composite membranes with the MWCNTs by using solution cast method. Basic process for the solution cast method is as shown in figure 16. The density of the PC granules is ~ 1.20 gm/cm^3 . PC membranes were also purchased from the Sterlitech Corporation, USA.

3.2.3 Functionalization of Membranes

Functionalization is the process through which we can enhance or control a specified property of our polymeric membranes as well as for other materials. In our work, we have functionalized PET membrane, PC membrane and MWCNTs.

For the functionalization of the PET membranes, KMnO_4 (Merck Millipore, India) was dissolved in aqueous H_2SO_4 (Sigma-Aldrich, India) solution having a concentration of 0.75 N. In this solution, PET membranes were dipped for different time 3, 6, 12 and 24 hours at room temperature. These treated membranes were washed four times with the concentration of 6 Mol/L HCl (Merck Millipore, India) and then washed twice with ethanol ($\text{C}_2\text{H}_6\text{O}$, Merck Millipore, India). These membranes were dried in the oven at 45°C for 24 hours.

For the functionalization of the PC membranes, a low cost and eco-friendly UV-irradiation process is used. For UV irradiation process, we have used G8T5 UV lamp of 25-W power. The wavelength of the UV lamp is approximately 253 nm, and this wavelength belongs from the C region of the UV spectra. UV region has sufficient energy that can split the molecules bonds of the polymer and be able to create free radicals. As per our experimental plan, porous PC membranes were systematically kept under the UV lamp so that the effects of the UV irradiation should be equal from both sides. The number of the created free radicals defines the quantitative functionalization of the PC membrane.

3.2.4 Functionalization of MWCNTs

The functionalization of MWCNTs were carried out as per chemical procedure [154,155]. For that a mixture H_2SO_4 (Fisher Scientific, India): HNO_3 (Merck Millipore, India) (1:3) were used at 80°C for 1 hour. Approximately 1 gm of the MWCNTs was suspended in 250 ml of the above-mentioned mix solution for 1 hour at 80°C . This process is complete by using the reflux with proper water supply. After completing the process, nearly 500 ml of DI water was mixed slowly in this solution and keep it to cool down. As it comes to room temperature, the solution was filtered and dried for overnight at 70°C . The filtration with DI water done till the pH of the solution become 6-7. This process leads to increase the number of carboxylic groups ($-\text{COOH}$) on MWCNTs wall.

3.2.5 Synthesis of Palladium Nanoparticles

Pd nanoparticle solution was prepared from palladium (II) chloride by chemical method [156]. The overall process of the Pd nanoparticle synthesis is shown in the figure 17. Palladium (II) chloride was dissolved in concentrated HCl (Merck Millipore, India) in a molar ratio of 1:2. To achieve the final metal precursor concentration of 10 mM, it was diluted with deionized water. The obtained precursor was filtered through $0.2\ \mu\text{m}$ pore size syringe filter (Sigma Aldrich, India). 88.5 ml deionized water was heated to $80^\circ\text{C} - 90^\circ\text{C}$ in a round bottom flask and then 2.5 ml of above-filtered solution was added at the same temperature. After 1 min, 2 ml of 1% sodium citrate (Sigma Aldrich, India) solution and 5.5 ml of freshly prepared 0.08% sodium borohydride (Sigma Aldrich, India) solution was quickly added and cool down till room temperature.

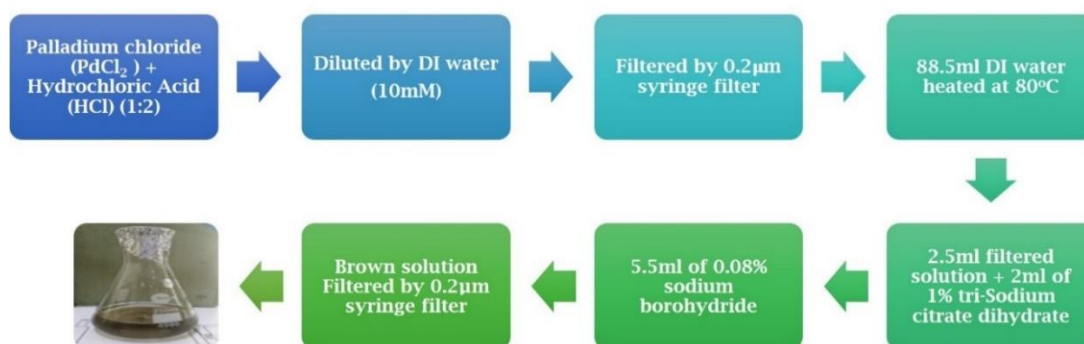


Figure 17: Synthesis process for the Pd nanoparticles.

At the room temperature, the solution again filtered through $0.2\ \mu\text{m}$ pore size syringe filter. The obtained brown solution have Pd nanoparticles.

3.3 Characterizations Techniques

3.3.1 Scanning Electron Microscopy (SEM)

Electron microscopy is a better microscopy due to its high magnification and resolving power less than 1 nm in size. In the electron microscopy signals used by interactions of the electron beam with materials atoms at various depths. The resolution of a microscope depends on wavelength on the source used to examine the sample.

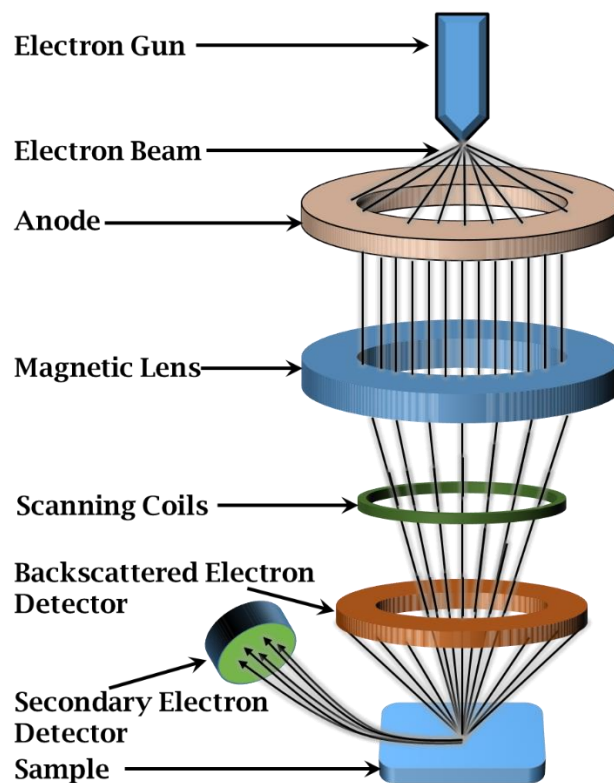


Figure 18: A schematic diagram of SEM system

Electronic console and the electron column are the two main components of the SEM instrument. A focused electron beam of electrons is used to producing signals from the sample surface. A vacuum environment is used to overcome the electron scattering problem by air molecules. A schematic diagram of the SEM is shown in the figure 18.

Basically SEM is operated in two type of modes; (1) secondary electron mode (2) backscattered electron mode. In most of the cases, secondary electron mode is used for the high-resolution image and the detailed information of the surface. The wavelength of the electron beam is controlled by the operating voltage. In the SEM setup, the electron

gun is used to produce a very fine and accurate beam in the range of the 1 – 40 KV. Condenser lens (Anode and magnetic lens) are used to control the electron beam and yield a fine pointed beam. The scanning coils are used to sweep the pointed electron beam over the sample. Backscattered and secondary electron detector are separately used to detect the generated electrons from the sample material as according to the operating mode. CRT monitor is used to displaying the collected information by the detectors.

In our case, we have used Nova Nano FE-SEM 450 FEI to examine the surface morphology as well as the porosity of the membrane with operating voltage of the 3kV.

3.3.2 Transmission Electron Microscopy (TEM)

TEM is one of the best technique for crystallography and inter-planner distance information. A representative schematic diagram for the TEM setup is shown in the figure 19.

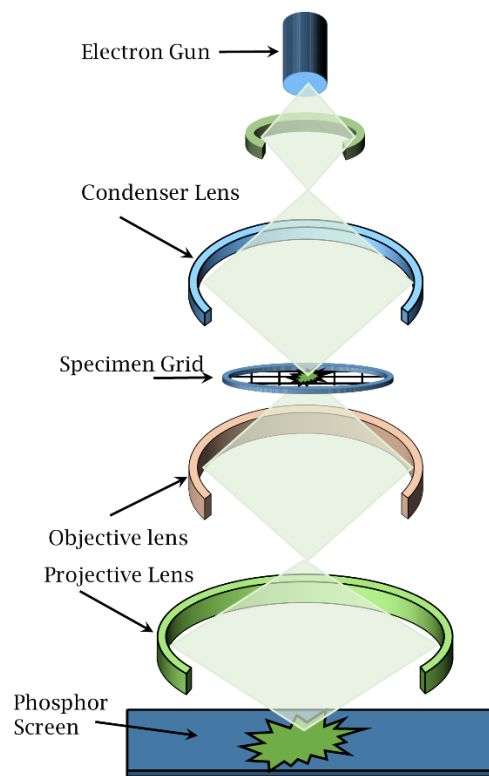


Figure 19: A schematic diagram of TEM system

Basically electron gun produces electron beam and the condenser lens control the beam. Further, these magnetic and condenser lenses accelerate the beam and pinpoint focused on the specimen grid having the sample on it. The accelerating voltage of the beam is in the range of the 100-400kV. Due to such have kinetic energy, electron

transmitted through the thin sample and fall on the CCD sensor of the system. CCD sensor is responsible to form a high-resolution image and send to on computer in the real time. The transmitted electron beam have all the information about the sample. Thus the transmitted beam replicates the patterns of the sample, forming an enlarged image when falling on the phosphor screen. Normally TEM is operated in the two-mode; (1) Bright field image mode and (2) Dark field image mode. For the normal microstructural image and analysis bright field image mode is used while the aperture blocks the direct beam in dark field image mode and then pass one or more diffracted beam. With the help of selected area diffraction pattern (SEAD) mode, lattice planes and interplanar distances of the sample can also easily observed.

In our case, we use TEM technique to analysis the crystallinity nature and particles size of Pd nanoparticles. SAED pattern is used for the observed lattice planes and their corresponding inter-planner distance. The setup used for the characterization of Pd nanoparticles is Tecnai G²S-TWIN Transmission Electron Microscope.

3.3.3 Fourier Transform Infra-Red Spectroscopy (FTIR)

FTIR is a perfect and complete technique to detect molecular structure as well as identification of the functional group.

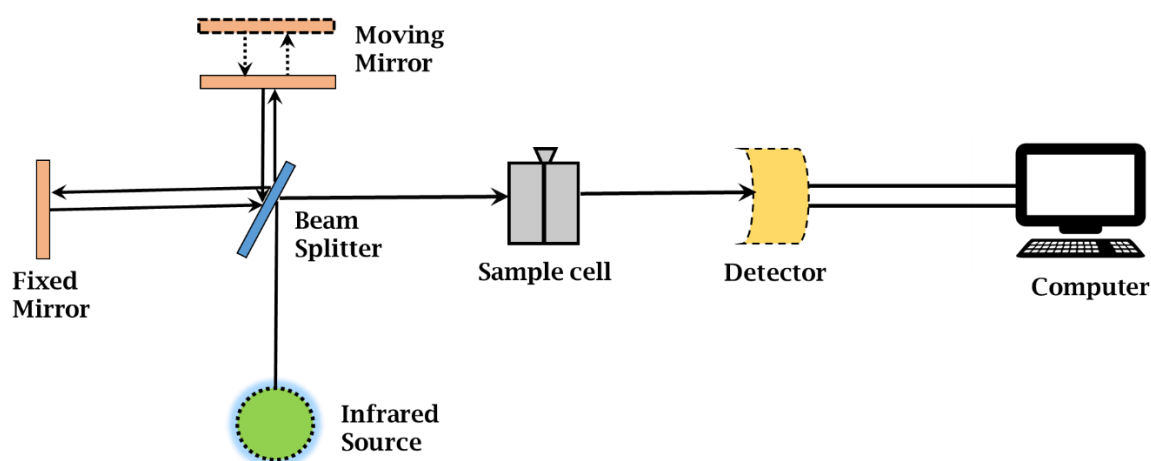


Figure 20: A schematic diagram for the FTIR technique

In most of the FTIR, consists a beam splitter, pair of mirror and detector. Beam splitter split the source generated beam into two parts (figure20). One of the part goes on the sample, and other goes to a reference sample. Because each different material is a unique combination of atoms, no two compounds produce the exact same infrared spectrum. So every functional group or the molecular bond absorbs a particular frequency in the infrared region. The sample absorbs additional frequency compare to the reference.

The detector collects the passed-out wavelength from the sample and the reference and compares its energy. Recorded energy with the frequency gives the complete information about the functional groups and the additional bonds.

In most of the FTIR's system, operating frequency is in the region of 400 to 4000 cm^{-1} . The advantage with the FTIR technique is that it can work with solid and liquid samples. In our case, we used FTIR technique for the comparative study of generated or attached functional group with the polymeric membrane surface. We have used Spectrum 2 Perkin Elmer FTIR instrument in the spectral range of 400 cm^{-1} -4000 cm^{-1} .

3.3.4 Raman Spectroscopy

Raman spectroscopy in combination with FTIR is a complete technique for molecular identification. Raman spectroscopy is used to observe the different modes of the sample such that vibrational, rotational and all other low-frequency modes.

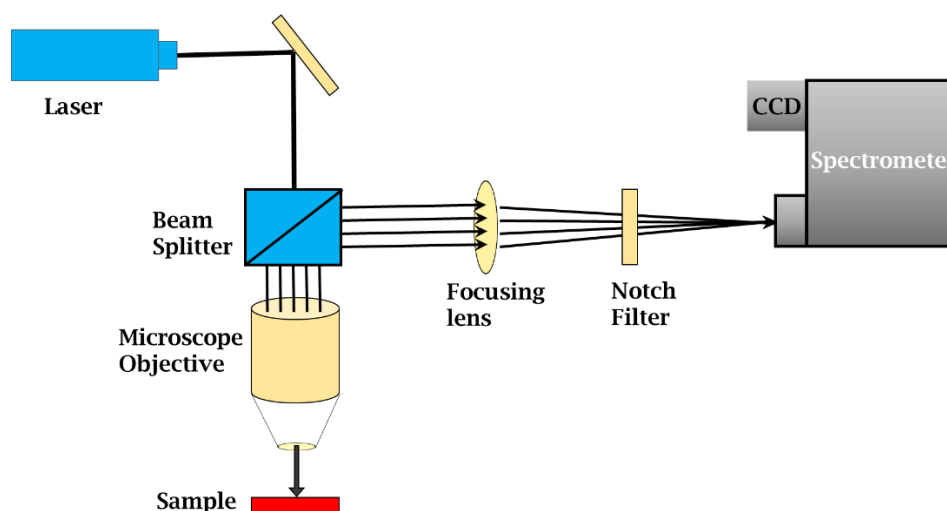


Figure 21: A schematic diagram for the Raman technique

It is based on the inelastic scattering of monochromatic light, generated by the laser source of the Raman setup. When the beam incident on the sample, nearly 0.0001% of photons frequency shifted from original laser frequency due to inelastic scattering. This shifting effect called as the Raman Effect and the shifted frequency have the information about the modes of the sample. Lower energy shift called as Stokes-Raman shift and vice versa phenomena called as anti-Stokes-Raman shift.

Usually, Raman spectroscopy gives quantitative and qualitative information for the molecular bond as well as functional group. A representative schematic diagram of

the Raman spectroscopy setup is shown in the figure 21. Raman technique can be used for the liquids, gels, powder and thin film samples.

In our case, we used Raman spectroscopy for the polymeric membranes such as PC and PET for their quantitative confirmation of functional groups. Raman spectroscopy was performed with a AIRIX STR 500 Raman microscope using a 532 nm excitation wavelength having the power of 10 mW, and 50X objective lens.

3.3.5 UV-Vis Spectroscopy

For the many molecules, photons from the UV-Vis region have enough energy to source a transitions between the different electronic energy levels of the molecule. When UV-radiation interacts with the material, many type processes can occur, which contains absorbance, reflection, fluorescence/phosphorescence, scattering, and photochemical reaction (absorbance and bond breaking). When a UV-Vis light passes through a sample, the amount of the absorbed light creates a difference between the incident light and the transmitted light. The transmitted light for sample compared with the reference sample.

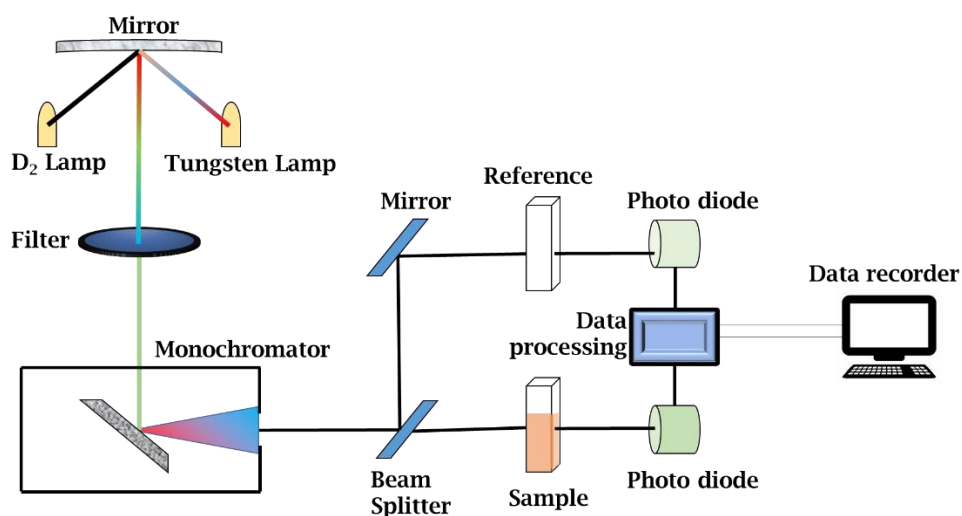


Figure 22: A schematic diagram for the UV-Vis technique

UV-Vis spectroscopy is based on the Beer-Lambert law. It states that “when a beam of monochromatic light is passed through a solution or sample of an absorbing substance, the rate of decrease of intensity of radiation with thickness of the absorbing solution is proportional to the incident radiation as well as the concentration of the solution.”

The expression equation of Beer-Lambert law is shown below;

$$A = \log (I_0/I) = Ecl \quad (9)$$

Where terms are defined such that A = absorbance, I_0 = intensity of incident light, I = intensity of light leaving sample cell, c = molar concentration of solute, E = molar absorptivity and l = length of the sample cell.

It is clear that greater the number of molecules capable of absorbing light of a given wavelength, the greater the extent of light absorption. A schematic diagram of the UV-Vis setup is shown in figure 22.

UV-Vis spectroscopy have many applications such as detection of functional groups, detection of extent of conjugation, identification of an unknown compound, determination of configurations of geometrical isomers, determination of the purity of a substance etc. In our study, we have used UV-Vis spectroscopy for the confirmation of functional group by using Agilent Technologies carry 60 UV-Vis setup in the range of 300nm – 900nm.

3.3.6 Gas Permeability

The permeability of the gases through polymeric membranes depends on the Fick's law. In general, for any kind permeation through the membrane, we need a gradient or difference in concentration/pressure/temperature etc. across the membrane. In the gas permeability setup as shown in the figure 23 [91,157], the gradient is pressure gradient. The permeability process involves; (a) dissolution (sorption) at high-pressure side (b) diffusion through membranes (c) desorption at the lower side. Permeation behaviour of the gases depends on the interaction of the gas molecule with membrane material, diffusion mechanism through the matrix, type of the membrane, filler matrix etc.

Based on the Fick's formula, the relation for the gas permeability [158,159] with other parameters is as shown below:

$$P = \frac{Kxdxs}{\Delta pxt} \quad (10)$$

In the formula, K, d, and s remain constant for a gas permeability setup.

The symbols are used as follow; K refers for cell constant, d for the thickness of the composite membrane, s for displacement of Hg slug in U-tube or displacement of the bubble in bubble flow meter of gas permeability setup, Δp for pressure gradient across the membrane and t used for the time taken to increased level of Hg slug or bubble. The

permeability was measured for three gases H₂, N₂ and CO₂. Also, the pressure range which we are using is the between 5psi - 15 psi. The setup used for the permeability measurement is self-developed in our lab.

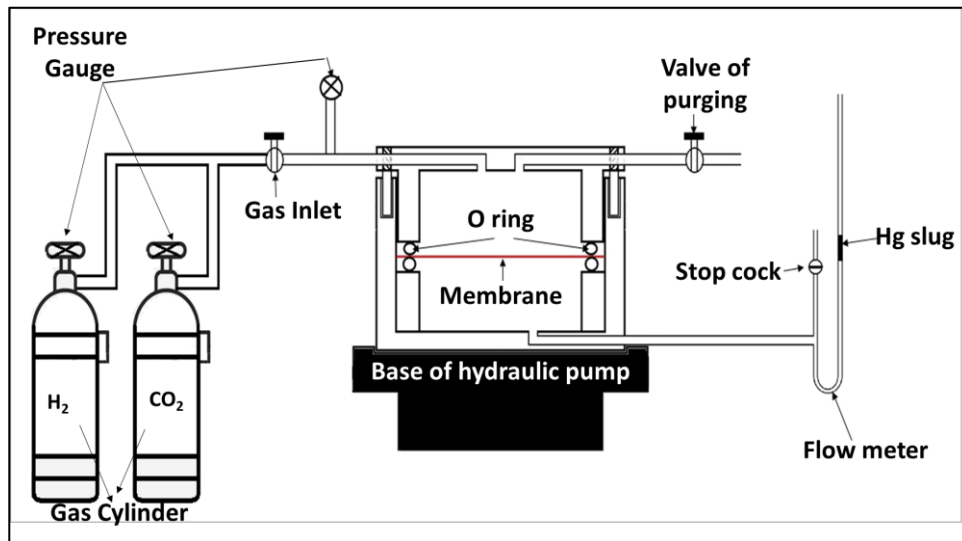


Figure 23: A schematic diagram for the gas permeability setup.

One more important parameter called as selectivity is also calculated by the permeability data of the gases. Selectivity is defined as the ratio of permeability of two gases as equation shown below;

$$S = P_A/P_B \quad (11)$$

Selectivity is the parameter which decides how membrane is efficient to permeate or not to permeate a particular gas in the reference of the other gas.

3.4 Conclusion

In this chapter, we have summarised the materials and the methods used during the experimental work. The details of the adopted methods, process and the techniques for the synthesis of the membranes and the modification of membrane for the functionalization have also been discussed. The same way brief introduction and working principle of the characterization technique also presented in one of the section.

Functionalized and Aligned MWCNTs in Polycarbonate

4.1 Introduction

Track-etched membranes are a good option due to construable properties. However, limitation of use of ion accelerator for the track creation direct us for other options. To overcome this issue, CNTs based polymeric membranes may be used an alternative option. The exceptional and unique properties of CNT's provides us advantage for the production of improved composites, and their application within a matrix depends primarily on the relationship between the matrix and CNT's interaction. Besides all the advantages, there are some limitations of CNTs based composite membrane like mechanical strength, the reaction of the polymer with a broad range of chemicals, low solubility, and agglomeration of CNTs, etc.

The functionalization is an effective method for different functionalities and subsequently desired nanomaterials can be incorporated into the polymer matrix. In functionalized membranes, properties (shape, size, and charge) of nanoparticles can be tailored as per required applications. Introduction of functional groups, such as carboxyl and amino group improve CNT's solubility in various solvents. Additionally, it also are useful for the further chemical link with other compounds such as biomolecules, inorganic compounds, polymers, and metal particles [143,151,160,161]. Attachment of various functional groups with CNT's is possible via oxidation by using concentrated acid. Functionalization of CNT's and deposition of nanomaterials is a beneficial method for enhancement in selectivity with permeability in the gas separation process.

Palladium (Pd) and its alloys are proved as the most important materials for high-quality hydrogen extraction from a mixture of gases. Therefore as per our primary application, Pd nanoparticles were used for the H₂ separation application [43,162–164].

The objective of present chapter is to examine the effect of functionalized MWCNTs and Pd nanoparticles deposition in PC matrix for H₂ separation. Further, we compare the selectivity of H₂ over other gases. These membranes have potential application in hydrogen separation / purification. This technique is easy and can be used for large area membranes with low cost. The results show that Pd nanoparticles with

functionalized MWCNTs dispersed in PC matrix may be used for hydrogen separation effectively. The schematic illustration of the process followed for this work is shown in figure 24.

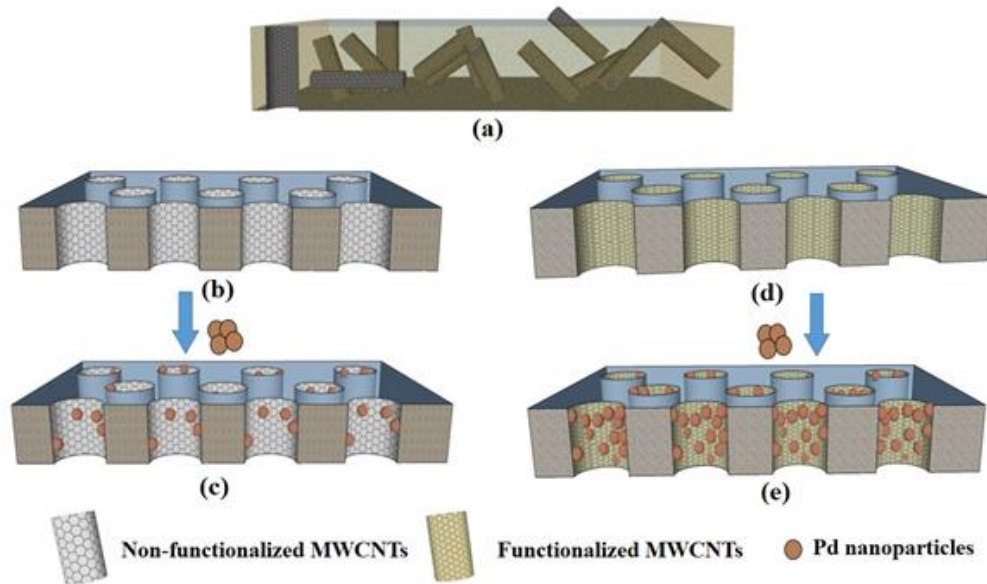


Figure 24: Schematic diagram of the process (a) Random distribution of MWCNTs in PC membrane (b) Magnetically alignment of non-functionalized MWCNTs in PC membrane (c) Pd deposition in the aligned non-functionalized MWCNTs-PC composite membrane (d) Magnetically alignment

4.2 Experimental Details

4.2.1 Sample Preparation

The PC membranes are prepared by solution cast method. The grains of PC were dissolved in chloroform for 3 hours to prepare the pristine PC membrane. To prepare the composite membranes of PC and MWCNTs, PC was dissolved in chloroform, and 1 wt% of MWCNTs sonicated with the polymer solution for 1 hour at room temperature. The obtained solution was spread in a mercury bath suspended in a petri dish of 4 cm diameter.

For alignment of MWCNTs in PC, the magnetic field of 1.9 kGauss was used in the perpendicular position of the membrane at room temperature for 24 hours. After the complete evaporation of the chloroform, the composite membrane was peeled off from the petri dish. The functionalization of MWCNTs was carried out as per the details mentioned in section 3.2.4. We have used, a mixture H_2SO_4 : HNO_3 (1:3) at 80°C for 1

hour to functionalize the MWCNTs [154,155]. Functionalization of MWCNTs leads to creating the –COOH group for better attachment of gas sensitive nanoparticles.

Pd nanoparticles were used to enhance the H₂ selectivity as well as permeability. For the synthesis of Pd nanoparticles, the chemical method is followed by using palladium (II) chloride as the base material for the synthesis process [156]. The synthesis process for the Pd nanoparticles was carried out as per the details mentioned in section 3.2.5. For deposition of Pd nanoparticles, membranes were kept in Pd nanoparticle solution for 6 hours in free standing position. So that deposition of Pd nanoparticles should uniform from both side. The nomenclature of prepared samples and their details are shown in table 3.

S. No.	Polymer	Type of MWCNT	Orientation	Pd deposition time	Symbol
1	Polycarbonate	---	---	0 hrs	PC
2	Polycarbonate	Pristine	Random	0 hrs	NFRPC
3	Polycarbonate	Pristine	Aligned	0 hrs	NFAPC
4	Polycarbonate	Functionalized	Random	0 hrs	FRPC
5	Polycarbonate	Functionalized	Aligned	0 hrs	FAPC
6	Polycarbonate	Pristine	Aligned	6 hrs	NFAPdPC
7	Polycarbonate	Functionalized	Aligned	6 hrs	FAPdPC

Table 3: Sample representation according to Type of MWCNTs, orientation and Pd deposition time

4.2.2 Characterization Details

For the characterization of the samples, Fourier transform infrared (FTIR) spectroscopy was conducted for the confirmation of the functionalization of MWCNTs. Raman spectroscopy was performed with a 532 nm excitation wavelength, a 50X objective lens, and power of 10 mW. The transmission measurements were done in a spectral range of 400 cm⁻¹ to 4000 cm⁻¹. Field Emission Scanning Electron Microscopy (FESEM) was used to examine the morphological and dispersion of MWCNTs in prepared membranes with the accelerating voltage of 3 kV. Transmission Electron Microscopy (TEM) images were taken for Pd nanoparticles size and the crystallography

features. I-V characteristic was performed on KEITHLEY Model 2600B within the voltage range of -6 volts to 6 volts by using pulse width time of 500 ms.

4.3 Result and Discussion

4.3.1 Transmission Electron Microscopy (TEM)

It has been observed that membranes with Pd nanoparticles have excellent hydrogen selectivity from a mixture of gases [151,165]. However, preparation of aligned MWCNTs and Pd containing composite PC membrane is sensibly exciting and may be a better candidate for separation technology.

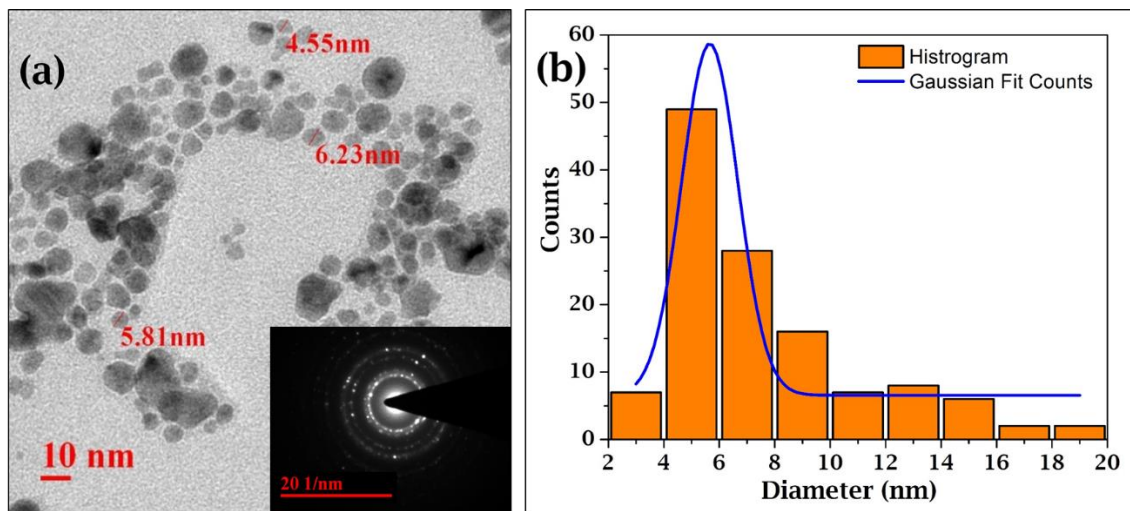


Figure 25: TEM image of (a) Pd nanoparticles distribution (b) histogram for average particle size.

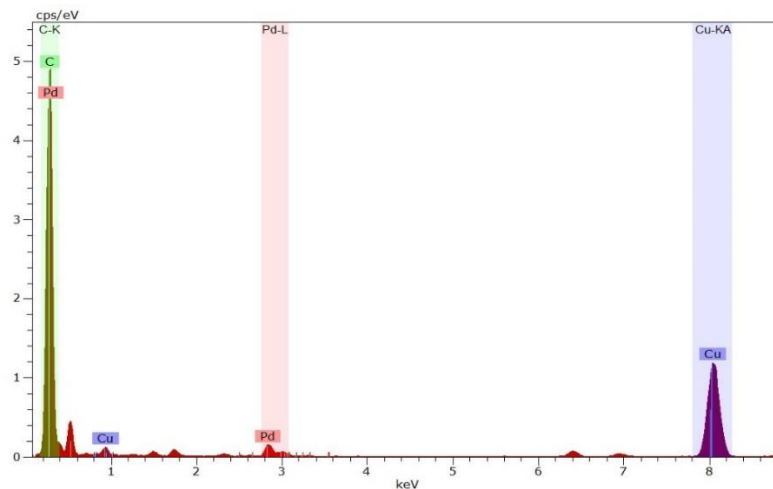


Figure 26: Energy-dispersive X-ray spectra (EDS) of Pd nanoparticles.

To achieve our objectives, we have synthesized Pd nanoparticles by a chemical method with average core diameter is 6 ± 1 nm as confirmed by the TEM images (figure 25). It is clear from figure 25(a) that all Pd nanoparticle lies within the range of 2-20 nm and have polycrystalline nature which is confirmed by Selected Area Electron Diffraction (SAED) pattern. The corresponding planes of Pd to the rings were found as (200), (311) and (400). After Gaussian fitting of the particle size distribution, maximum number of particles were found to be in the range of 4 nm – 8 nm and average particle size were found to be 6 ± 1 nm as shown in histogram (figure 25(b)). Energy-dispersive X-ray spectra (EDS) also confirm the presence of Pd particles as shown in the figure 26.

4.3.2 Raman Spectroscopy

Functionalization process leads to increase the number of carboxylic groups (-COOH) on MWCNTs inner wall as well as the outer surface.

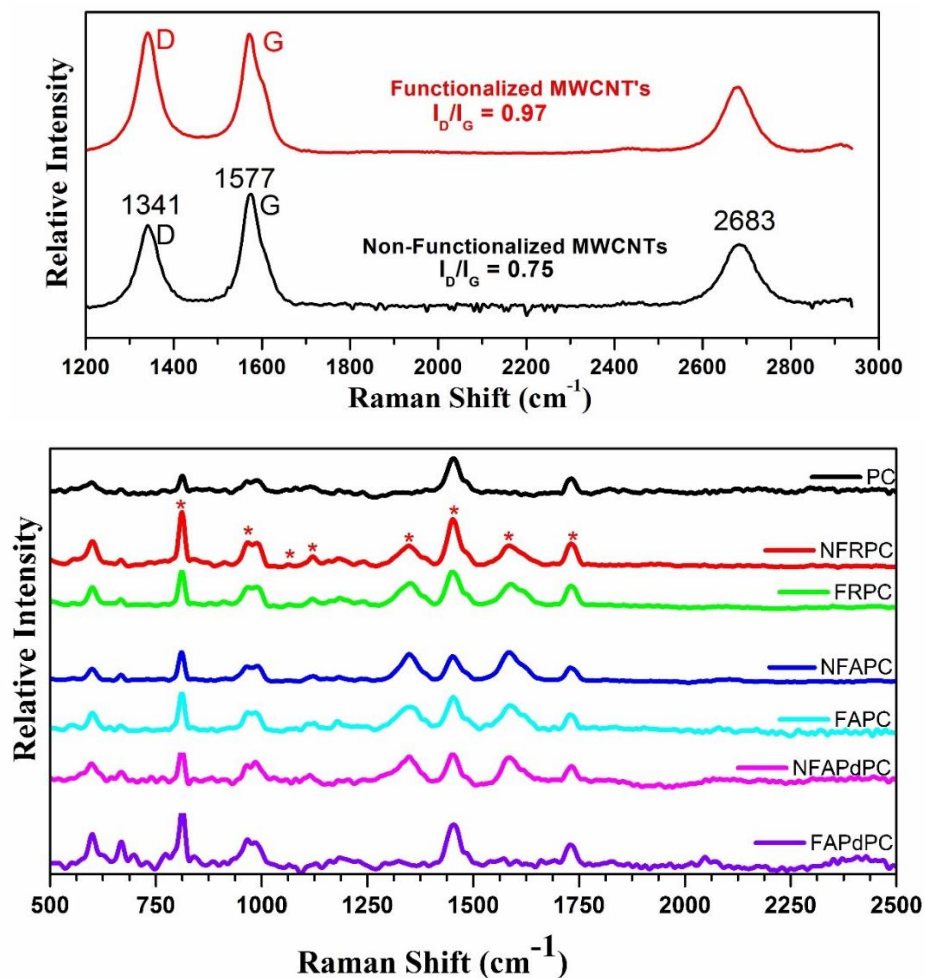


Figure 27: Raman spectra of (a) Non-functionalized and functionalized MWCNTs (b) all composite membranes (symbols; N: non, F: functionalized, R: random, A: aligned, Pd: Palladium, PC: Polycarbonate).

From the Raman spectra analysis, it was found that there are more number of a carboxylic group (-COOH) at the wall of functionalized MWCNTs as compared to non-functionalized MWCNTs. In both type of MWCNTs, the fundamental bands of MWCNTs have been found at 1341 cm^{-1} and 1577 cm^{-1} as shown in figure 27(a). These bands are called D-band & G-band respectively. The relative intensity ratio of D-band (I_D) and G-band (I_G) was estimated to confirm the functionalization [166,167].

I_D / I_G was known as a ratio of sp^3 – hybridized carbon atoms (disordered carbon) relative to sp^2 bonded carbon atoms (graphite carbon). In the functionalized state of MWCNTs, there are more numbers of sp^3 hybridized carbon as compared to non-functionalized MWCNTs. It can be clearly seen from Raman spectra that I_D / I_G ratio for non-functionalized MWCNTs and functionalize MWCNTs is 0.75 and 0.97, respectively. Since I_D / I_G ratio of functionalized MWCNTs are relatively high and hence it indicates that some moieties are covalently introduced onto the surface of MWCNTs during the functionalization process. These changes due to the functionalization process help to enhance the Pd attachment as well as the hydrogen acceptance during the permeation process.

Peak (cm^{-1})	Corresponding bond
813,964	C-H Wagging
1081	C-O-C stretching
1114	C-H wagging
1184	C-O-C stretching
1238	C-O-C stretching
1319	CH_3 symmetric bending, C-O-C stretching
1346	D-band of MWCNT(disorder in carbon system)
1452	CH_3 deformation
1586	C-C bond vibration (G band)
1730	C=O stretch

Table 4: Raman peaks and corresponding bond for all the composite samples.

Both functionalized and non-functionalized MWCNTs were dispersed in PC to prepare the composite membranes. Raman spectra have been recorded for all the synthesized PC-MWCNTs composite membranes. It can be seen from figure 27(b), that

there is a little bit shift in Raman spectra for composite membranes in comparison to pure MWCNTs fundamental peaks. The shift of G-band peak of MWCNTs revealed that it has good dispersion as well as the interaction between MWCNTs and PC matrix. All observed major peaks in the Raman spectra of the composite membranes are listed in table 4 with their corresponding bond.

4.3.3 Fourier-Transform Infrared Spectroscopy (FTIR)

In a polymer, each molecular group has their characteristic frequency of vibration, and it depends on the nature of the chemical bond present in that group. To determine the vibrational mode of a chemical bond, infrared (IR) spectroscopy is admirable technique. IR spectra of material give us information about the type, position of bonds and the presence of the functional group. Valence or stretching vibration corresponds to vibrations along the axis of bonding while rotation or bending vibrations are related to angular modifications.

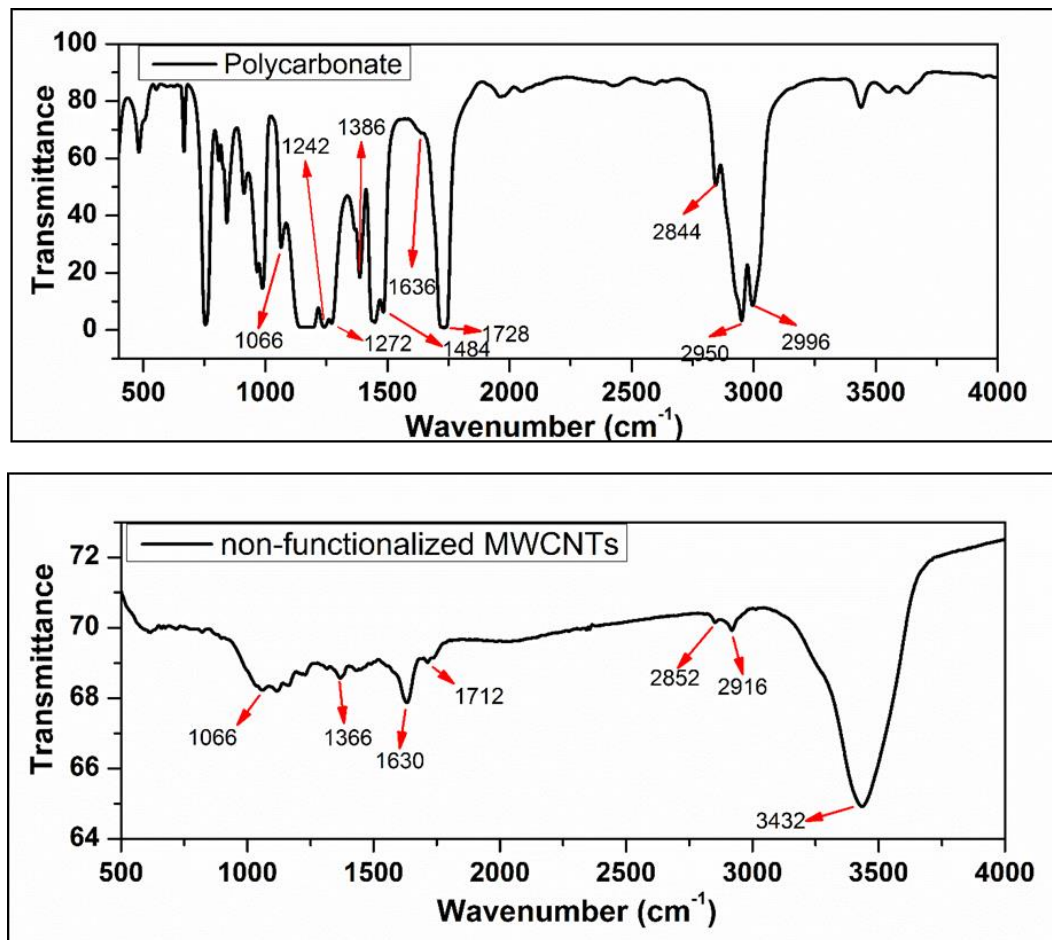


Figure 28: FTIR spectra of (a) Polycarbonate membrane (b) Non-functionalized MWCNTs.

Figure 28 shows the FTIR spectra of PC and MWCNTs and have all elementary bonds. It is clear from FTIR spectra of PC (figure 28 (a)) that it has all associated peaks and peak observed at 1066 cm^{-1} , 1242 cm^{-1} and 1272 cm^{-1} are due to $\text{Csp}^2\text{-O}$ bond stretching. In these peaks, the intensity at 1066 cm^{-1} is lower because of resonance of -C=O molecule. One more observed peak at 1386 cm^{-1} appears due to $\text{Csp}^3\text{-H}$ bending vibration. For $\text{Csp}^2\text{-H}$, there is a peak in the range $1442\text{-}1457\text{ cm}^{-1}$ and this range also includes C=C stretching. Another C=C stretching appears at 1636 cm^{-1} and 1484 cm^{-1} due to an aromatic ring carbon. For C=O , peak at 1728 cm^{-1} was observed. It can be noted from figure 28 (a) that for $\text{Csp}^3\text{-H}$ band peaks appears at 2844 cm^{-1} , 2950 cm^{-1} while $\text{Csp}^2\text{-H}$ band peak appears at 2996 cm^{-1} . In the fingerprint range $400\text{-}1000\text{ cm}^{-1}$, other peaks are found to be related with C-C bond stretching.

The intensive band at wavenumbers 3432 cm^{-1} is due to stretching vibrations of isolated surface -OH moieties and / or -OH in carboxyl groups and absorbed water. The bands in the $1750\text{-}1550\text{ cm}^{-1}$ range can be assigned to C=O groups in different environments such as carboxylic acid, ketone/quinone. And C=C in aromatic rings, whereas the bands in the range of $1300\text{ cm}^{-1} - 950\text{ cm}^{-1}$ prove the presence of C-O bonds in various chemical surroundings. A band of wavenumber at 1630 cm^{-1} most probably due to aromatic and unsaturated structural of C=C bonds. 2852 cm^{-1} & 2916 cm^{-1} peaks are due to the presence of CH_2 group (C-H stretching) and the presence of CH_3 group (C-H stretching), respectively.

4.3.4 Scanning Electron Microscope (SEM)

The distribution of MWCNTs in the PC matrix and morphology of samples have been confirmed with SEM images. It can be observed from figure 29(a) that there was no homogeneity in MWCNTs distribution due to the random orientation of the MWCNTs but in figure 29(b) have perfect distribution as expected due to the magnetic alignment of MWCNTs in PC matrix [168]. Further, the observed pore size of composite membrane matches with a diameter of MWCNTs, which is in the range of $20\text{nm} - 30\text{nm}$. Opening of MWCNTs over the surface confirms that alignment of MWCNTs serves as a channel in the range of $20\text{-}30\text{ nm}$. figure 29(c) have the bright points and rings which confirms the presence of Pd nanoparticles in aligned-functionalized MWCNT-PC membrane. It was observed that Pd nanoparticles deposited not only inside of MWCNTs but also on surface of the composite membrane. In case of functionalized MWCNTs,

there is significant loading of Pd nanoparticles while non-functionalized MWCNTs have only few Pd nanoparticles.

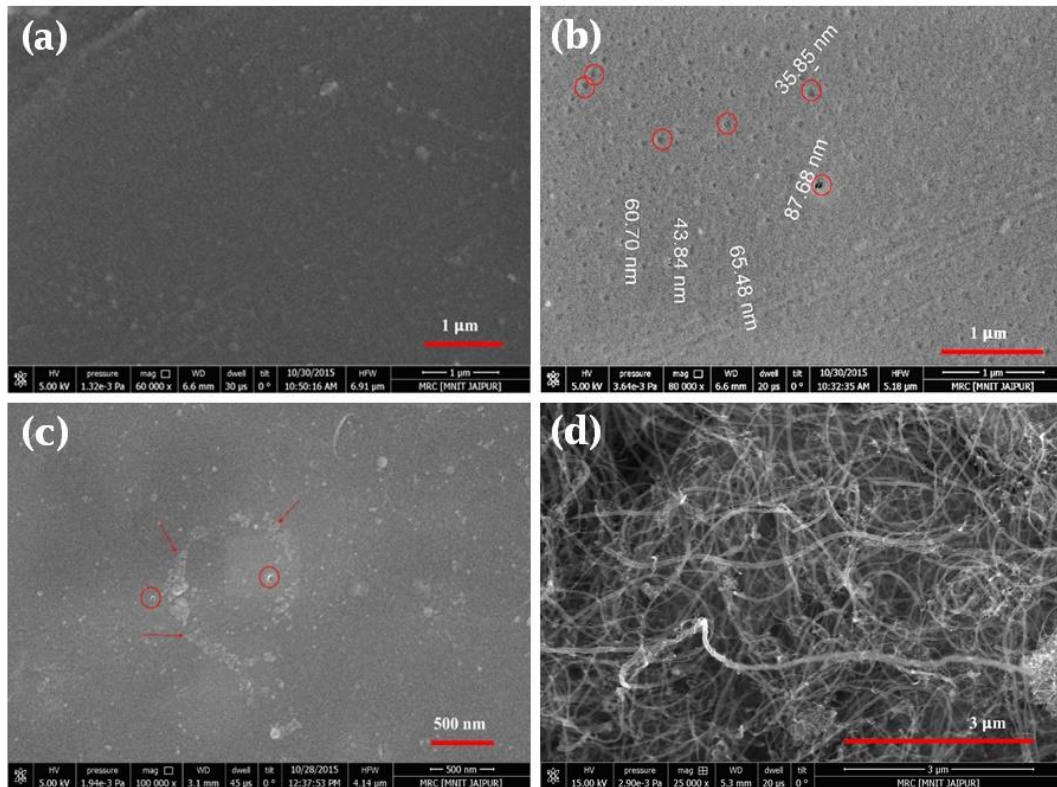


Figure 29: SEM image of (a) MWCNTs distribution in random orientation (b) in aligned orientation (c) aligned MWCNTs with Pd nanoparticles (d) non-functionalized MWCNTs.

Based on the observation from SEM images of independent MWCNTs (figure 29(d)), the average diameter was in the range 20 nm - 30 nm and length of MWCNTs was in the range of 7 μm -12 μm.

4.3.5 Current-Voltage Measurement (I-V)

For confirmations of MWCNTs alignment and Pd deposition, current-voltage measurement (I-V curve) was recorded as shown in figure 30. To perform the current-voltage measurement, we have sandwiched [169] the membrane sample within the copper disc.

Figure 30 (a) represents the I-V characteristics for all the non-functionalized MWCNTs samples and figure 30 (b) for all the functionalized MWCNTs samples. It has been found that in randomly distributed MWCNTs have lower current in comparison to aligned MWCNTs. It is due to less agglomeration of MWCNTs and increase of path

numbers between opposite site by formation of MWCNTs network during the existence of magnetic field.

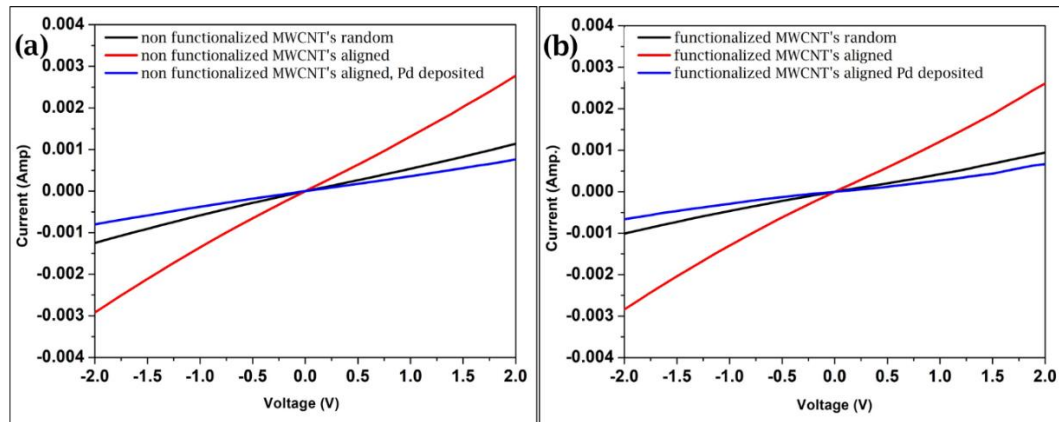


Figure 30: I-V curve of (a) non-functionalized MWCNTs composite samples (b) functionalized MWCNTs composite samples.

The same behaviour is observed for both functionalized and non-functionalized cases. In the case of aligned MWCNTs, conductivity is decreased after deposition of Pd nanoparticles. This is probably due to the Pd nanoparticles absorbed hydrogen during gas separation process. During separation, hydrogen gas molecules occupy the octahedral voids of Face Center Cubic (FCC) lattice of Pd and convert it in semiconductor [170]. So this absorption of hydrogen reduces the conductivity of the composite membrane.

4.3.6 Permeability and Selectivity Measurements

The gas permeation measurements for hydrogen (H_2), nitrogen (N_2) and carbon dioxide (CO_2) were carried out for all samples. The permeability of H_2 was always higher than the CO_2 , N_2 for all type of composite membrane due to higher diffusion of hydrogen as well as smaller molecular diameter relatively to larger ones of CO_2 and N_2 . The estimated molecular diameter of H_2 , CO_2 and N_2 are 2.89 Å, 3.3 Å and 3.64 Å respectively [87,91]. The permeability of gases also depends on the activation energy for diffusion, the activation energy for solubility and polarity of gases along with the molecular diameter. The mechanism for the permeation of gases through CNT-PC composite membrane is due to combine effect of solution diffusion and molecular sieving model. In the case of CO_2 and N_2 , permeability of CO_2 is a slightly lower than N_2 because of the activation energy of diffusion is higher for CO_2 due to liner shape of the molecule

and high polarity [171,172]. Whereas in the case of N₂ required activation energy of diffusion be less due to the spherical shape of the molecule and low polarity of this gas. The results of gas permeability are shown in table 5.

Gas	PC+CNT (Non-functionalized)		PC+CNT (Functionalized)	PC+CNT (non-functionalized) + Pd deposited		PC+CNT (Functionalized) + Pd deposited
	Random	Aligned	Random	Aligned	Aligned	Aligned
H ₂	1763	9997	2213	12211	4712	4758
N ₂	859	3075	1342	2958	2125	1135
CO ₂	688	1640	823	1907	1208	598

Table 5: Permeability data for composite membrane.

It is evident from figure 31 (a and b) that there was a significant change in permeation of all three gases in aligned MWCNTs-PC membranes. It is thought that the aligned MWCNTs provides a channel.

The permeability process involves (a) dissolution (sorption) at high-pressure side (b) diffusion through membranes (c) desorption at lower side. It is expected that aligned MWCNTs in PC provided more dissolution in comparison to randomly distributed MWCNTs.

Pd nanoparticles have high surface-volume ratio and show more absorption properties for H₂. With H₂ gas molecules, Pd nanoparticles produce two different phases, both of which contain palladium metal atoms in FCC lattice. At low concentration of H₂ up to PdH_{0.2}, Pd lattice expands from 3.889 Å to 3.895 Å. For higher concentration, the second phase appears with a lattice constant of 4.025 Å. The absorption of H₂ is reversible and H₂ rapidly diffuse through the Pd metal lattice and metallic conductivity also reduces as hydrogen is absorbed. Due to that in the case of Pd deposited composite membrane permeability decreases as indicated by figure 31 (c).

Table 6 shows selectivity of H₂ over N₂ and CO₂. It can be conclude from the data that the selectivity increases in the aligned case for both types of MWCNTs (non-functionalized as well as functionalized).

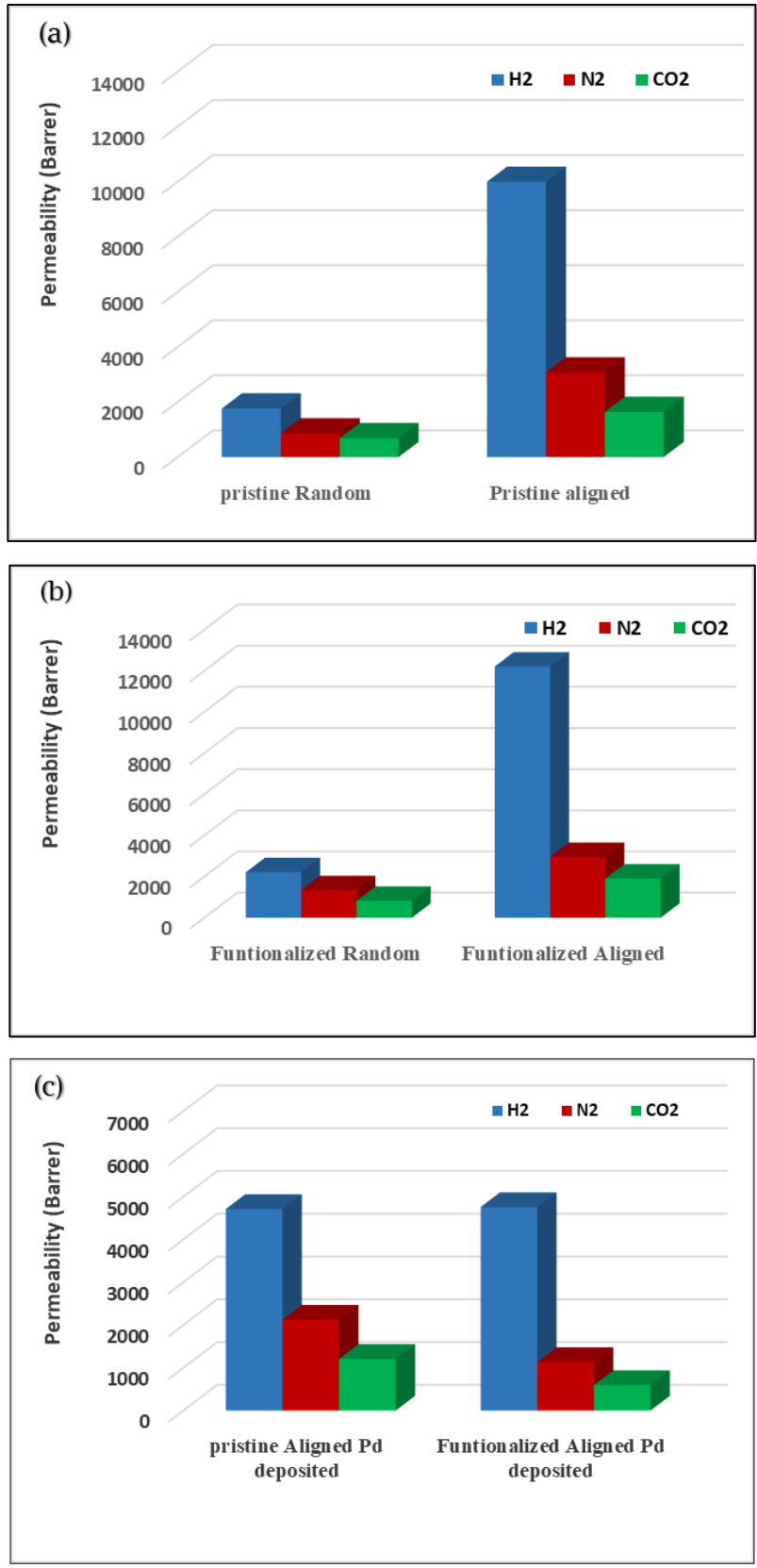


Figure 31: Graph of gas permeability for (a) non-functionalized MWCNTs (b) functionalized MWCNTs in both orientation (c) Pd deposited aligned sample.

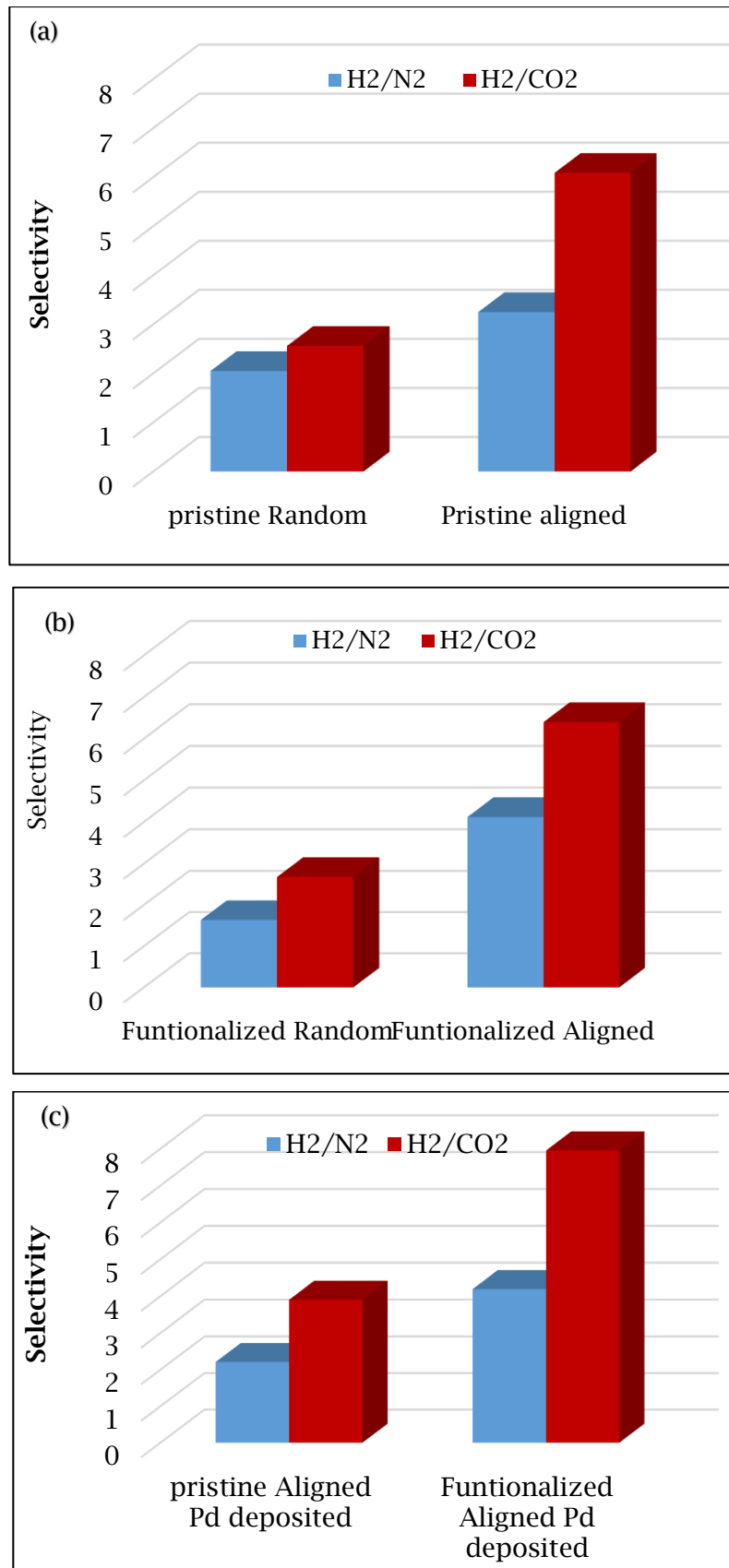


Figure 32: Selectivity data for (a) non-functionalized MWCNTs (b) functionalized MWCNTs in both orientation (c) Pd deposited aligned sample.

Selectivity	PC+CNT (Non-functionalized)		PC+CNT (Functionalized)		PC+CNT (non-functionalized) + Pd deposited	PC+CNT (Functionalized) + Pd deposited
	Random	Aligned	Random	Aligned	Aligned	Aligned
H ₂ /N ₂	2.05	3.25	1.65	4.13	2.22	4.19
H ₂ /CO ₂	2.56	6.10	2.69	6.40	3.90	7.96

Table 6: Selectivity data for composite membrane.

Figure 32 shows the selectivity of H₂ over other gases in possible combinations. It can be revealed that selectivity is maximum in case of functionalized MWCNTs because of more attachment of Pd nanoparticles with carboxylic group in case of functionalized MWCNTs. In functionalized MWCNTs, more attachment of Pd nanoparticles causes the more absorption of H₂ compared to other two gases. Maximum selectivity for H₂/N₂ and H₂/CO₂ was found 4.19 and 7.96, respectively for the sample Pd deposited functionalized aligned composite membrane. Improvement in selectivity suggests that functionalized CNTs and membranes can be used for hydrogen gas separation.

4.4 Conclusions

The permeability of composite polymer membranes can be modified by using different form of MWCNTs. It was concluded from this study that orientation of MWCNTs affects the permeability as well as selectivity of gases. For aligned orientation, permeability and selectivity was found more than the random orientated MWCNTs in PC matrix. It can be concluded that functionalization of MWCNTs has played important role to control the permeability and selectivity of the gases. Functionalized aligned MWCNTs with Pd nanoparticles in PC matrix has maximum selectivity of H₂ in comparison to other gases. It is noticeable that functionalization of MWCNTs and selective deposition of Pd nanoparticles is a useful methods for improvement of H₂ selectivity with higher permeability. We believe that such type of composite membranes can be used to develop hydrogen-selective nano-filter for purification/separation technology.

Chemical Functionalized PET Membranes

5.1 Introduction

To meet economic demands for a substitute and efficient fuel, it is essential to purify and separate high-quality H₂. Therefore, it is necessary to remove undesired components from mixtures of solvents, gases (e.g. CO₂, N₂ etc.) and impurities. Uniform and homogeneous distributed track etched porous membranes have great potential for the selective and higher permeation of hydrogen. Chemical modification of the surface as well as pore wall of the membrane plays an important role in the process of the gas separation. Functionalization of porous membrane and deposition of nanoparticles within pores is an efficient technique for hydrogen separation.

Membranes will be functionalized by a specific group such as carboxyl and amino group then it can improve selectivity of H₂. It is also supportive for the chemical link with nanomaterials, polymer and inorganic compounds. Since different functionalities can be obtained after functionalization and desired nanomaterials can be attached into the pore walls. Among the available option for the H₂ selectivity, Pd exhibit amazing absorbing properties for H₂ gas and directed to use for the H₂ separation application.

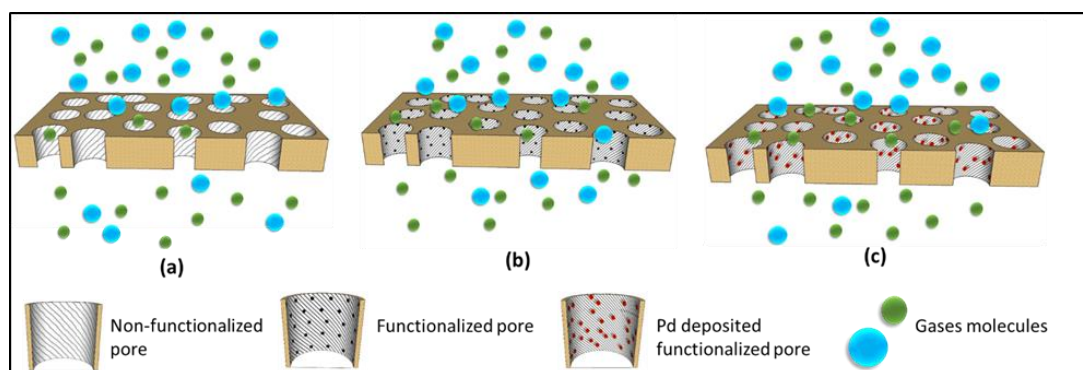


Figure 33: Schematic diagram of the process (a) Gas permeation through the non-functionalized membrane (b) Gas permeation through the functionalized membrane (c) Gas permeation through the Pd nanoparticles deposited functionalized membrane

The objective of in present chapter is to observe the effect of functionalization time on permeability and selectivity of H₂ over other gases in functionalized PET

membranes. Further, Pd nanoparticles deposited into the pores of these functionalized membranes. The easy preparation process and low cost of these membranes are the favourable parameters for the commercial use of such membranes for H₂ separation applications. The process followed for the chemical functionalization is shown in figure 33. In the schematic diagram, huge molecules in sky blue color are representing the CO₂ and N₂ gases as they have approximately same diameter. H₂ molecules are represented by small molecules with green color. Layered structure of brown color is used for porous Polyethylene terephthalate (PET) membrane having average pore diameter approximately 0.2 μm.

5.2 Experimental Details

5.2.1 Sample Preparation

Track-etched PET membranes are used as a porous membrane with average pore diameter of 0.2 μm. Pd nanoparticles were also used for track etched membranes to have H₂ selective membranes.

S. No.	Polymer	Functionalization time	Pd nanoparticles deposition time	Symbol
1	PET	0 hour	0 hour	PET
2	PET	3 hours	0 hour	C3
3	PET	6 hours	0 hour	C6
4	PET	12 hours	0 hour	C12
5	PET	24 hours	0 hour	C24
6	PET	3 hours	6 hours	C3-Pd6
7	PET	6 hours	6 hours	C6-Pd6
8	PET	12 hours	6 hours	C12-Pd6
9	PET	24 hours	6 hours	C24-Pd6

Table 7: Sample representation based on the carboxylation and Pd nanoparticles deposition time (c; carboxylated, C-Pd; carboxylated membranes with Pd nanoparticles, numbers represents hours).

Synthesis [173] and details of Pd nanoparticles solution are given in section 3.2.5. Functionalization of the PET membranes used for the better H₂ selectivity and permeability properties in comparison to pristine PET membranes. For chemical

functionalization, 4 g of KMnO_4 was dissolved in 80 ml of aqueous H_2SO_4 solution of concentration 0.75N. Track-etched PET membranes were dipped in the above mentioned solution for 3, 6, 12 and 24 hours at room temperature. These membranes were then dried in the oven at 45°C for 24 hours. Further, these modified membranes were dipped in Pd nanoparticles solution for 6 hours. Finally, these membranes were washed with DI water to remove loosely bounded Pd nanoparticles from the surface of the membrane. The nomenclature of these membranes are listed in the table 7 on the basis of the carboxylation time and Pd nanoparticles deposition time.

5.2.2 Characterization Details

For the analysis of $-\text{COOH}$ group in all the samples, Fourier transform infrared (FTIR) spectra were recorded in the range of 400 cm^{-1} - 4000 cm^{-1} . Surface morphology including cross-sectional image and distribution of pores were examined by FESEM at accelerating voltage of 3 kV. Pd nanoparticles size was examined by TEM. For the separation measurements, gas permeability setup was used with the H_2 , N_2 and CO_2 gases.

5.3 Results and Discussion

5.3.1 Fourier Transform Infrared Spectroscopy (FTIR)

The FTIR spectra of PET membranes contains several bonds belonging to essential components of PET polymer, which are highly infrared active and shows the characteristic peaks.

Figure 34 (a and b) shows the FTIR spectra of functionalized and non-functionalized PET membranes. All the elementary bonds of the spectra and their corresponding bond presented in table 8. Functionalization of PET membranes can be confirmed by the intensity and broadening of FTIR peaks in the belonging region of $2500\text{-}3300\text{ cm}^{-1}$ because of the stretching $-\text{OH}$ bond of $-\text{COOH}$ group. Due to the existence of H_2 bonding in all the samples, the fundamental peak for stretching vibration of O-H was found at 2968 cm^{-1} (figure 34), and it has been found that the intensity and broadening increases with time of functionalization. With functionalization time, the intensity of stretching vibration of carboxyl bond $\text{C}=\text{O}$ at 1716 cm^{-1} also increases due to the enhancement of molecules of carboxylic group.

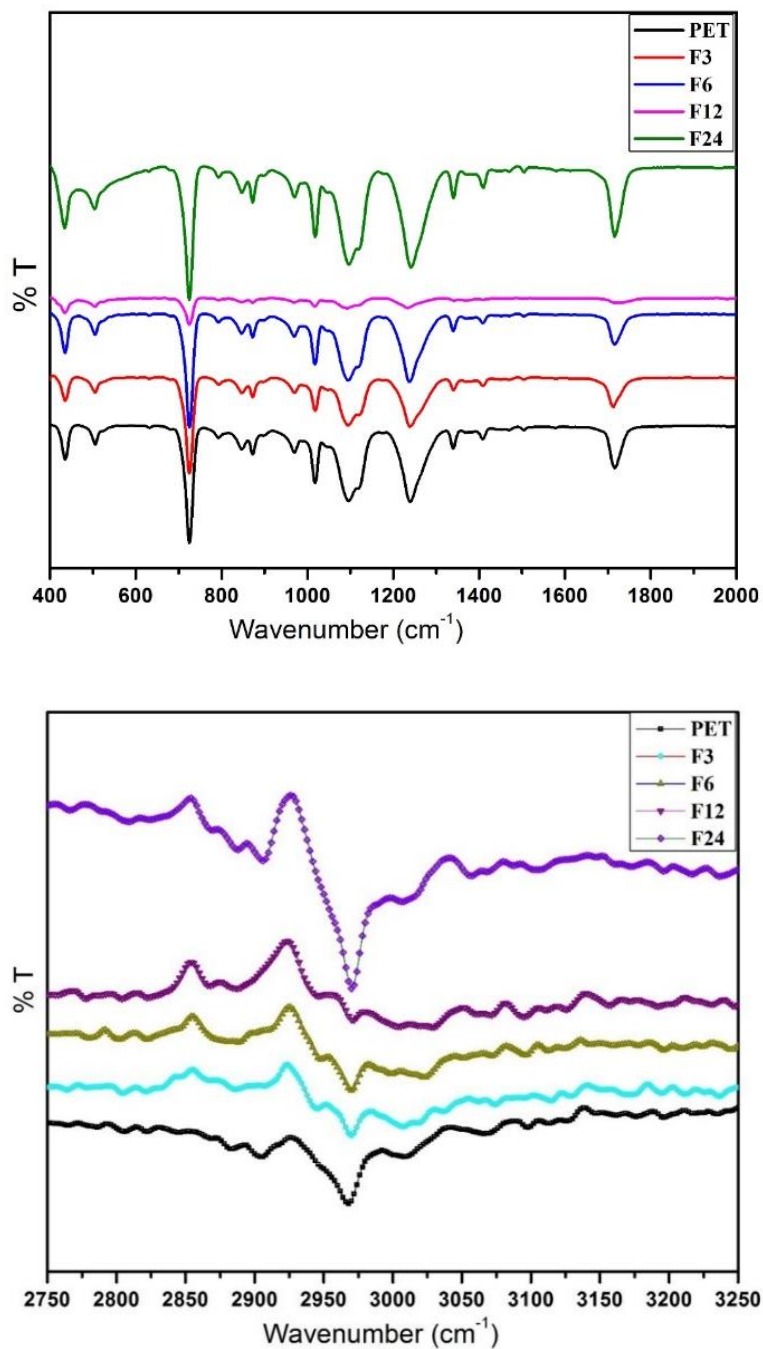


Figure 34: FTIR spectra of (a) functionalized membranes (b) correspond to carboxylation peak

So, increased intensity for both the peaks (1716 cm^{-1} and 2968 cm^{-1}) confirms more functionalization of membranes. F24 and F24-Pd6 had maximum carboxylic group compared to other samples which are due to more oxidation of hydroxyl group by the KMnO_4 on the pore and surface of PET polymer as shown in figure 36.

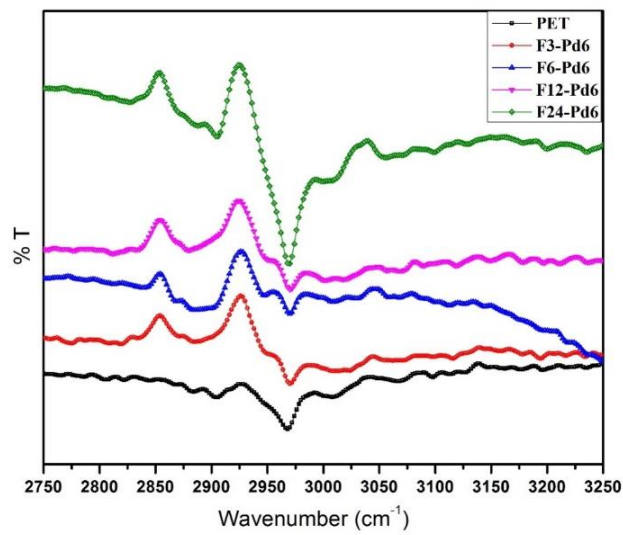
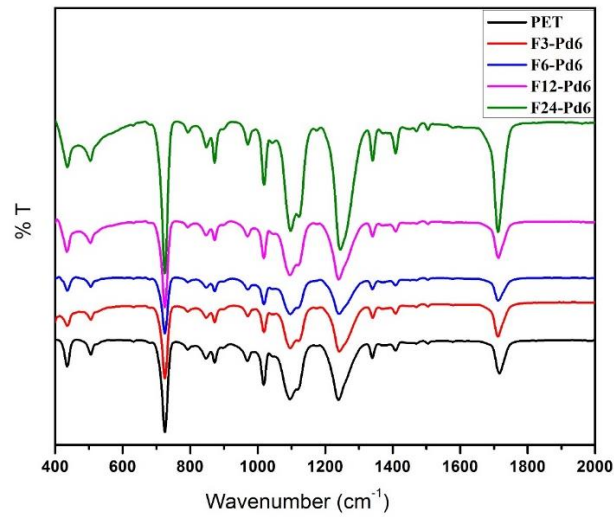


Figure 35: FTIR spectra of (a) functionalized Pd deposited membranes (b) correspond to carboxylation peak.

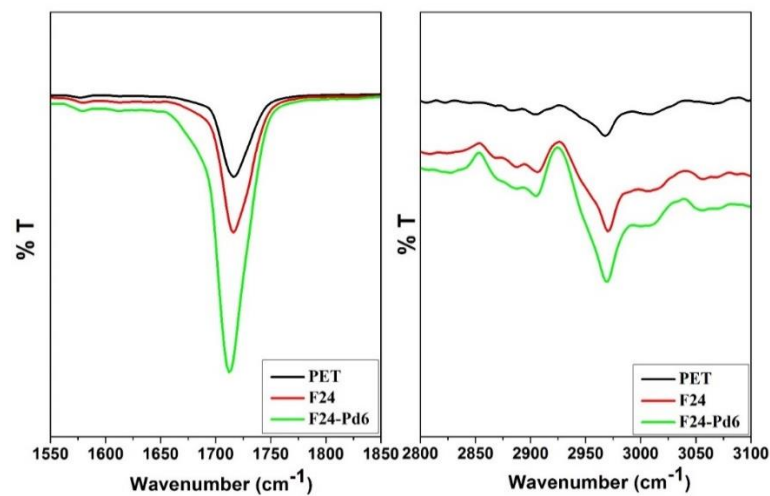


Figure 36: FTIR spectra for comparison of functionalization peak of PET, F24 and F24-Pd6

Peak	Bonds
506,632,682	Out-of-plane banding of -C=O
724	Stretching vibration of -C-H (aromatic)
792, 846	In-plane bending vibration (C-H)
872	Stretching vibration of =C-H (aromatic)
970	Out-of-plane banding of -COOH
1018, 1096, 1240	Stretching vibration of ester bond C-O
1174	Out-of-plane bending vibration (C-H)
1340	Stretching vibration of -C-H (alkane)
1408, 1504, 1578	Stretching vibration of C=C (aromatic)
1716	Stretching vibration of carboxyl bond C=O
2968	Stretching vibration of O-H

Table 8: FTIR peaks and corresponding bond.

5.3.2 Scanning Electron Microscopy (SEM)

For the morphological study, all the samples were characterized by FESEM. SEM images show that the pore distribution is uniform and diameter is approximately $0.2 \mu\text{m}$. The presence and quantitative analysis of Pd nanoparticles were confirmed by using the bright points in the SEM images. It was observed that as the time of functionalization increases, the brightness of these pore boundary points enhanced. However, if we compare with and without Pd deposited samples, without Pd deposited samples show low brightness while Pd deposited samples show more brightness (figure 37 to figure 40).

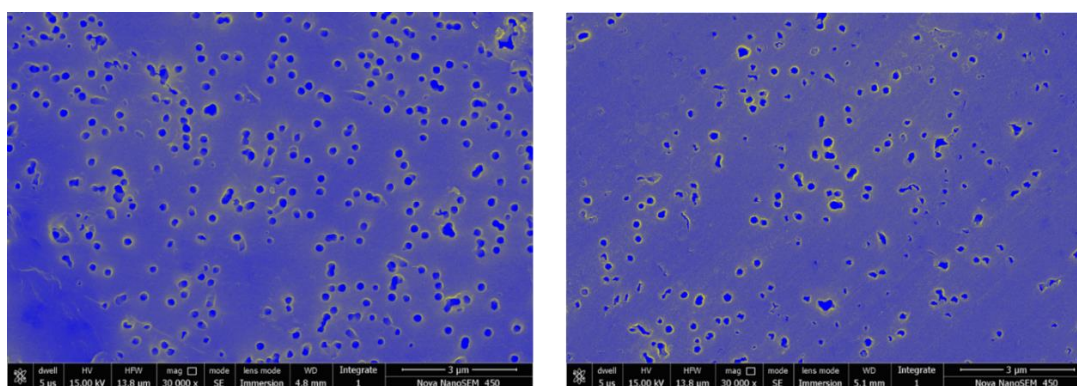


Figure 37: Scanning electron micrograph of 3 hours functionalized PET membrane (a) before Pd deposition (b) after Pd deposition for 6 hours.

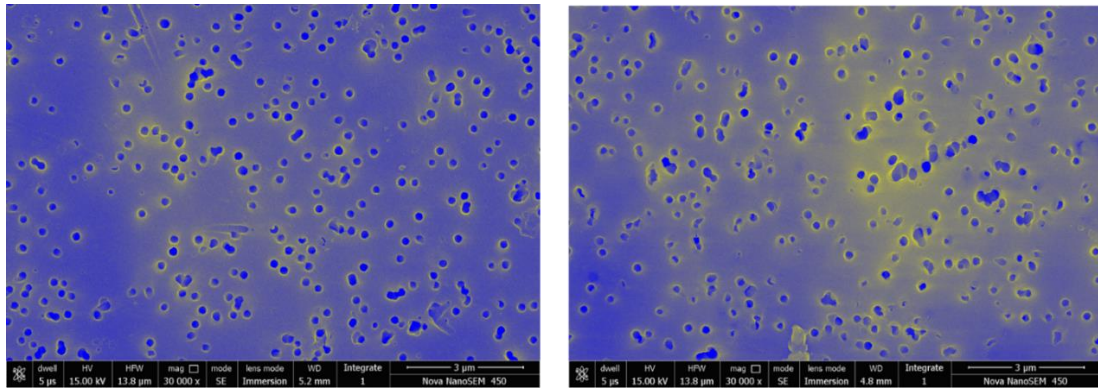


Figure 38: Scanning electron micrograph of 6 hours functionalized PET membrane (a) before Pd deposition (b) after Pd deposition for 6 hours.

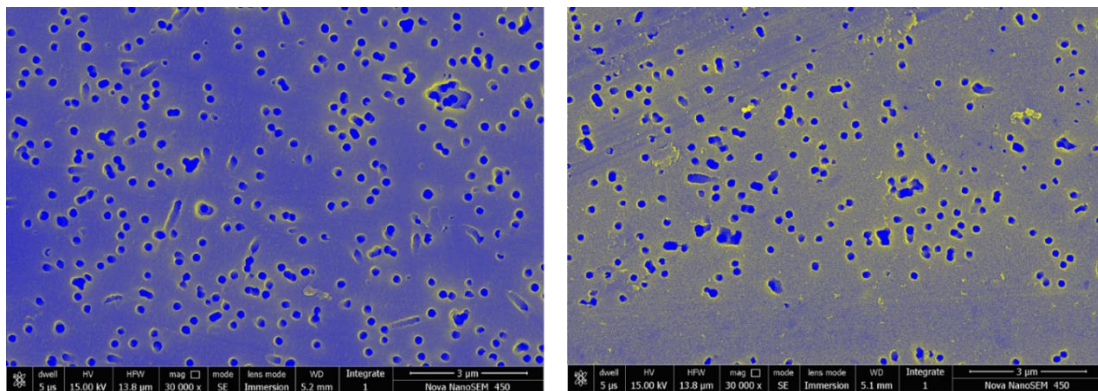


Figure 39: Scanning electron micrograph of 12 hours functionalized PET membrane (a) before Pd deposition (b) after Pd deposition for 6 hours.

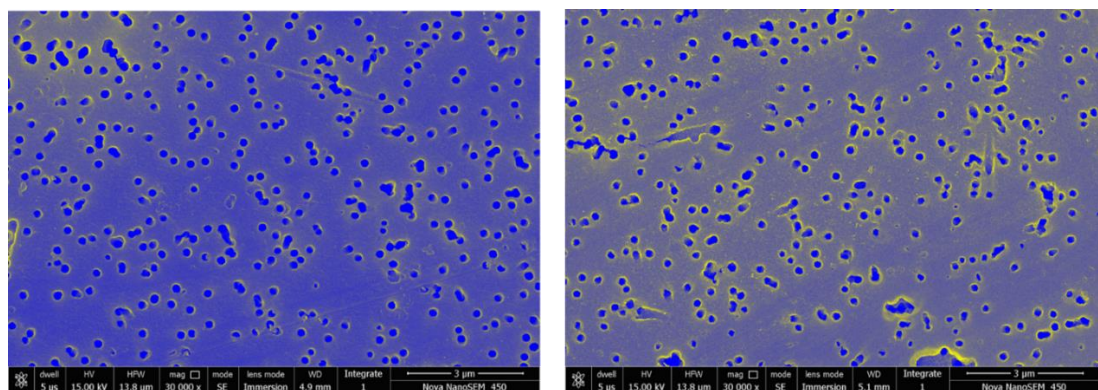


Figure 40: Scanning electron micrograph of 24 hours functionalized PET membrane (a) before Pd deposition (b) after Pd deposition for 6 hours.

Bright surface morphology gives a direct indication of more number of attached Pd nanoparticles. The bright boundary of pores also provides a sign of deposition of Pd

nanoparticles inside the pore wall. The size of Pd nanoparticles lies in the range of 6 ± 1 nm which was confirmed by TEM in our previous chapter. Probability of covering the complete pore is very less because the diameter of the pore was nearly 200 nm.

5.3.3 Permeability and Selectivity

The gas permeation measurements of all samples for H₂, N₂ and CO₂ were carried out with the help of a gas separation setup. The corresponding results of permeability and selectivity of H₂ are shown in table 9 and table 10, respectively. As H₂ has a smaller molecular diameter (2.89 Å) compared to CO₂ (3.3 Å) and N₂ (3.64 Å), that is why hydrogen has the highest diffusion rate and shows higher permeability for all samples as shown by figure 41 and figure 43.

Beside molecular diameter, other parameters like activation energy for diffusion, the activation energy for solubility and polarity of gases also affect the permeability of the porous membrane. For the comparison of CO₂ and N₂ permeability, CO₂ has a little bit lower permeability than N₂. It occurs because of the linear shape of CO₂ gas molecule and it requires higher activation energy to diffuse in comparison to the spherical shape of N₂. Also, CO₂ molecule has more polarity than the N₂ molecule.

Sample	PET	F3	F6	F12	F24	F3-Pd6	F6-Pd6	F12-Pd6	F24-Pd6
CO ₂	2827	2429	2411	2405	2275	2330	2187	2139	2129
N ₂	3747	3490	3733	3690	3607	3621	3515	3490	3465
H ₂	9478	9692	10832	10742	10653	11017	12047	12394	12890

Table 9: Permeability data for all functionalized and Pd deposited PET samples.

Sample	PET	F3	F6	F12	F24	F3-Pd6	F6-Pd6	F12-Pd6	F24-Pd6
H ₂ /CO ₂	3.35	3.99	4.49	4.47	4.68	4.73	5.51	5.79	6.05
H ₂ /N ₂	2.53	2.78	2.90	2.91	2.95	3.04	3.43	3.55	3.72

Table 10: Selectivity data for all functionalized and Pd deposited PET samples

As the functionalization time of the PET membranes increases, the permeability of CO₂ and N₂ shows a slight decrease and which improves the selectivity of H₂ as compared to other gases (figure 42). The selective H₂ gas permeability for a

functionalized PET was probably due to carbonyl functional groups; carboxylic acids contribute in H₂ bonding as in both situation H₂ acceptors and H₂ donors [174]. The maximum selectivity of H₂/CO₂ and H₂/N₂ was found 4.68 and 2.95, respectively.

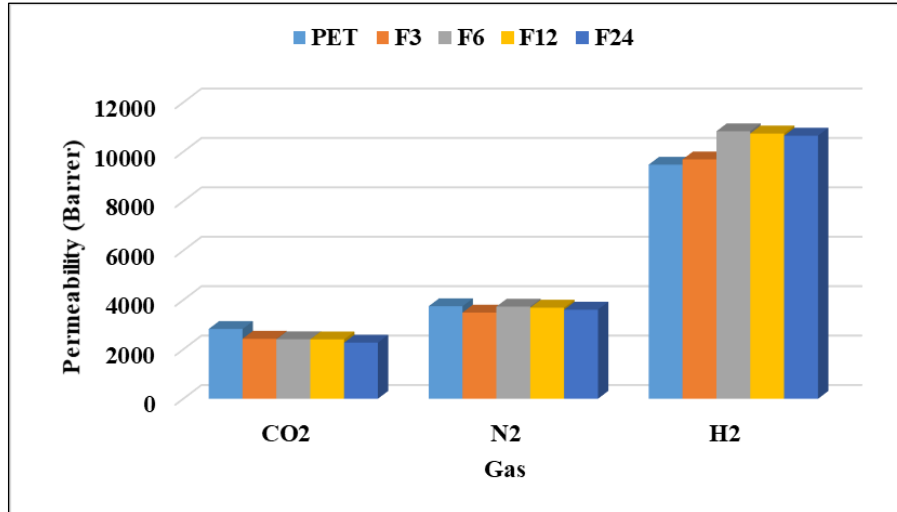


Figure 41: Graph of gas permeability for all functionalized samples.

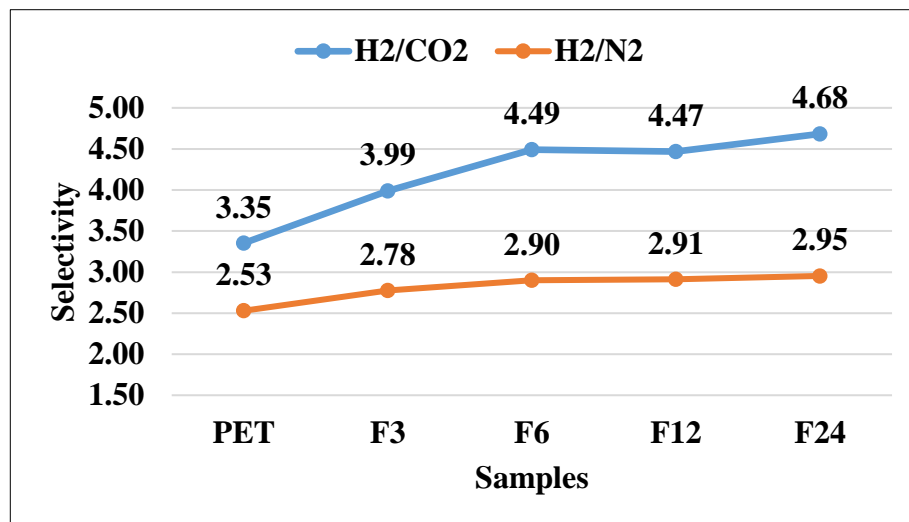


Figure 42: Selectivity data for functionalized samples

After the deposition of Pd nanoparticles for 6 hours in these samples, it is found improvement in the H₂ selectivity. This is because of Pd shows maximum absorption property for hydrogen. In contact with H₂, Pd lattice obtained two different phases α and β (sometimes called α'). In both state Pd lattice structure will be FCC, and H₂ atoms randomly occupy the octahedral void of the lattice [170,175,176]. At the low concentration of H₂ till PdH_{0.02}, Pd lattice occurs α phase and lattice expands slightly

from 3.889 Å to 3.895 Å. Above this concentration of H₂, β phase appears with a lattice constant of 4.025 Å. The absorption of H₂ is also reversible that means H₂ can rapidly diffuse through the Pd metal lattice.

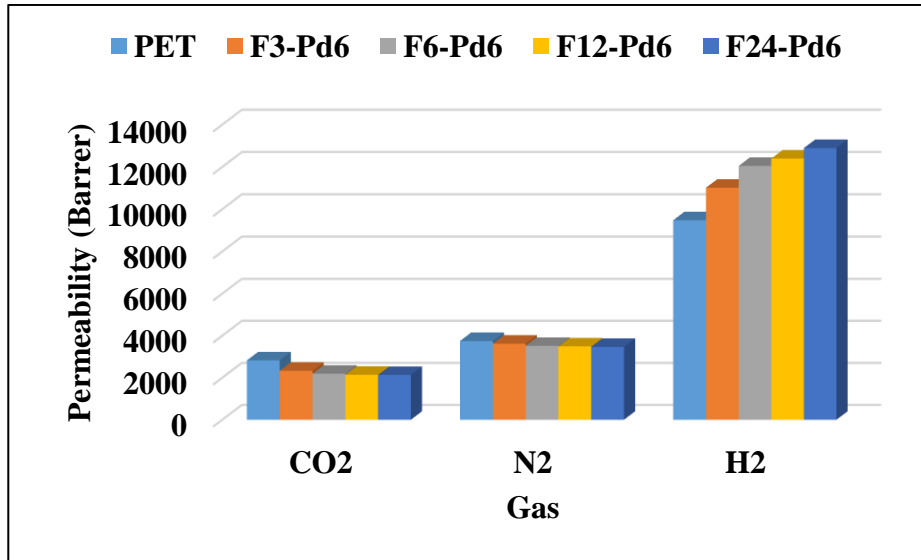


Figure 43: Graph of gas permeability for all functionalized Pd deposited samples

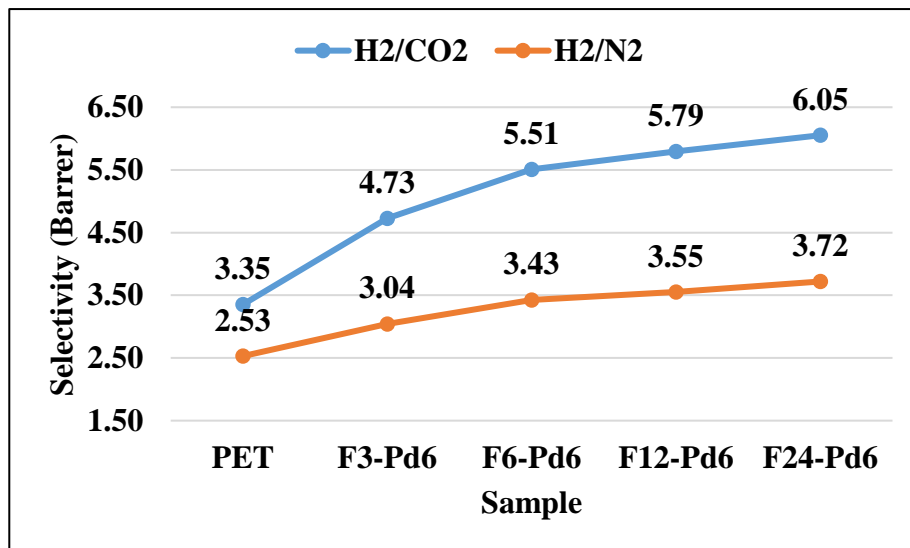


Figure 44: Selectivity data for all functionalized Pd deposited samples

Functionalization of the membrane provides more vacant space to attach nanoparticles within the pore as well as on surface. Due to this, both permeability and selectivity for H₂ in all Pd deposited sample found to be increased. From figure 44, the maximum selectivity in Pd deposited sample of H₂/CO₂ and H₂/N₂ was found 6.05 and

3.72, respectively. So for the hydrogen-selective and purification application Pd deposition pores membrane has played a significant role.

5.4 Conclusions

Functionalization with carboxylic groups of polymeric membranes can be an efficient way to modify the permeability and selectivity. It was concluded that functionalization of PET membrane affects the permeability of gases and increase the selectivity of H₂ with functionalization time in comparison with other gases. To fulfill our aim, selective deposition of Pd nanoparticles in pores PET membranes shows significant improvement in selectivity of hydrogen with considerable permeability. Maximum selectivity found 6.05 and 3.72 for H₂/CO₂ and H₂/N₂, respectively in maximum functionalized PET membrane with 6-hour deposition of Pd nanoparticles. Because of the improved permeability and selectivity, such type of membranes having functionalization and nanoparticles deposition can be used commercially in the application of H₂ separation and purification.

UV Functionalized PC Membranes

6.1 Introduction

To overcome problem with fossil fuels, it is necessary to explore new sustainable clean energy sources such as H₂ energy. New materials and methods are being developed for the hydrogen purification/separation. However, the membrane-based separation process is the advanced, reliable and low-cost with better results. Functionalization of the membrane is a technique to alter the polymeric membranes surface and molecular structure by providing the direct or indirect energy source. Use of gas sensitive nanoparticles with such functionalized membrane is a noble strategy in the sense of higher permeability and selectivity for a particular gas.

There are various functionalization methods available for polymeric surface, such as chemical, plasma, UV irradiation, ion irradiation etc. Out of these functionalization approaches, UV irradiation is one of the best approach due to its simplicity and controlled surface modification. Because of the outstanding interaction of the Pd with H₂ molecule, we select Pd nanoparticles for the H₂ separation over other nanoparticles like Platinum [177], Nickel [178], Titanium and metal Alloys [179,180] etc.

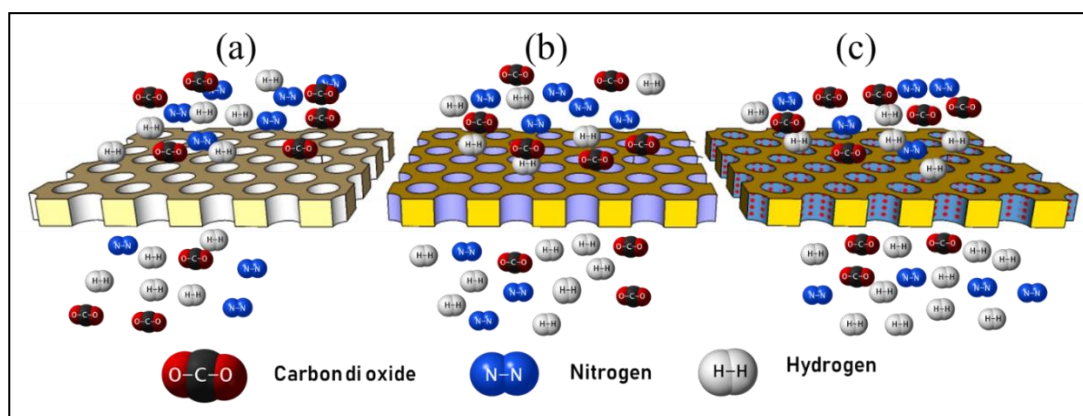


Figure 45: Schematic diagram of process Gas permeation through (a) Pristine PC membrane (b) UV irradiated PC membrane and (c) Pd Nanoparticles deposited in UV irradiated PC membrane.

In present chapter, functionalization of track-etched PC membranes have been carried out via UV-irradiation with time difference, and its effect on gas permeability and selectivity of H₂ over CO₂ and N₂ gases have been reported. Further, to enhance H₂

selectivity, Pd nanoparticles have deposited into the pores as well as on the surface of the PC membrane. We have also use Polyvinylpyrrolidone (PVP), which act as a binder for the Pd nanoparticles to improve the H₂ selectivity over other gases. These membranes show improved permeability and selectivity and can be used for H₂ separation. This method gives an opportunity to use these membranes with easy fabrication process and low cost for commercial use. The process followed for this study is briefly represented by the schematic diagram as shown in figure 45.

6.2 Experimental Details

6.2.1 Sample Preparation

Track-etched PC membranes having pore diameter of 0.1 μm are used for present work. For the Pd nanoparticles synthesis, chemical method is followed as described in the section 3.2.5. For the time-based UV irradiation process, UV lamp having the power of 25 Watt and approximately wavelength of 253 nm was used. It belongs to the C-region in the UV spectra. The samples were UV-irradiated for different intervals of time.

S. No.	Membrane (pore size)	UV irradiation time	Pd nanoparticles deposition time	Sample name	Symbol
1	PC (0.1 μm)	0	0	PC_0.1	S0
2	PC (0.1 μm)	36 hours	0	PC_0.1_UV_36	S1
3	PC (0.1 μm)	36 hours	24 hours	PC_0.1_UV_36 _Pd_24	S2
4	PC (0.1 μm)	36 hours	24 hours (with PVP)	PC_0.1_UV_36 _Pd_PVP_24	S3
5	PC (0.1 μm)	48 hours	0	PC_0.1_UV_48	S4
6	PC (0.1 μm)	48 hours	24 hours	PC_0.1_UV_48 _Pd_24	S5
7	PC (0.1 μm)	48 hours	24 hours (with PVP)	PC_0.1_UV_48 _Pd_PVP_24	S6

Table 11: Sample representation based on the UV irradiation time and Pd nanoparticles deposition time.

6.2.2 Characterization Details

For the Pd nanoparticles deposition process, UV-irradiated membranes kept for fixed time and volume in the Pd nanoparticles solution. During the time of deposition, it was also checked that the deposition of particles equally from both sides of membrane. For the use of PVP as a binder for Pd nanoparticles, we used a concentration of 0.001 gm/ml solution of PVP in Pd nanoparticles solution. The samples are listed as in the table 11 are based on the UV irradiation time, Pd nanoparticles deposition time and use of PVP.

For the gas permeability measurements, we have used the gas permeability setup for the H₂, N₂ and CO₂ gases and details of set up have been explained in section 3.3.6. Surface morphology of functionalized and Pd nanoparticles deposited membranes were studied by the FESEM. To analyze, the characteristic bonds of pristine PC and structural changes after the functionalization, FTIR was used in the range of 400 cm⁻¹ - 4000 cm⁻¹. Raman scattering spectra were recorded for all the samples on Raman spectroscopy having an excitation source laser of 785 nm and power intensity of 50 mW. The UV-Vis spectra confirmed carbonate bond cleavage phenomena by using the UV-Vis setup in the range of 300nm - 900 nm.

6.3 Results and Discussion

Electronic energy of the polymer molecule changes when the polymer irradiated in the UV region.

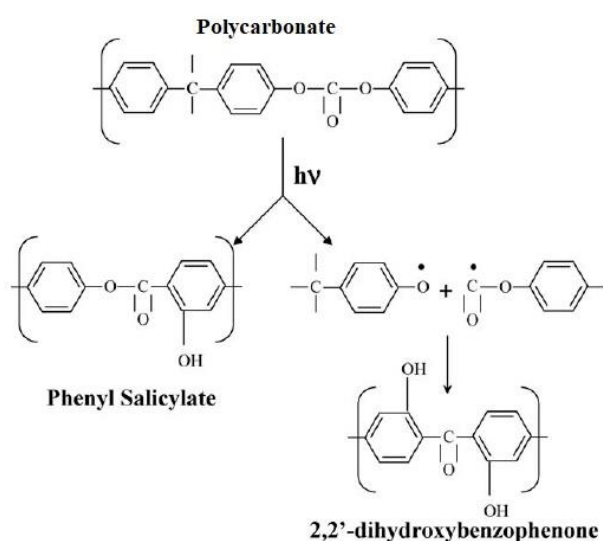


Figure 46: A schematic representation of the photo-degradation process

These electronic changes outcome in the form of physical and chemical changes. UV region has sufficient energy that it can split the molecules bonds of the polymer and be able to create free radicals [181]. In our case, when PC is irradiated by UV radiation, photo-degradation (bond splitting) phenomena arises. Photo-degradation can be understood by photo-fries rearrangement mechanism and it is well reported in the literature [182,183].

In UV region, the wavelength shorter than 350 nm have enough energy that can cleave or break the C-O bond from carbonate group in the PC molecular structure. The completion of the process is the formation of the phenyl free radicals. The free radicals can initiate further reactions such as crosslinking process, chain scission process. The schematic representation of the bond degradation process is shown in the figure 46. Carbonate group selectively absorbed the energy in the UV region and the process of the cross-linking continued by the small molecules. Irradiation of PC causes the aromatic carbonate unit to reorganize itself into dihydroxybenzophenone and phenylsalicylate derivatives. These free radicals are helpful in the improvement of H₂ selectivity over other gases. The UV irradiated PC membranes were analyzed by different characterization techniques.

6.3.1 UV-Visible Spectroscopy

The UV-Vis absorption spectroscopy measurements were done in the range of 200 nm - 900 nm for all the fabricated samples (S0 – S6). Samples S1, S2 and S3 have the irradiation time of 36 hours and the sample S4, S5 and S6 have the irradiation time of 48 hours.

Equal time of UV-irradiation of the sample leads the same amount of the photo-fries mechanism. Because of this sample S1, S2 and S3 have similar UV-Vis spectra and the sample S4, S5 and S6 and the similar UV-Vis spectra. So, we are comparing the fitted data of UV-Vis spectra for the un-irradiated sample S0 and irradiated samples S1 & S4 as shown in figure 47.

In the observed data of the UV-Vis spectra, two shoulder bands nearly 365 nm and 320 nm can be clearly seen in figure 47. The presence of both bands can be interpret by the photo-fries mechanism of the PC. These two bands most probably due to the $\pi - \pi^*$ (~320 nm) and $n - \pi^*$ (~365 nm) transmission of carbonyl group, respectively. The intensity of both the band's increases with the UV-irradiation time. This intensity

increment of the bands is a clear sign of higher bond-cleavage of carbonate group with UV-irradiation time. This is the reason for same time irradiated samples shows the same intensity of spectra. As the irradiation time increases the bond intensity enhanced due to high number of bond splitting phenomena.

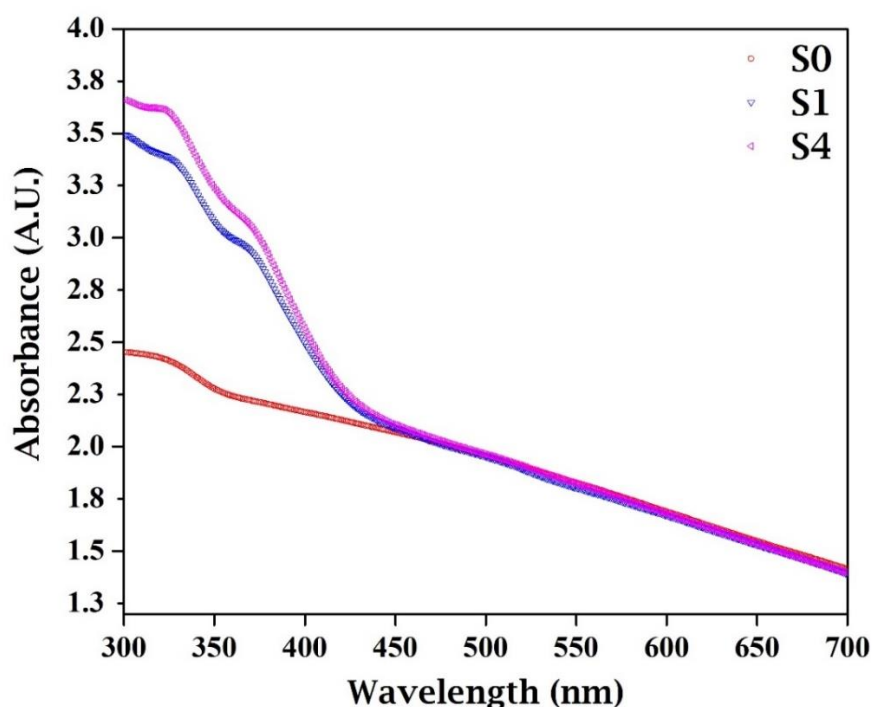


Figure 47: UV-Vis spectra for the sample S0, S1 and S4 in the range of 300-700 nm, those are resembled to the pristine PC, UV irradiated PC for 36 hours and UV irradiated PC for 48 hours respectively

6.3.2 Raman Spectroscopy

Figure 48 shows the Raman spectra of all the samples (S0 - S6) in the observed range of range of 500 cm^{-1} - 2000 cm^{-1} and all fundamental peaks of PC are present.

But there was small shift in the Raman frequencies of pristine PC membrane (S0) and UV-irradiated PC membrane samples (S1-S6). These shifts are due to change in the structure of surfaces for UV-irradiated membrane as compared to pristine PC.

Because there is no UV-irradiation on the pristine PC membranes, so the sample S0 remains in the actually structure of the PC. All the observed peak frequencies and corresponding bonds are presented in table 12. This shift or changes in frequency also show that the UV irradiation has small effect on Raman frequencies in the range of 2000 cm^{-1} - 4000 cm^{-1} .

Wavenumber (cm ⁻¹)	Type of Vibration
574, 634	Phenyl ring vibration
703,731	C-H out-of-plane bending
826	Phenyl ring vibration
886	O-C(O)-O stretching
918, 1109, 1146, 1177, 1234	C-O-C stretching
1005	C-H bending in-plane
1387,1441, 1462	CH ₃ deformation
1601	Phenyl ring vibration
1773	C=O stretching

Table 12: Raman peaks and corresponding bonds.

If we enlarge the region 2750-3150 cm⁻¹ as shown in figure 49, we observe the peaks at 2937 cm⁻¹ and 3071 cm⁻¹ shows intensity growth after the UV irradiation samples (S1-S6) as a result of the photo-fries process on the PC surface.

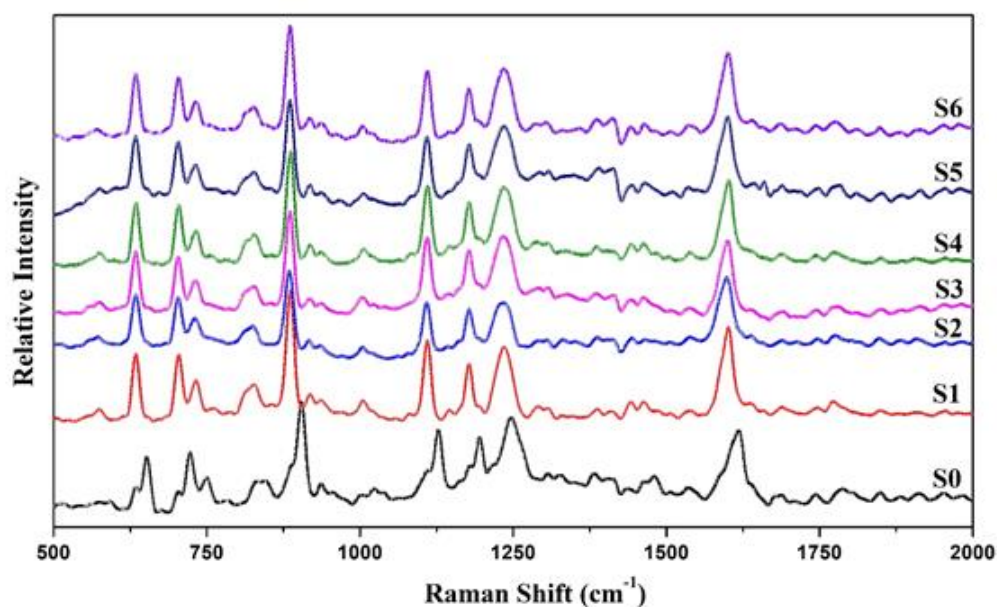


Figure 48: Raman spectra of all the samples (S0-S6) in the range of 500-2000 cm⁻¹.

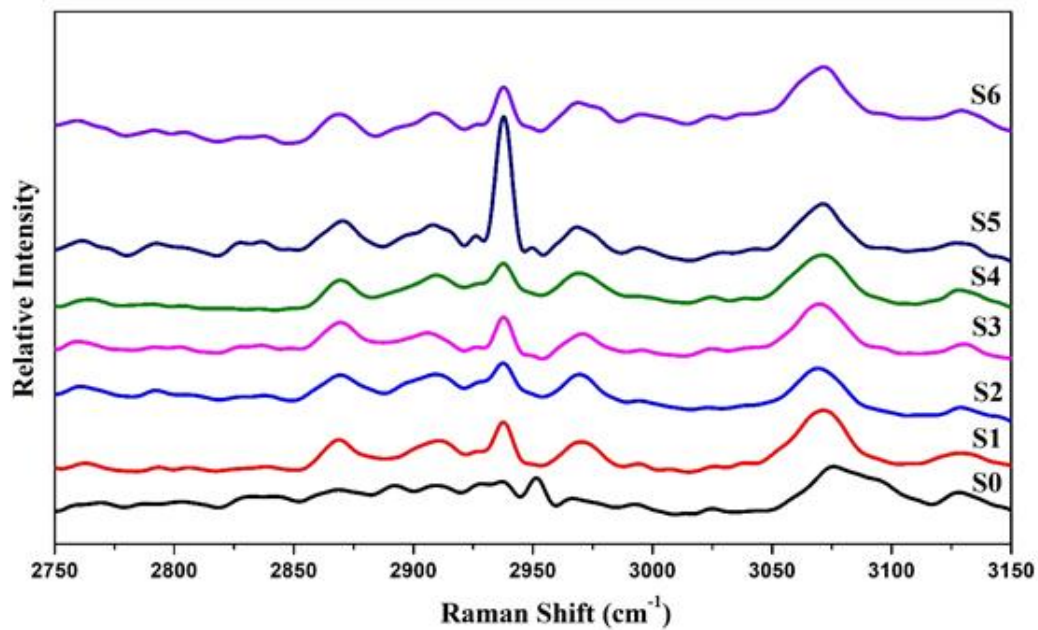


Figure 49: Raman spectra of all the samples (S0-S6) in the range of 2750-3150 cm^{-1} .

6.3.3 Fourier Transform Infrared Spectroscopy (FTIR)

Figure 50 shows the FTIR spectrum of all samples (S0-S6) in the range of 400 cm^{-1} - 4000 cm^{-1} .

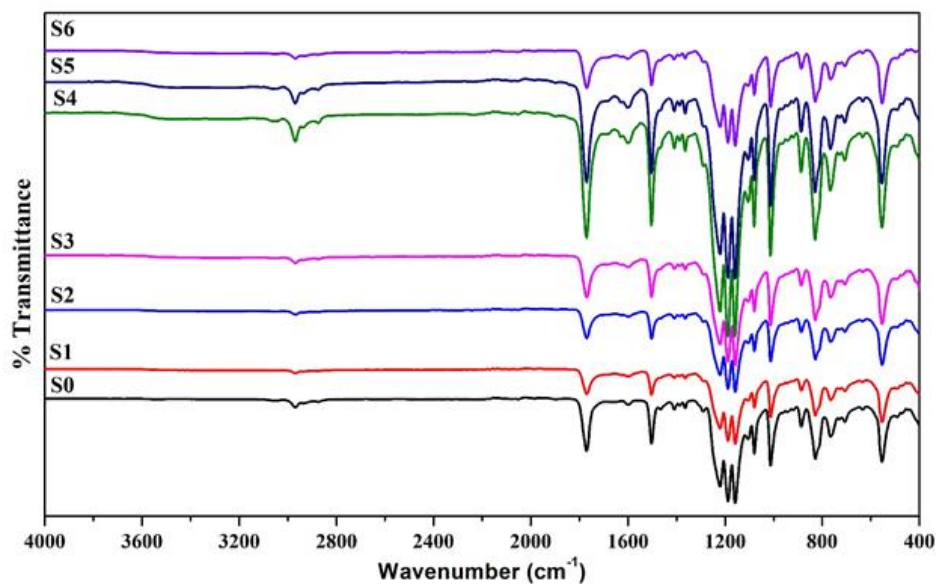


Figure 50: FTIR spectra of all the samples (S0-S6) in the range of 400 cm^{-1} - 3100 cm^{-1} .

All the peaks corresponding to elementary bonds of PC polymer [184,185]. For the analysis samples (S1-S6) are compared with the base sample of PC, S0. There was no remarkable shift in the spectra (400 cm^{-1} - 4000 cm^{-1}), but peaks related to carbonated group shows intensity variation. Peak at 2965 cm^{-1} is corresponding to C-H₃ stretching vibration, 1768 cm^{-1} corresponding to free carbonyl stretching motion and 1168 cm^{-1} represents C-O stretching from carbonyl group of PC.

When the UV irradiation time of samples is increased, a slight increment has been observed for both the peaks at 1768 cm^{-1} and 1168 cm^{-1} . These peaks are corresponding to the carbonyl group, and the increment is due to enhancement in stretching of the C-O bond. Also, the absorption peak around 2965 cm^{-1} associated with C-H stretching arises due to UV irradiation. It means that when the samples have been exposed to UV light, then bond formation takes place due to the photo-fries mechanism. UV irradiation generate the changes in the PC surface as well as the molecular structure, which is responsible for the variation in carbonate (1780 cm^{-1}) to phenylene (1520 cm^{-1}) intensity ratio.

6.3.4 Scanning Electron Microscopy (SEM)

The morphological study of the samples was done with the help of SEM and obtained SEM images are shown in the figure 51.

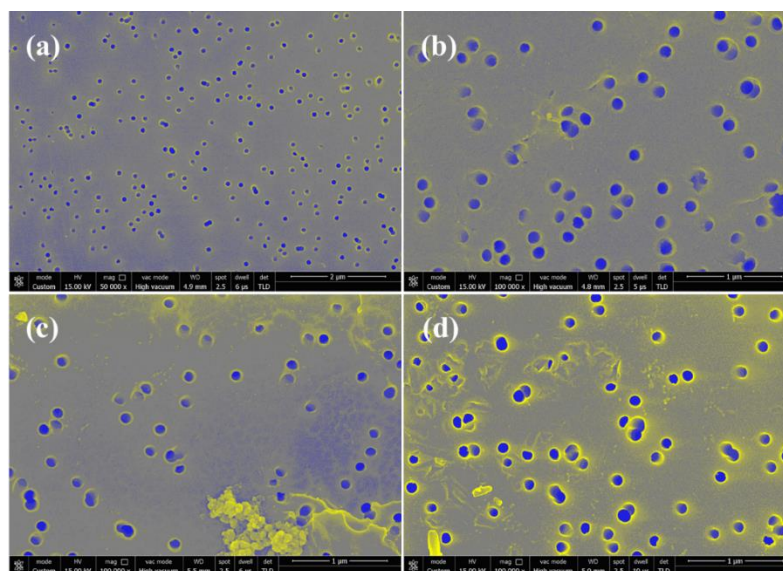


Figure 51: Scanning electron microscope (SEM) of the sample (a) Pristine PC (S0) (b) UV irradiated for 48 hours (S4) (c) UV irradiated for 48 hours with deposition of Pd Nanoparticles for 24 hours (S5) (d) UV irradiated for 48 hours with deposition of Pd nanoparticles

The morphological study of the samples was done with the help of SEM and obtained SEM images are shown in the figure 51. From the SEM images, it is clear that the average pore size of all the sample is approximately 0.1 μm . These membranes were dipped in Pd nanoparticle solution, and there is very less possibility to cover the pore by the Pd nanoparticles because the Pd nanoparticle size in the range of 6 ± 1 nm and pore size is 0.1 μm . In the SEM images, bright points (yellowish) indicates the number of Pd nanoparticles on the surface as well as in pores. In the figure 51(C), it can be seen that the Pd nanoparticles are in the pores as well as on the surface too. However, the clustering of Pd nanoparticles on the surface of membranes as well as in pores can be controlled by using the PVP as binder.

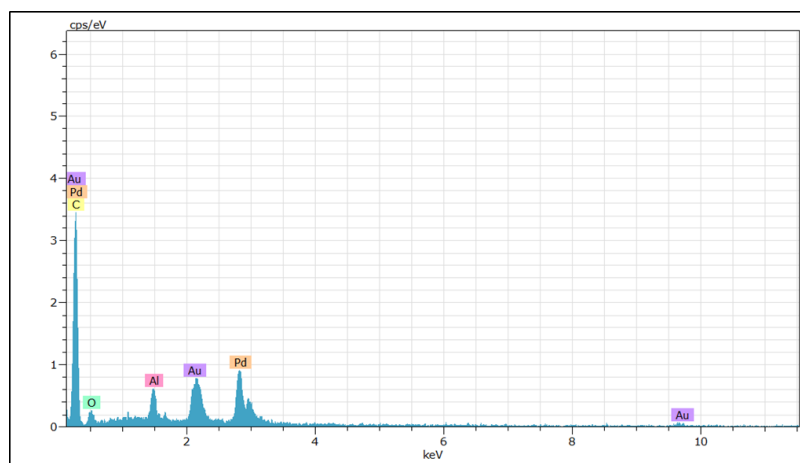


Figure 52: Energy Dispersive Spectroscopy (EDS) spectra of the Sample S2 for the confirmation of palladium (Pd) NP's.

From the figure 51(d), it can be observed that when PVP is used with Pd nanoparticles, there is minimum clustering on the surface and as a result, the surface, as well as the pores boundary have enhanced brightness in sample S6 with uniform distribution of nanoparticles. Energy-dispersive X-ray spectroscopy (EDS) spectra of sample S2 also confirms the existence of Pd (figure 52). So using PVP binder with Pd nanoparticles is an effective way to have maximum attachment of nanoparticles on polymer surface as well as in pores.

6.3.5 Permeability and Selectivity

For the gas separation application, we used H_2 , N_2 and CO_2 gases to examine the gas permeability and selectivity for all the samples. The obtained data of the gas permeability are shown in figure 53 and figure 54. It is evident from the gas permeability

measurements, H₂ shows the maximum permeability because of the smallest molecular size in comparison to the other two gases (N₂ & CO₂).

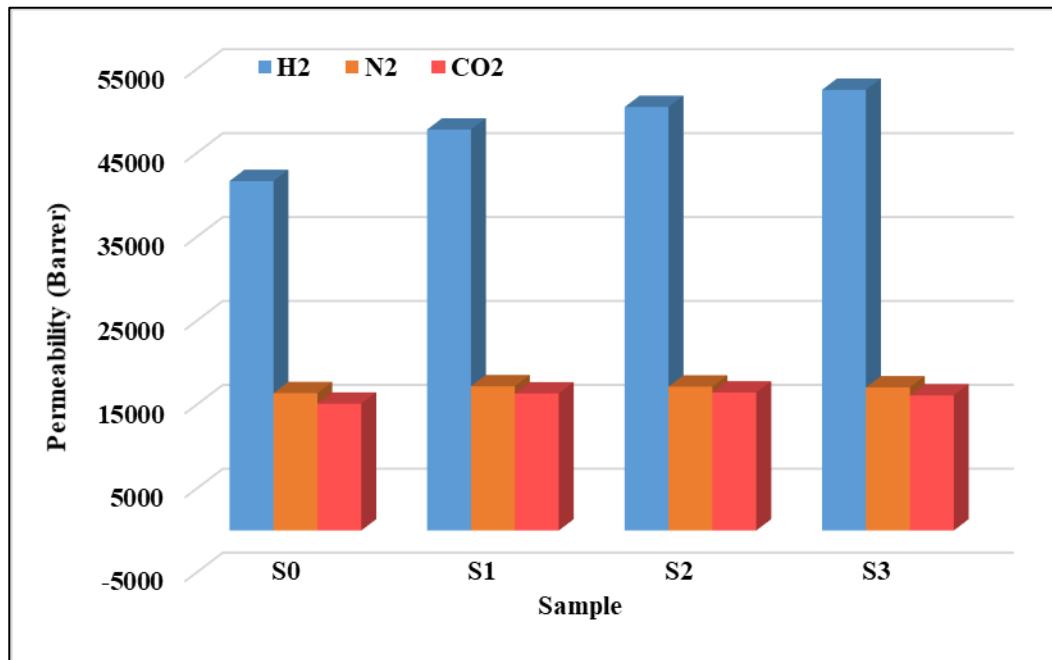


Figure 53: Graph of the gas permeability data for the samples (S0 - S3). S0 is for the without UV irradiation pristine PC and S1-S3 samples having the UV irradiation time of 36 hours.

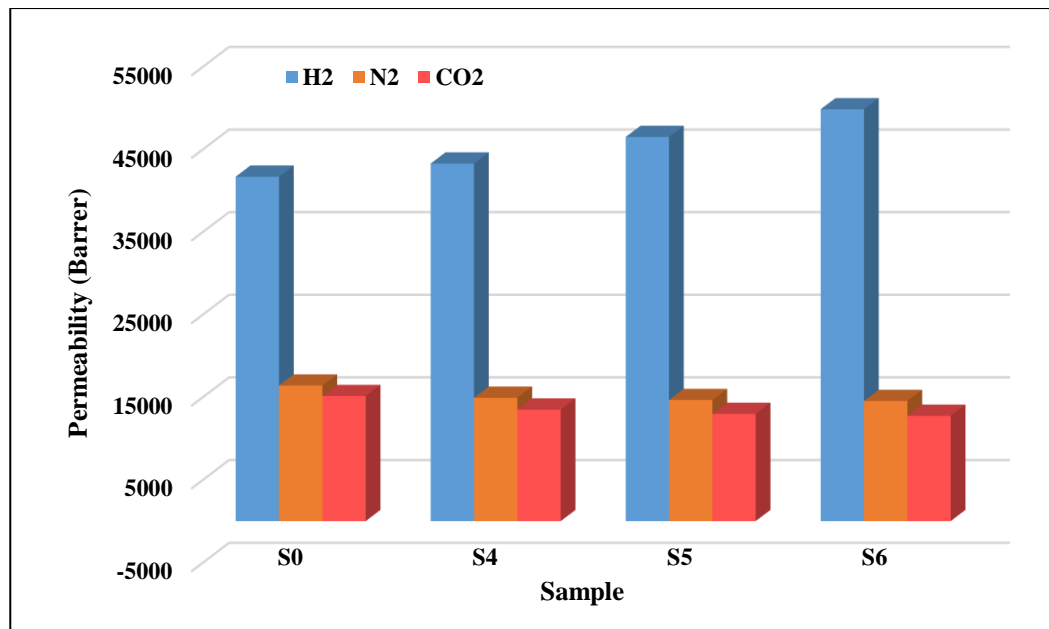


Figure 54: Graph of the gas permeability data for the samples (S0, S4 – S6). S0 is for the without UV irradiation pristine PC and S4-S6 samples having the UV irradiation time of 48 hours.

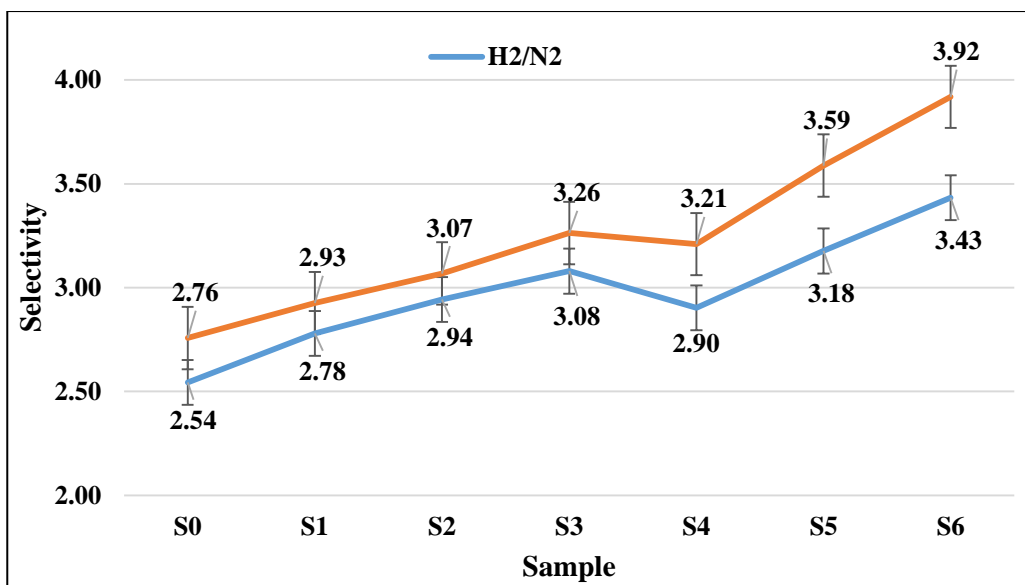


Figure 55: Graph of selectivity data of H₂ over CO₂ and N₂ for all the samples (S0-S6).

Along with the molecular size other factors like gas molecule interaction with the surface, action energy and diffusion rate in the polymeric medium, all are favorable for the higher permeation of H₂ gas. The spherical shape of H₂ molecules as well helps in the higher permeability rate than N₂ and CO₂. In the contrast of CO₂ and N₂, CO₂ has smaller molecular (3.30 Å) size than N₂ (3.64 Å). But because of the linear shape gas molecule of CO₂ requires more activation energy for diffusion through pores membrane than N₂ gas molecules, which front-runners for CO₂ to lower permeation compared to N₂.

The UV-irradiation process of the membrane increases the number of free radicals/group on the surface as well as on inner pore walls. These free groups are continuously ready to accept the H₂ molecules as according to the functionalize mechanism. In the presence of pressure gradient of H₂, group donates or transport H₂ to the next group or molecule of polymer in the low concentration zone of H₂. Such action of these free group increases the permeability of H₂. But for N₂ and CO₂ these group works as obstacle. So, there was not effective increment or decrement found in the CO₂ and N₂ permeability in all the samples. Comparison of only UV irradiated sample S1 and S4 the selectivity H₂/N₂ and H₂/CO₂ is higher (figure 55) in the S4 because of the more time UV-irradiation (48 hours). In the next stage of the sample series, we deposited Pd nanoparticles in the UV-irradiated samples (S2, S5) without PVP and (S3, S6) with PVP. Pd nanoparticles have supreme absorption property of H₂ due to its lattice structure. With

a low concentration of H₂, Pd shows α phase and β phases obtained with high concentration. Due to face centred cubic (FCC) structure of Pd and the octahedral void of the FCC lattice is perfect place to grip the H₂ because of its smaller molecular size. The absorption phenomena also reversible, means diffusion of H₂ through lattice will be higher if there was temperature/pressure gradient is available. So in our case, we use pressure gradient, so that why all the Pd deposited samples shows the higher permeability and selectivity of hydrogen.

The UV irradiation of the samples improves the attachment of Pd Nanoparticles with membrane compare to pristine sample. More attachment of Pd Nanoparticles with PC membrane is responsible for higher permeability and selectivity H₂. On the same pattern for more attachment of Pd nanoparticles with polymer, we used PVP with Pd nanoparticles solution, which works as a binder for nanoparticles. Use of binder increase the numbers of Pd nanoparticles attached with PC membranes. The maximum UV irradiation time and highest number of Pd nanoparticles in sample S6 we found the highest permeability of H₂. Also the maximum selectivity found in sample S6 for H₂/N₂ and H₂/CO₂, 3.43 and 3.92 respectively.

6.4 Conclusions

The permeability and selectivity of the gases through the polymeric membrane can be controlled by UV irradiation process and selective deposition of nanoparticles. It was concluded from obtained results that with increase in UV irradiation time the attachment of Pd nanoparticles greater. Better attachment of the nanoparticles directed the higher selectivity of H₂. Use of a binder with the polymeric membrane is an important factor for the Pd nanoparticles attachment. Maximum selectivity was found 3.43 and 3.92 for H₂/N₂ and H₂/CO₂, respectively in sample S6. We have faith in the fact that such kind of the membrane has potential use in the field of the gas separation and purification. And UV irradiation process over polymeric membranes to modify the surface and molecular structure.

Conclusions and Future Scope of the Work

7.1 Conclusions

The present thesis represents the gas separation of engineered nanochannels and functionalized porous polymeric membranes by different methods for the fabrication of H₂ gas selective membrane. The following conclusions are made on the basis of the studies carried out:

- ✓ Membrane-based gas separation always face the trade-off relation problem between the permeability and the selectivity. That means as the permeability of gases increases the selectivity of the gases decreases and vice versa. To overcome this issue, our objectives are focused to enhance H₂ permeability as well as selectivity by using functionalized porous polymeric membranes.
- ✓ Porous polymeric composite membranes of chemically functionalised MWCNTs and PC successfully fabricated by using solution cast method. Different orientation of MWCNTs were obtained by the help of high magnetic field. It was found that aligned orientation of the MWCNTs have higher permeability and selectivity as compared to random orientated MWCNTs.
- ✓ Functionalization is a well-known tool to alter the nonomaterials /polymeric membranes surface and molecular structure of the polymer. We can modify a specific property of the membrane as according to our required application. So we used different type of functionalization process for the membranes to alter the permeability and selectivity of the porous polymeric membranes.
- ✓ Functionalization of MWCNTs plays a significant role to control the permeability and selectivity in comparison to pristine MWCNTs.

- ✓ Functionalization of PET membrane affects the permeability of gases and increase the selectivity of H₂ with functionalization time in comparison to other gases.
- ✓ Pd have maximum absorption properties for the H₂, so Pd nanoparticles have used as a gas (H₂) sensitive material.
- ✓ To accomplish the trade-off relation between permeability and selectivity, PET membranes having Pd nanoparticles in their pores as well as on surface shows enhanced selectivity of H₂ with considerable permeability. Maximum selectivity was found 6.05 and 3.72 for H₂/CO₂ and H₂/N₂ respectively in maximum functionalized PET membrane with 6-hour deposition of Pd nanoparticles.
- ✓ UV-irradiation process is a low cost and effective process for the functionalization of porous PC membranes. It was found that with increasing the UV-irradiation time, permeability and selectivity has increased considerably and also it binds more number of Pd nanoparticles as compared to pristine PC membrane.
- ✓ Use of PVP as a binder for Pd nanoparticles with the membrane found effective for controlling the gas permeability and selectivity. 48 hours UV irradiated functionalized and 24 hours Pd deposited PC membranes shows the maximum selectivity for the H₂ with the significant permeability.

So, based on the above finding, we have faith in the fact that such kind of functionalized polymeric membrane and use of gas sensitive materials with them have potential use in the field of the gas separation and purification. Such membranes can be used to develop hydrogen-selective nanofilters.

7.2 Future Scope of the Work

Although, plenty of work has been carried out on the functionalized porous polymeric membrane for H₂ gas separation. Based on the findings in the present work, future scope of the work can be proposed as follows:

- ✓ Besides CNT's, composite membranes of the other carbon nanomaterials such as graphene, reduced graphene oxide etc. can be functionalized and may be used for the H₂ selective gas separation applications.
- ✓ Other functionalization methods can be explored for the better functionalization of the membranes and attachment of gas sensitive nanomaterials.
- ✓ Due to the limitation of the SHI process for track-etched membranes, another highly porous membranes may be useful for the gas separation application.
- ✓ Graft polymerisation method can be carried out in future, through which we can control the gas sensitive properties of the membrane during the sample synthesis process.
- ✓ Other gas sensitive materials such as core-shell, bimetallic and ion implanted materials may be useful for the gas separation application.

So, the use of membrane-based H₂ separation applications will be beneficial for the future energy solution of world energy crises and the pollution problems.

References

- [1] Ockwig NW, Nenoff TM. Membranes for Hydrogen Separation 2007;107:4078–110. doi:10.1021/cr0501792.
- [2] Thomas C., James BD, Lomax FD, Kuhn IF. Fuel options for the fuel cell vehicle: hydrogen, methanol or gasoline? *Int J Hydrogen Energy* 2000;25:551–67. doi:10.1016/S0360-3199(99)00064-6.
- [3] Isfahani SNR, Sedaghat A. A hybrid micro gas turbine and solid state fuel cell power plant with hydrogen production and CO2 capture. *Int J Hydrogen Energy* 2016;41:9490–9. doi:https://doi.org/10.1016/j.ijhydene.2016.04.065.
- [4] Fernández RÁ, Cilleruelo FB, Martínez IV. A new approach to battery powered electric vehicles: A hydrogen fuel-cell-based range extender system. *Int J Hydrogen Energy* 2016;41:4808–19. doi:https://doi.org/10.1016/j.ijhydene.2016.01.035.
- [5] Chen Y-H, Chen C-Y, Lee S-C. Technology forecasting and patent strategy of hydrogen energy and fuel cell technologies. *Int J Hydrogen Energy* 2011;36:6957–69. doi:10.1016/J.IJHYDENE.2011.03.063.
- [6] Dicks AL. Hydrogen generation from natural gas for the fuel cell systems of tomorrow. *J Power Sources* 1996;61:113–24. doi:https://doi.org/10.1016/S0378-7753(96)02347-6.
- [7] Yilanci A, Dincer I, Ozturk HK. A review on solar-hydrogen/fuel cell hybrid energy systems for stationary applications. *Prog Energy Combust Sci* 2009;35:231–44. doi:10.1016/J.PECS.2008.07.004.
- [8] Castel C, Favre E. Membrane separations and energy efficiency. *J Memb Sci* 2018;548:345–57. doi:https://doi.org/10.1016/j.memsci.2017.11.035.
- [9] Pandey P, Chauhan RS. Membranes for gas separation. *Prog Polym Sci* 2001;26:853–93. doi:10.1016/S0079-6700(01)00009-0.
- [10] HAMID SBEEBOAABD. Membrane-based Gas Separation: Principle, Applications and Future Potential 2014.

- [11] Ockwig NW, Nenoff TM. Membranes for hydrogen separation. *Chem Rev* 2007;107:4078–110.
- [12] Yampolskii Y. Polymeric Gas Separation Membranes. *Macromolecules* 2012;45:3298–311. doi:10.1021/ma300213b.
- [13] Sanders DF, Smith ZP, Guo R, Robeson LM, McGrath JE, Paul DR, et al. Energy-efficient polymeric gas separation membranes for a sustainable future: A review. *Polymer (Guildf)* 2013;54:4729–61. doi:10.1016/J.POLYMER.2013.05.075.
- [14] Denny Kamaruddin H, Koros WJ. Some observations about the application of Fick's first law for membrane separation of multicomponent mixtures. *J Memb Sci* 1997;135:147–59. doi:https://doi.org/10.1016/S0376-7388(97)00142-7.
- [15] Javaid A. Membranes for solubility-based gas separation applications. *Chem Eng J* 2005;112:219–26. doi:https://doi.org/10.1016/j.cej.2005.07.010.
- [16] Rahimpour MR, Samimi F, Babapoor A, Tohidian T, Mohebi S. Palladium membranes applications in reaction systems for hydrogen separation and purification: A review. *Chem Eng Process Process Intensif* 2017;121:24–49. doi:https://doi.org/10.1016/j.cep.2017.07.021.
- [17] Wijmans JG, Baker RW. The solution-diffusion model: a review. *J Memb Sci* 1995;107:1–21. doi:https://doi.org/10.1016/0376-7388(95)00102-1.
- [18] Zito PF, Caravella A, Brunetti A, Drioli E, Barbieri G. Knudsen and surface diffusion competing for gas permeation inside silicalite membranes. *J Memb Sci* 2017;523:456–69.
- [19] Wijmans JG, Baker RW. The solution-diffusion model: a review. *J Memb Sci* 1995;107:1–21.
- [20] Wijmans JGH, Baker RW. *The Solution-Diffusion Model: A Unified Approach to Membrane Permeation*. Mater. Sci. Membr. Gas Vap. Sep., Chichester, UK: John Wiley & Sons, Ltd; 2006, p. 159–89. doi:10.1002/047002903X.ch5.
- [21] Ismail AF, Rana D, Matsuura T, Foley HC. Carbon-based Membranes for Separation Processes. *Carbon-Based Membr ...* 2011:17–27. doi:10.1007/978-0-387-78991-0.

- [22] Ma X, Swaidan R, Teng B, Tan H, Salinas O, Litwiller E, et al. Carbon molecular sieve gas separation membranes based on an intrinsically microporous polyimide precursor. *Carbon N Y* 2013;62:88–96. doi:<https://doi.org/10.1016/j.carbon.2013.05.057>.
- [23] Liu Q, Gupta KM, Xu Q, Liu G, Jin W. Gas permeation through double-layer graphene oxide membranes: The role of interlayer distance and pore offset. *Sep Purif Technol* 2019;209:419–25. doi:<https://doi.org/10.1016/j.seppur.2018.07.044>.
- [24] Zhang W, Gaggl M, Gluth GJG, Behrendt F. Gas separation using porous cement membrane. *J Environ Sci* 2014;26:140–6. doi:[https://doi.org/10.1016/S1001-0742\(13\)60389-7](https://doi.org/10.1016/S1001-0742(13)60389-7).
- [25] Jones CW, Koros WJ. Carbon molecular sieve gas separation membranes-I. Preparation and characterization based on polyimide precursors. *Carbon N Y* 1994;32:1419–25. doi:10.1016/0008-6223(94)90135-X.
- [26] Isfahani SNR, Sedaghat A, Ma S, Sun D, Wang X Sen, Zhou HC, et al. Functionalization of a polymer using nanoparticles immobilized in supercritical carbon dioxide. *Int J Hydrogen Energy* 2015;41:59–64. doi:10.1143/JJAP.48.06FF13.
- [27] Liu J, Wei J. Knudsen diffusion in channels and networks. *Chem Eng Sci* 2014;111:1–14. doi:<https://doi.org/10.1016/j.ces.2014.01.014>.
- [28] Zito PF, Caravella A, Brunetti A, Drioli E, Barbieri G. Discrimination among gas translation, surface and Knudsen diffusion in permeation through zeolite membranes. *J Memb Sci* 2018;564:166–73. doi:<https://doi.org/10.1016/j.memsci.2018.07.023>.
- [29] Damle AS, Gangwal SK, Venkataraman VK. Carbon membranes for gas separation: Developmental studies. *Gas Sep Purif* 1994;8:137–47. doi:[https://doi.org/10.1016/0950-4214\(94\)80024-3](https://doi.org/10.1016/0950-4214(94)80024-3).
- [30] Jose AJ, Kappen J, Alagar M. 2 - Polymeric membranes: Classification, preparation, structure physiochemical, and transport mechanisms. In: Thomas S, Balakrishnan P, Sreekala MSBT-FBP, editors. Woodhead Publ. Ser. Biomater.,

Woodhead Publishing; 2018, p. 21–35. doi:<https://doi.org/10.1016/B978-0-08-102194-1.00002-5>.

- [31] Ng LY, Mohammad AW, Leo CP, Hilal N. Polymeric membranes incorporated with metal/metal oxide nanoparticles: A comprehensive review. *Desalination* 2013;308:15–33. doi:<https://doi.org/10.1016/j.desal.2010.11.033>.
- [32] De Falco M, Salladini A, Palo E, Iaquaniello G. Reformer and membrane modules (RMM) for methane conversion powered by a nuclear reactor. *Nucl. Power-Deployment, Oper. Sustain., InTech*; 2011.
- [33] Bakhtiari O, Sadeghi N. Mixed matrix membranes' gas separation performance prediction using an analytical model. *Chem Eng Res Des* 2015;93:710–9. doi:<https://doi.org/10.1016/j.cherd.2014.06.013>.
- [34] Shimekit B, Mukhtar H, Murugesan T. Prediction of the relative permeability of gases in mixed matrix membranes. *J Memb Sci* 2011;373:152–9. doi:<https://doi.org/10.1016/j.memsci.2011.02.038>.
- [35] Carreon M, Dahe G, Feng J, Venna SR. Mixed Matrix Membranes for Gas Separation Applications. *Membr. Gas Sep., vol. Volume 1, World Scientific*; 2016, p. 1–57. doi:[doi:10.1142/9789813207714_0001](https://doi.org/10.1142/9789813207714_0001).
- [36] Wang M, Wang Z, Zhao S, Wang J, Wang S. Recent advances on mixed matrix membranes for CO₂ separation. *Chinese J Chem Eng* 2017;25:1581–97. doi:<https://doi.org/10.1016/j.cjche.2017.07.006>.
- [37] Sadykov VA, Krasnov A V, Fedorova YE, Lukashevich AI, Bepalko YN, Eremeev NF, et al. Novel nanocomposite materials for oxygen and hydrogen separation membranes. *Int J Hydrogen Energy* 2018. doi:<https://doi.org/10.1016/j.ijhydene.2018.02.182>.
- [38] Dolan MD. Non-Pd BCC alloy membranes for industrial hydrogen separation. *J Memb Sci* 2010;362:12–28. doi:<https://doi.org/10.1016/j.memsci.2010.06.068>.
- [39] Dolan MD, Dave NC, Ilyushechkin AY, Morpeth LD, McLennan KG. Composition and operation of hydrogen-selective amorphous alloy membranes. *J Memb Sci* 2006;285:30–55. doi:<https://doi.org/10.1016/j.memsci.2006.09.014>.
- [40] Lin R-B, Xiang S, Xing H, Zhou W, Chen B. Exploration of porous metal–organic

- frameworks for gas separation and purification. *Coord Chem Rev* 2019;378:87–103. doi:<https://doi.org/10.1016/j.ccr.2017.09.027>.
- [41] Li B, Wen H-M, Yu Y, Cui Y, Zhou W, Chen B, et al. Nanospace within metal–organic frameworks for gas storage and separation. *Mater Today Nano* 2018;2:21–49. doi:<https://doi.org/10.1016/j.mtnano.2018.09.003>.
- [42] Bepalko Y, Sadykov V, Ereemeev N, Skryabin P, Krieger T, Sadovskaya E, et al. Synthesis of tungstates/Ni_{0.5}Cu_{0.5}O nanocomposite materials for hydrogen separation cermet membranes. *Compos Struct* 2018;202:1263–74. doi:<https://doi.org/10.1016/j.compstruct.2018.06.004>.
- [43] David E, Kopac J. Development of palladium/ceramic membranes for hydrogen separation. *Int J Hydrogen Energy* 2011;36:4498–506. doi:<https://doi.org/10.1016/j.ijhydene.2010.12.032>.
- [44] Malzbender J. Mechanical aspects of ceramic membrane materials. *Ceram Int* 2016;42:7899–911. doi:<https://doi.org/10.1016/j.ceramint.2016.02.136>.
- [45] Thakkar H, Lawson S, Rownaghi AA, Rezaei F. Development of 3D-printed polymer-zeolite composite monoliths for gas separation. *Chem Eng J* 2018;348:109–16. doi:<https://doi.org/10.1016/j.cej.2018.04.178>.
- [46] Gao H, Lin YS, Li Y, Zhang B. Chemical stability and its improvement of palladium-based metallic membranes. *Ind Eng Chem Res* 2004;43:6920–30.
- [47] Paglieri SN, Way JD. INNOVATIONS IN PALLADIUM MEMBRANE RESEARCH. *Sep Purif Methods* 2002;31:1–169. doi:10.1081/SPM-120006115.
- [48] Patel AK, Acharya NK. Metal coated and nanofiller doped polycarbonate membrane for hydrogen transport. *Int J Hydrogen Energy* 2018;43:21675–82. doi:<https://doi.org/10.1016/j.ijhydene.2018.03.205>.
- [49] Moss TS, Peachey NM, Snow RC, Dye RC. Multilayer metal membranes for hydrogen separation. *Int J Hydrogen Energy* 1998;23:99–106. doi:[https://doi.org/10.1016/S0360-3199\(97\)00030-X](https://doi.org/10.1016/S0360-3199(97)00030-X).
- [50] Ward TL, Dao T. Model of hydrogen permeation behavior in palladium membranes. *J Memb Sci* 1999;153:211–31.

- [51] Ghasemzadeh K, Sadati Tilebon SM, Basile A. Chapter 10 - Silica Membranes Application for Hydrogen Separation. In: Basile A, Ghasemzadeh KBT-CT and FD on (Bio-) M, editors., Elsevier; 2017, p. 243–64. doi:<https://doi.org/10.1016/B978-0-444-63866-3.00010-8>.
- [52] Nwogu NC, Anyanwu EE, Gobina E. An initial investigation of a nano-composite silica ceramic membrane for hydrogen gas separation and purification. *Int J Hydrogen Energy* 2016;41:8228–35. doi:<https://doi.org/10.1016/j.ijhydene.2015.11.162>.
- [53] Verweij H. Ceramic membranes: morphology and transport. *J Mater Sci* 2003;38:4677–95.
- [54] Khatib SJ, Oyama ST. Silica membranes for hydrogen separation prepared by chemical vapor deposition (CVD). *Sep Purif Technol* 2013;111:20–42. doi:<https://doi.org/10.1016/j.seppur.2013.03.032>.
- [55] Kosinov N, Gascon J, Kapteijn F, Hensen EJM. Recent developments in zeolite membranes for gas separation. *J Memb Sci* 2016;499:65–79. doi:<https://doi.org/10.1016/j.memsci.2015.10.049>.
- [56] Wee S-L, Tye C-T, Bhatia S. Membrane separation process—Pervaporation through zeolite membrane. *Sep Purif Technol* 2008;63:500–16. doi:<https://doi.org/10.1016/j.seppur.2008.07.010>.
- [57] Koohsaryan E, Anbia M. Nanosized and hierarchical zeolites: A short review. *Chinese J Catal* 2016;37:447–67. doi:[https://doi.org/10.1016/S1872-2067\(15\)61038-5](https://doi.org/10.1016/S1872-2067(15)61038-5).
- [58] Ismail AF, David LIB. A review on the latest development of carbon membranes for gas separation. *J Memb Sci* 2001;193:1–18. doi:[https://doi.org/10.1016/S0376-7388\(01\)00510-5](https://doi.org/10.1016/S0376-7388(01)00510-5).
- [59] Hamm JBS, Ambrosi A, Griebeler JG, Marcilio NR, Tessaro IC, Pollo LD. Recent advances in the development of supported carbon membranes for gas separation. *Int J Hydrogen Energy* 2017;42:24830–45. doi:[10.1016/J.IJHYDENE.2017.08.071](https://doi.org/10.1016/J.IJHYDENE.2017.08.071).
- [60] Haider S, Lindbråthen A, Lie JA, Hägg M-B. Regenerated cellulose based carbon

membranes for CO₂ separation: Durability and aging under miscellaneous environments. *J Ind Eng Chem* 2018. doi:<https://doi.org/10.1016/j.jiec.2018.10.037>.

- [61] Iijima S. Helical microtubules of graphitic carbon. *Nature* 1991;354:56.
- [62] Iijima S, Ichihashi T. Single-shell carbon nanotubes of 1-nm diameter. *Nature* 1993;363:603.
- [63] Kholmanov I, Kim J, Ou E, Ruoff RS, Shi L. Continuous Carbon Nanotube–Ultrathin Graphite Hybrid Foams for Increased Thermal Conductivity and Suppressed Subcooling in Composite Phase Change Materials. *ACS Nano* 2015;9:11699–707. doi:10.1021/acs.nano.5b02917.
- [64] Tersoff J, Ruoff RS. Structural Properties of a Carbon-Nanotube Crystal. *Phys Rev Lett* 1994;73:676–9. doi:10.1103/PhysRevLett.73.676.
- [65] Swain SS, Unnikrishnan L, Mohanty S, Nayak SK. Carbon nanotubes as potential candidate for separation of H₂CO₂ gas pairs. *Int J Hydrogen Energy* 2017;42:29283–99. doi:<https://doi.org/10.1016/j.ijhydene.2017.09.152>.
- [66] Babu DJ, Lange M, Cherkashinin G, Issanin A, Staudt R, Schneider JJ. Gas adsorption studies of CO₂ and N₂ in spatially aligned double-walled carbon nanotube arrays. *Carbon N Y* 2013;61:616–23. doi:<https://doi.org/10.1016/j.carbon.2013.05.045>.
- [67] Sanip SM, Ismail AF, Goh PS, Soga T, Tanemura M, Yasuhiko H. Gas separation properties of functionalized carbon nanotubes mixed matrix membranes. *Sep Purif Technol* 2011;78:208–13. doi:10.1016/J.SEPPUR.2011.02.003.
- [68] Ma P-C, Siddiqui NA, Marom G, Kim J-K. Dispersion and functionalization of carbon nanotubes for polymer-based nanocomposites: A review. *Compos Part A Appl Sci Manuf* 2010;41:1345–67. doi:<https://doi.org/10.1016/j.compositesa.2010.07.003>.
- [69] Tao Y, Xue Q, Liu Z, Shan M, Ling C, Wu T, et al. Tunable Hydrogen Separation in Porous Graphene Membrane: First-Principle and Molecular Dynamic Simulation. *ACS Appl Mater Interfaces* 2014;6:8048–58. doi:10.1021/am4058887.

- [70] Wei S, Zhou S, Wu Z, Wang M, Wang Z, Guo W, et al. Mechanistic insights into porous graphene membranes for helium separation and hydrogen purification. *Appl Surf Sci* 2018;441:631–8. doi:<https://doi.org/10.1016/j.apsusc.2018.02.111>.
- [71] Robeson LM. Correlation of separation factor versus permeability for polymeric membranes. *J Memb Sci* 1991;62:165–85. doi:[https://doi.org/10.1016/0376-7388\(91\)80060-J](https://doi.org/10.1016/0376-7388(91)80060-J).
- [72] Sun M, Li J. Graphene oxide membranes: Functional structures, preparation and environmental applications. *Nano Today* 2018;20:121–37. doi:<https://doi.org/10.1016/j.nantod.2018.04.007>.
- [73] Wang Y, Yang Q, Zhong C, Li J. Theoretical investigation of gas separation in functionalized nanoporous graphene membranes. *Appl Surf Sci* 2017;407:532–9. doi:<https://doi.org/10.1016/j.apsusc.2017.02.253>.
- [74] Zhang J, Xin Q, Li X, Yun M, Xu R, Wang S, et al. Mixed matrix membranes comprising aminosilane-functionalized graphene oxide for enhanced CO₂ separation. *J Memb Sci* 2019;570–571:343–54. doi:<https://doi.org/10.1016/j.memsci.2018.10.075>.
- [75] Ebrahimi S, Mollaiy-Berneti S, Asadi H, Peydayesh M, Akhlaghian F, Mohammadi T. PVA/PES-amine-functional graphene oxide mixed matrix membranes for CO₂/CH₄ separation: Experimental and modeling. *Chem Eng Res Des* 2016;109:647–56. doi:<https://doi.org/10.1016/j.cherd.2016.03.009>.
- [76] Chakarvarti SK. Track-etch membranes enabled nano-/microtechnology: A review. *Radiat Meas* 2009;44:1085–92. doi:<https://doi.org/10.1016/j.radmeas.2009.10.028>.
- [77] Gómez Álvarez-Arenas TE, Apel PY, Orelovitch OL, Muñoz M. New ultrasonic technique for the study of the pore shape of track-etched pores in polymer films. *Radiat Meas* 2009;44:1114–8. doi:<https://doi.org/10.1016/j.radmeas.2009.09.002>.
- [78] Yamazaki IM, Paterson R, Geraldo LP. A new generation of track etched membranes for microfiltration and ultrafiltration. Part I. Preparation and characterisation. *J Memb Sci* 1996;118:239–45. doi:[https://doi.org/10.1016/0376-7388\(96\)00098-1](https://doi.org/10.1016/0376-7388(96)00098-1).

- [79] Sudowe R, Vater W, Ensinger W, Vetter J, Penzhorn R-D, Brandt R. Basic research on nuclear track microfilters for gas separation. *Radiat Meas* 1999;31:691–6. doi:[https://doi.org/10.1016/S1350-4487\(99\)00179-1](https://doi.org/10.1016/S1350-4487(99)00179-1).
- [80] Apel PY, Blonskaya I V, Dmitriev SN, Orelovitch OL, Sartowska B. Structure of polycarbonate track-etch membranes: Origin of the “paradoxical” pore shape. *J Memb Sci* 2006;282:393–400. doi:<https://doi.org/10.1016/j.memsci.2006.05.045>.
- [81] Xu Z, Wan L, Huang X, editors. *Functionalization Methods for Membrane Surfaces BT - Surface Engineering of Polymer Membranes*, Berlin, Heidelberg: Springer Berlin Heidelberg; 2009, p. 64–79. doi:10.1007/978-3-540-88413-2_3.
- [82] Xiao L, Davenport DM, Ormsbee L, Bhattacharyya D. Polymerization and Functionalization of Membrane Pores for Water Related Applications. *Ind Eng Chem Res* 2015;54:4174–82. doi:10.1021/ie504149t.
- [83] Ulbricht M. Advanced functional polymer membranes. *Polymer (Guildf)* 2006;47:2217–62. doi:<https://doi.org/10.1016/j.polymer.2006.01.084>.
- [84] Awang N, Ismail AF, Jaafar J, Matsuura T, Junoh H, Othman MHD, et al. Functionalization of polymeric materials as a high performance membrane for direct methanol fuel cell: A review. *React Funct Polym* 2015;86:248–58. doi:<https://doi.org/10.1016/j.reactfunctpolym.2014.09.019>.
- [85] Ma Z, Lu X, Wu C, Gao Q, Zhao L, Zhang H, et al. Functional surface modification of PVDF membrane for chemical pulse cleaning. *J Memb Sci* 2017;524:389–99. doi:<https://doi.org/10.1016/j.memsci.2016.11.063>.
- [86] Al-Gharabli S, Kujawski W, Arafat HA, Kujawa J. Tunable separation via chemical functionalization of polyvinylidene fluoride membranes using piranha reagent. *J Memb Sci* 2017;541:567–79. doi:<https://doi.org/10.1016/j.memsci.2017.07.047>.
- [87] Kumar R, Kamakshi, Shisodia S, Kumar M, Awasthi K. Effect of UV irradiation on PC membrane and use of Pd nanoparticles with/without PVP for H₂ selectivity enhancement over CO₂ and N₂ gases. *Int J Hydrogen Energy* 2018. doi:10.1016/J.IJHYDENE.2018.06.094.
- [88] Ng LY, Ahmad A, Mohammad AW. Alteration of polyethersulphone membranes

- through UV-induced modification using various materials: A brief review. *Arab J Chem* 2017;10:S1821–34. doi:<https://doi.org/10.1016/j.arabjc.2013.07.009>.
- [89] Ohland AL, Salim VMM, Borges CP. Plasma functionalized hydroxyapatite incorporated in membranes for improved performance of osmotic processes. *Desalination* 2019;452:87–93. doi:<https://doi.org/10.1016/j.desal.2018.11.008>.
- [90] Upadhyaya L, Qian X, Ranil Wickramasinghe S. Chemical modification of membrane surface—overview. *Curr Opin Chem Eng* 2018;20:13–8. doi:<https://doi.org/10.1016/j.coche.2018.01.002>.
- [91] Kumar R, Kamakshi, Kumar M, Awasthi K. Functionalized Pd-decorated and aligned MWCNTs in polycarbonate as a selective membrane for hydrogen separation. *Int J Hydrogen Energy* 2016. doi:10.1016/j.ijhydene.2016.09.008.
- [92] Kamakshi, Kumar R, Saraswat VK, Kumar M, Awasthi K. Palladium nanoparticle binding in functionalized track etched PET membrane for hydrogen gas separation. *Int J Hydrogen Energy* 2017;42:16186–94. doi:10.1016/J.IJHYDENE.2017.05.040.
- [93] Gohil JM, Choudhury RR. Chapter 2 - Introduction to Nanostructured and Nano-enhanced Polymeric Membranes: Preparation, Function, and Application for Water Purification. In: Thomas S, Pasquini D, Leu S-Y, Gopakumar DABT-NM in WP, editors. *Micro Nano Technol.*, Elsevier; 2019, p. 25–57. doi:<https://doi.org/10.1016/B978-0-12-813926-4.00038-0>.
- [94] Altintas Z, Chianella I, Ponte G Da, Paulussen S, Gaeta S, Tothill IE. Development of functionalized nanostructured polymeric membranes for water purification. *Chem Eng J* 2016;300:358–66. doi:<https://doi.org/10.1016/j.cej.2016.04.121>.
- [95] Saleh TA, Gupta VK. Chapter 9 - Application of Nanomaterial-Polymer Membranes for Water and Wastewater Purification. In: Saleh TA, Gupta VKBT-N and PM, editors., Elsevier; 2016, p. 233–50. doi:<https://doi.org/10.1016/B978-0-12-804703-3.00009-7>.
- [96] Aghaeinejad-Meybodi A, Ghasemzadeh K. Chapter 11 - Solar Energy for Pure Hydrogen Production Using Inorganic Membrane Reactor. In: Basile A, Cassano A, Figoli ABT-CT and FD on (Bio-) M, editors., Elsevier; 2019, p. 261–92.

doi:<https://doi.org/10.1016/B978-0-12-813545-7.00011-8>.

- [97] Mohammadi A, Mehrpooya M. A comprehensive review on coupling different types of electrolyzer to renewable energy sources. *Energy* 2018;158:632–55. doi:<https://doi.org/10.1016/j.energy.2018.06.073>.
- [98] Weitemeyer S, Kleinhans D, Vogt T, Agert C. Integration of Renewable Energy Sources in future power systems: The role of storage. *Renew Energy* 2015;75:14–20. doi:<https://doi.org/10.1016/j.renene.2014.09.028>.
- [99] Eder L V, Provornaya I V, Filimonova I V, Kozhevin VD, Komarova A V. World energy market in the conditions of low oil prices, the role of renewable energy sources. *Energy Procedia* 2018;153:112–7. doi:<https://doi.org/10.1016/j.egypro.2018.10.068>.
- [100] Kannan N, Vakeesan D. Solar energy for future world: - A review. *Renew Sustain Energy Rev* 2016;62:1092–105. doi:<https://doi.org/10.1016/j.rser.2016.05.022>.
- [101] Marchenko O V, Solomin S V. The future energy: Hydrogen versus electricity. *Int J Hydrogen Energy* 2015;40:3801–5. doi:<https://doi.org/10.1016/j.ijhydene.2015.01.132>.
- [102] Jha SK, Bilalovic J, Jha A, Patel N, Zhang H. Renewable energy: Present research and future scope of Artificial Intelligence. *Renew Sustain Energy Rev* 2017;77:297–317. doi:<https://doi.org/10.1016/j.rser.2017.04.018>.
- [103] Khandelwal B, Karakurt A, Sekaran PR, Sethi V, Singh R. Hydrogen powered aircraft: The future of air transport. *Prog Aerosp Sci* 2013;60:45–59. doi:<https://doi.org/10.1016/j.paerosci.2012.12.002>.
- [104] Naghadeh SB, Vahdatifar S, Mortazavi Y, Khodadadi AA, Abbasi A. Functionalized MWCNTs effects on dramatic enhancement of MWCNTs/SnO₂ nanocomposite gas sensing properties at low temperatures. *Sensors Actuators B Chem* 2016;223:252–60. doi:10.1016/J.SNB.2015.09.088.
- [105] Van Amerongen GJ. The Permeability of Different Rubbers to Gases and Its Relation to Diffusivity and Solubility. *J Appl Phys* 1946;17:972–85. doi:10.1063/1.1707667.
- [106] Barrer RM. Permeability in relation to viscosity and structure of rubber. *Trans*

Faraday Soc 1942;38:322–30. doi:10.1039/TF9423800322.

- [107] Stern SA, Wang SC. Countercurrent and cocurrent gas separation in a permeation stage. Comparison of computation methods. *J Memb Sci* 1978;4:141–8. doi:[https://doi.org/10.1016/S0376-7388\(00\)83290-1](https://doi.org/10.1016/S0376-7388(00)83290-1).
- [108] Robeson LM. Correlation of separation factor versus permeability for polymeric membranes. *J Memb Sci* 1991;62:165–85. doi:10.1016/0376-7388(91)80060-J.
- [109] Paul DR, Kemp DR. The diffusion time lag in polymer membranes containing adsorptive fillers. *J Polym Sci Polym Symp* 1973;41:79–93. doi:10.1002/polc.5070410109.
- [110] Kulprathipanja S, Neuzil RW, Li NN. Separation of gases by means of mixed matrix membranes 1992.
- [111] Barbari TA, Koros WJ, Paul DR. Polymeric membranes based on bisphenol-A for gas separations. *J Memb Sci* 1989;42:69–86.
- [112] Mohammadi AT, Matsuura T, Sourirajan S. Gas separation by silicone-coated dry asymmetric aromatic polyamide membranes. *Sep Puri* 1995;9:181–7.
- [113] Hu Q, Marand E, Dhingra S, Fritsch D, Wen J. Poly (amide-imide) / TiO₂ nanocomposite gas separation membranes " Fabrication and characterization. *J Memb Sci* 1997;135:65–79. doi:[http://dx.doi.org/10.1016/S0376-7388\(97\)00120-8](http://dx.doi.org/10.1016/S0376-7388(97)00120-8).
- [114] Jahan Z, Niazi MBK, Hägg M-B, Gregersen ØW. Cellulose nanocrystal/PVA nanocomposite membranes for CO₂ /CH₄ separation at high pressure. *J Memb Sci* 2018;554:275–81. doi:10.1016/j.memsci.2018.02.061.
- [115] Kim S, Shamsaei E, Lin X, Hu Y, Simon GP, Seong JG, et al. The enhanced hydrogen separation performance of mixed matrix membranes by incorporation of two-dimensional ZIF-L into polyimide containing hydroxyl group. *J Memb Sci* 2018;549:260–6. doi:10.1016/j.memsci.2017.12.022.
- [116] Molki B, Aframehr WM, Bagheri R, Salimi J. Mixed matrix membranes of polyurethane with nickel oxide nanoparticles for CO₂ gas separation. *J Memb Sci* 2018;549:588–601. doi:10.1016/j.memsci.2017.12.056.
- [117] Rodenas T, Luz I, Prieto G, Seoane B, Miro H, Corma A, et al. Metal–organic

framework nanosheets in polymer composite materials for gas separation. *Nat Mater* 2014;14:48.

- [118] Liu D, Li X, Geng H, Chen R, Rettenmayr M, Su Y, et al. Development of Nb₃₅Mo₅Ti₃₀Ni₃₀ alloy membrane for hydrogen separation applications. *J Memb Sci* 2018;553:171–9. doi:10.1016/j.memsci.2018.02.052.
- [119] Cheng YS, Peña MA, Fierro JL, Hui DCW, Yeung KL. Performance of alumina, zeolite, palladium, Pd-Ag alloy membranes for hydrogen separation from Towngas mixture. *J Memb Sci* 2002;204:329–40. doi:10.1016/S0376-7388(02)00059-5.
- [120] Gallucci F, Fernandez E, Corengia P, van Sint Annaland M. Recent advances on membranes and membrane reactors for hydrogen production. *Chem Eng Sci* 2013;92:40–66.
- [121] Hatlevik Ø, Gade SK, Keeling MK, Thoen PM, Davidson AP, Way JD. Palladium and palladium alloy membranes for hydrogen separation and production: history, fabrication strategies, and current performance. *Sep Purif Technol* 2010;73:59–64.
- [122] Chen Y, Wei Y, Zhuang L, Xie H, Wang H. Effect of Pt layer on the hydrogen permeation property of La_{5.5}W_{0.45}Nb_{0.15}Mo_{0.4}O_{11.25}- Δ membrane. *J Memb Sci* 2018;552:61–7. doi:10.1016/j.memsci.2018.01.068.
- [123] Fasolin S, Barison S, Boldrini S, Ferrario A, Romano M, Montagner F, et al. Hydrogen separation by thin vanadium-based multi-layered membranes. *Int J Hydrogen Energy* 2018;43:3235–43. doi:https://doi.org/10.1016/j.ijhydene.2017.12.148.
- [124] Sharma A, Kumar S, Tripathi B, Singh M, Vijay YK. Aligned CNT/Polymer nanocomposite membranes for hydrogen separation. *Int J Hydrogen Energy* 2009;34:3977–82. doi:10.1016/j.ijhydene.2009.02.068.
- [125] Sharma A, Vijay YK. Effect of electric field variation in alignment of SWNT/PC nanocomposites. *Int J Hydrogen Energy* 2012;37:3945–8. doi:https://doi.org/10.1016/j.ijhydene.2011.03.166.
- [126] Kumar S, Srivastava S, Agrawal S, Tripathi B, Vijay YK. Effect of Electric Field

Alignment of MWCNT in PMMA Matrix for Hydrogen Gas Purification. AIP Conf Proc 2011;1349:1061–2. doi:10.1063/1.3606228.

- [127] Sharma A, Tripathi B, Vijay YK. Dramatic Improvement in properties of magnetically aligned CNT/polymer nanocomposites. *J Memb Sci* 2010;361:89–95. doi:<https://doi.org/10.1016/j.memsci.2010.06.005>.
- [128] Li L, Song C, Jiang D, Wang T. Preparation and enhanced gas separation performance of Carbon/Carbon nanotubes (C/CNTs) hybrid membranes. *Sep Purif Technol* 2017;188:73–80. doi:<https://doi.org/10.1016/j.seppur.2017.07.019>.
- [129] He X. Techno-economic feasibility analysis on carbon membranes for hydrogen purification. *Sep Purif Technol* 2017;186:117–24. doi:10.1016/j.seppur.2017.05.034.
- [130] Hashim SS, Somalu MR, Loh KS, Liu S, Zhou W, Sunarso J. Perovskite-based proton conducting membranes for hydrogen separation: A review. *Int J Hydrogen Energy* 2018;43:15281–305. doi:10.1016/j.ijhydene.2018.06.045.
- [131] Song N, Gao X, Ma Z, Wang X, Wei Y, Gao C. A review of graphene-based separation membrane: Materials, characteristics, preparation and applications. *Desalination* 2018;437:59–72. doi:10.1016/J.DESAL.2018.02.024.
- [132] Al-Mufachi NA, Rees N V, Steinberger-Wilkens R. Hydrogen selective membranes: A review of palladium-based dense metal membranes. *Renew Sustain Energy Rev* 2015;47:540–51. doi:<https://doi.org/10.1016/j.rser.2015.03.026>.
- [133] Khatib SJ, Oyama ST. Silica membranes for hydrogen separation prepared by chemical vapor deposition (CVD). *Sep Purif Technol* 2013;111:20–42. doi:10.1016/j.seppur.2013.03.032.
- [134] Dolan MD. Non-Pd BCC alloy membranes for industrial hydrogen separation. *J Memb Sci* 2010;362:12–28. doi:10.1016/j.memsci.2010.06.068.
- [135] Moghadam F, Park HB. Two-dimensional materials: an emerging platform for gas separation membranes. *Curr Opin Chem Eng* 2018;20:28–38. doi:<https://doi.org/10.1016/j.coche.2018.02.004>.
- [136] Yoo BM, Shin JE, Lee HD, Park HB. Graphene and graphene oxide membranes for gas separation applications. *Curr Opin Chem Eng* 2017;16:39–47.

doi:10.1016/J.COCHE.2017.04.004.

- [137] Acharya NK, Kulshrestha V, Awasthi K, Kumar R, Jain AK, Singh M, et al. Gas permeation study of Ti-coated, track-etched polymeric membranes. *Vacuum* 2006;81:389–93.
- [138] Ibrahim A, Lin YS. Gas permeation and separation properties of large-sheet stacked graphene oxide membranes. *J Memb Sci* 2018;550:238–45. doi:10.1016/j.memsci.2017.12.081.
- [139] Favvas EP, Heliopoulos NS, Karousos DS, Devlin E, Papageorgiou SK, Petridis D, et al. Mixed matrix polymeric and carbon hollow fibers with magnetic iron-based nanoparticles and their application in gas mixture separation. *Mater Chem Phys* 2018;223:220–9. doi:https://doi.org/10.1016/j.matchemphys.2018.10.047.
- [140] Van Gestel T, Barthel J. New types of graphene-based membranes with molecular sieve properties for He, H₂ and H₂O. *J Memb Sci* 2018;554:378–84. doi:https://doi.org/10.1016/j.memsci.2018.02.034.
- [141] Nour M, Berean K, Balendhran S, Ou JZ, Du Plessis J, McSweeney C, et al. CNT/PDMS composite membranes for H₂ and CH₄ gas separation. *Int J Hydrogen Energy* 2013;38:10494–501. doi:https://doi.org/10.1016/j.ijhydene.2013.05.162.
- [142] Nour M, Berean K, Griffin MJ, Matthews GI, Bhaskaran M, Sriram S, et al. Nanocomposite carbon-PDMS membranes for gas separation. *Sensors Actuators B Chem* 2012;161:982–8. doi:https://doi.org/10.1016/j.snb.2011.11.079.
- [143] Kulshrestha V, Awasthi K, Vijay Y. Swift heavy ion (SHI) irradiated polymer blend membranes for hydrogen permeation. *Int J Hydrogen Energy* 2007;32:3105–8. doi:10.1016/j.ijhydene.2007.01.014.
- [144] Ensinger W, Sudowe R, Brandt R, Neumann R. Gas separation in nanoporous membranes formed by etching ion irradiated polymer foils. *Radiat Phys Chem* 2010;79:204–7. doi:https://doi.org/10.1016/j.radphyschem.2009.08.045.
- [145] Kulshrestha V, Acharya NK, Awasthi K, Singh M, Avasthi DK, Vijay YK. Study of gas permeation for asymmetric track-etched polymer blends. *Int J Hydrogen Energy* 2006;31:1266–70.

- [146] Kulshrestha V, Acharya NK, Awasthi K, Singh M, Avasthi DK, Vijay YK. Study of gas permeation for asymmetric track-etched polymer blends. *Int J Hydrogen Energy* 2006;31:1266–70. doi:10.1016/j.ijhydene.2005.12.004.
- [147] Vijay YK. Nuclear track filters for hydrogen purification. *Int J Hydrogen Energy* 2008;33:340–5. doi:https://doi.org/10.1016/j.ijhydene.2007.07.062.
- [148] Kumar R, Saraswat VK, Kumar M, Awasthi K, Stamm M. Hydrogen gas separation with controlled selectivity via efficient and cost effective block copolymer coated PET membranes. *Int J Hydrogen Energy* 2017. doi:10.1016/j.ijhydene.2017.06.113.
- [149] Ibrahim AFM, Lin YS. Synthesis of graphene oxide membranes on polyester substrate by spray coating for gas separation. *Chem Eng Sci* 2018;190:312–9. doi:10.1016/j.ces.2018.06.031.
- [150] Iwasa R, Suizu T, Yamaji H, Yoshioka T, Nagai K. Gas separation in polyimide membranes with molecular sieve-like chemical/physical dual crosslink elements onto the top of surface. *J Memb Sci* 2018;550:80–90. doi:10.1016/j.memsci.2017.12.064.
- [151] Awasthi K, Choudhury S, Komber H, Simon F, Formanek P, Sharma A, et al. Functionalization of track-etched poly (ethylene terephthalate) membranes as a selective filter for hydrogen purification. *Int J Hydrogen Energy* 2014;39:9356–65.
- [152] Wang Z, Knebel A, Grosjean S, Wagner D, Bräse S, Wöll C, et al. Tunable molecular separation by nanoporous membranes. *Nat Commun* 2016;7:13872.
- [153] Jue ML, Lively RP. Targeted gas separations through polymer membrane functionalization. *React Funct Polym* 2015;86:88–110. doi:https://doi.org/10.1016/j.reactfunctpolym.2014.09.002.
- [154] Kar P, Choudhury A. Carboxylic acid functionalized multi-walled carbon nanotube doped polyaniline for chloroform sensors. *Sensors Actuators, B Chem* 2013;183:25–33. doi:10.1016/j.snb.2013.03.093.
- [155] Choudhury A, Kar P. Doping effect of carboxylic acid group functionalized multi-walled carbon nanotube on polyaniline. *Compos Part B Eng* 2011;42:1641–7.

doi:10.1016/j.compositesb.2011.04.005.

- [156] Awasthi K, Choudhury S, Komber H, Simon F, Formanek P, Sharma A, et al. Functionalization of track-etched poly (ethylene terephthalate) membranes as a selective filter for hydrogen purification. *Int J Hydrogen Energy* 2014;39:9356–65. doi:10.1016/j.ijhydene.2014.03.240.
- [157] Kumar R, Kamakshi, Kumar M, Awasthi K. Selective deposition of Pd nanoparticles in porous PET membrane for hydrogen separation. *Int J Hydrogen Energy* 2017;42. doi:10.1016/j.ijhydene.2017.03.202.
- [158] Vijay YK, Acharya NK, Wate S, Avasthi DK. Nanofilter for hydrogen purification. *Int J Hydrogen Energy* 2003;28:1015–8. doi:https://doi.org/10.1016/S0360-3199(02)00166-0.
- [159] Liu Y, Wang R, Chung T-S. Chemical cross-linking modification of polyimide membranes for gas separation. *J Memb Sci* 2001;189:231–9. doi:https://doi.org/10.1016/S0376-7388(01)00415-X.
- [160] Jue ML, Lively RP. Targeted gas separations through polymer membrane functionalization. *React Funct Polym* 2015;86:40–3. doi:10.1016/j.reactfunctpolym.2014.09.002.
- [161] Kuwahara Y, Morita M, Nagami T, Tanaka A, Iwanaga T, Kumamaru K, et al. Functionalization of a polymer using nanoparticles immobilized in supercritical carbon dioxide. *Jpn J Appl Phys* 2009;48:06FF13.
- [162] Jewell LL, Davis BH. Review of absorption and adsorption in the hydrogen–palladium system. *Appl Catal A Gen* 2006;310:1–15. doi:https://doi.org/10.1016/j.apcata.2006.05.012.
- [163] Yun S, Ted Oyama S. Correlations in palladium membranes for hydrogen separation: A review. *J Memb Sci* 2011;375:28–45. doi:https://doi.org/10.1016/j.memsci.2011.03.057.
- [164] Zhang K, Way JD. Palladium-copper membranes for hydrogen separation. *Sep Purif Technol* 2017;186:39–44. doi:https://doi.org/10.1016/j.seppur.2017.05.039.
- [165] Favier F, Walter EC, Zach MP, Benter T, Penner RM. Hydrogen Sensors and Switches from Electrodeposited Palladium Mesowire Arrays. *Science* (80-)

2001;293:2227 LP-2231.

- [166] Bokobza L, Zhang J. Raman spectroscopic characterization of multiwall carbon nanotubes and of composites. *Express Polym Lett* 2012;6.
- [167] Choudhury A, Kar P. Doping effect of carboxylic acid group functionalized multi-walled carbon nanotube on polyaniline. *Compos Part B Eng* 2011;42:1641–7. doi:<https://doi.org/10.1016/j.compositesb.2011.04.005>.
- [168] LARIJANI MM, KHAMSE EJ, ASADOLLAHI Z, ASADI M. Effect of aligned carbon nanotubes on electrical conductivity behaviour in polycarbonate matrix. *Bull Mater Sci* 2012;35:305–11. doi:10.1007/s12034-012-0299-1.
- [169] Kumar A, Jangir LK, Kumari Y, Kumar M, Kumar V, Awasthi K. Electrical behavior of dual-morphology polyaniline. *J Appl Polym Sci* 2016;133. doi:10.1002/app.44091.
- [170] Zeng XQ, Latimer ML, Xiao ZL, Panuganti S, Welp U, Kwok WK, et al. Hydrogen Gas Sensing with Networks of Ultrasmall Palladium Nanowires Formed on Filtration Membranes. *Nano Lett* 2011;11:262–8. doi:10.1021/nl103682s.
- [171] Acharya NK, Yadav PK, Vijay YK. Study of temperature dependent gas permeability for polycarbonate membrane 2004.
- [172] Skoulidas AI, Sholl DS, Johnson JK. Adsorption and diffusion of carbon dioxide and nitrogen through single-walled carbon nanotube membranes. *J Chem Phys* 2006;124:54708. doi:10.1063/1.2151173.
- [173] Kumar R, Kamakshi, Kumar M, Awasthi K. Functionalized Pd-decorated and aligned MWCNTs in polycarbonate as a selective membrane for hydrogen separation. *Int J Hydrogen Energy* 2016;41:23057–66. doi:10.1016/j.ijhydene.2016.09.008.
- [174] Fukuzumi H, Fujisawa S, Saito T, Isogai A. Selective Permeation of Hydrogen Gas Using Cellulose Nanofibril Film. *Biomacromolecules* 2013;14:1705–9. doi:10.1021/bm400377e.
- [175] Lee E, Lee JM, Koo JH, Lee W, Lee T. Hysteresis behavior of electrical resistance in Pd thin films during the process of absorption and desorption of hydrogen gas.

Int J Hydrogen Energy 2010;35:6984–91.
doi:<https://doi.org/10.1016/j.ijhydene.2010.04.051>.

- [176] Sun Y, Wang HH. High-Performance, Flexible Hydrogen Sensors That Use Carbon Nanotubes Decorated with Palladium Nanoparticles. *Adv Mater* 2007;19:2818–23. doi:10.1002/adma.200602975.
- [177] Sankir M, Semiz L, Serin RB, Sankir ND. Hydrogen generation from nanoflower platinum films. *Int J Hydrogen Energy* 2015;40:8522–9. doi:<https://doi.org/10.1016/j.ijhydene.2015.04.137>.
- [178] Wang M, Song J, Wu X, Tan X, Meng B, Liu S. Metallic nickel hollow fiber membranes for hydrogen separation at high temperatures. *J Memb Sci* 2016;509:156–63. doi:<https://doi.org/10.1016/j.memsci.2016.02.025>.
- [179] Acharya NK, Kulshrestha V, Awasthi K, Kumar R, Jain AK, Singh M, et al. Gas permeation study of Ti-coated, track-etched polymeric membranes. *Vacuum* 2006;81:389–93. doi:10.1016/j.vacuum.2006.03.027.
- [180] Jo YS, Lee CH, Kong SY, Lee K-Y, Yoon CW, Nam SW, et al. Characterization of a Pd/Ta composite membrane and its application to a large scale high-purity hydrogen separation from mixed gas. *Sep Purif Technol* 2018;200:221–9. doi:10.1016/J.SEPPUR.2017.12.019.
- [181] Jaleh B, Shahbazi N. Surface properties of UV irradiated PC–TiO₂ nanocomposite film. *Appl Surf Sci* 2014;313:251–8. doi:<https://doi.org/10.1016/j.apsusc.2014.05.197>.
- [182] Ayoub A, Massardier-Nageotte V. The effect of UV-irradiation and molten medium on the mechanical and thermal properties of polystyrene–polycarbonate blends. *J Appl Polym Sci* 2011;124:1096–105. doi:10.1002/app.35094.
- [183] Hareesh K, Pandey AK, Sangappa Y, Bhat R, Venkataraman A, Sanjeev G. Changes in the properties of Lexan polycarbonate by UV irradiation. *Nucl Instruments Methods Phys Res Sect B Beam Interact with Mater Atoms* 2013;295:61–8. doi:<https://doi.org/10.1016/j.nimb.2012.10.011>.
- [184] Mendonça da Rocha Oliveira L, Vedovello P, Paranhos CM. Polycarbonate/1-(2-hydroxyethyl)-2, 3-dimethylimidazolium chloride composite membranes and

short-range chain mobility analysis. *J Appl Polym Sci* 2017;134:45117.

- [185] Resta V, Quarta G, Lomascolo M, Maruccio L, Calcagnile L. Raman and Photoluminescence spectroscopy of polycarbonate matrices irradiated with different energy $^{28}\text{Si}^+$ ions. *Vacuum* 2015;116:82–9. doi:<https://doi.org/10.1016/j.vacuum.2015.03.005>.

BIO-DATA

Name: Rajesh Kumar

Father's Name: Mr. Mahaveer Prasad

Mother's Name: Mrs. Chukesh Devi

Date of Birth: 10/10/1990

Marital Status: Single

Education Qualification: M.Sc. Applied Physics (2014)
Malaviya National Institute of Technology Jaipur
Rajasthan, India

B.Sc. (2012)
Seth G. R. Chamaria College, Fatehpur Sikar
Rajasthan, India

Awards: Awarded by CSIR-Senior Research Fellowship (SRF)
Awarded for best poster presentation in "International workshop on polymer-metal Nanocomposite 2015"
Awarded for best oral presentation in conference on "Applied science and humanities in engineering-2016"
Awarded best oral presentation in "International conference on Soft Materials 2018".

Publications: International Journals (03)
Allied International Journals (03)

Conferences: International Conferences (06)
National Conferences (02)

Workshops: 03 attended